การเตรียมตัวเร่งปฏิกิริยา Ni_{core} – Pt $alloy_{shell}$ สำหรับเซลล์เชื้อเพลิงพีอีเอ็ม

นางสาวเสาวลักษณ์ ผลาพิบูลย์

วิทยานิพนธ์นี้เป็นส่วนหนึ่งของการศึกษาตามหลักสูตรปริญญาวิทยาศาสตรดุษฎีบัณฑิต

สาขาวิชาเคมีเทคนิค ภาควิชาเคมีเทคนิค

คณะวิทยาศาสตร์ จุฬาลงกรณ์มหาวิทยาลัย

ปีการศึกษา 2555

PREPARATION OF Ni_{core} – Pt $ALLOY_{shell}$ CATALYSTS FOR PEM FUEL CELL

Miss Saowaluck Bhlapibul

A Dissertation Submitted in Partial Fulfillment of the Requirements
for the Degree of Doctor of Philosophy Program in Chemical Technology
Department of Chemical Technology
Faculty of Science
Chulalongkorn University
Academic Year 2012

Thesis Title	PREPARATION OF Ni_{core} – Pt $ALLOY_{shell}$ CATALYSTS FOR PEM FUEL CELL
By	Miss Saowaluck Bhlapibul
Field of Study	Chemical Technology
Thesis Advisor	Associate Professor Pornpote Piumsomboon, Ph.D.
Thesis Co-advisor	Associate Professor Kejvalee Pruksathorn, Dr. de l'INPT

Accepted by the Faculty of Science, Chulalongkorn University in Partial Fulfillment of the Requirements for the Doctoral Degree

.....Dean of the Faculty of Science
(Professor Supot Hannongbua, Dr. rer. nat.)

THESIS COMMITTEE

.....Chairman
(Associate Professor Somkiat Ngamprasertsith, Dr. de l'INPT.)

.....Thesis Advisor
(Associate Professor Pornpote Piumsomboon, Ph.D.)

.....Thesis Co-advisor
(Associate Professor Kejvalee Pruksathorn, Dr. de l'INPT.)

.....Examiner
(Associate Professor Mali Hunsom, Ph.D.)

.....Examiner
(Kunakorn Poochinda, Ph.D.)

.....Examiner
(Professor Orawon Chailapakul, Ph.D.)

.....External Examiner
(Associate Professor Supaporn Therdthianwong, Ph.D.)

เสาวลักษณ์ ผลาพิบูลย์ : การเตรียมตัวเร่งปฏิกิริยา Ni_{core} – Pt $alloy_{shell}$ สำหรับเซลล์เชื้อเพลิงพีอีเอ็ม. (PREPARATION OF Ni_{core} – Pt $ALLOY_{shell}$ CATALYSTS FOR PEM FUEL CELL) อ.ที่ปรึกษาวิทยานิพนธ์หลัก: รศ.ดร.พรพจน์ เปี่ยมสมบูรณ์, อ.ที่ปรึกษาวิทยานิพนธ์ร่วม: รศ.ดร.เก็จวลี พฤกษาทร, 120 หน้า.

ความพยายามในการพัฒนาตัวเร่งปฏิกิริยาเชิงไฟฟ้าของเซลล์เชื้อเพลิงพีอีเอ็มโดยการลดปริมาณโลหะมีค่าในองค์ประกอบได้รับการกล่าวถึงอย่างกว้างขวาง ตัวเร่งปฏิกิริยาที่มีโครงสร้าง core – shell บนตัวรองรับคาร์บอนนับเป็นทางเลือกที่น่าสนใจสำหรับการปรับปรุงสมบัติและเสถียรภาพของตัวเร่งปฏิกิริยา ในการศึกษาเบื้องต้นของงานวิจัยนี้ เป็นการสังเคราะห์ตัวเร่งปฏิกิริยา Ni_{core} – Pt_{shell} บนตัวรองรับคาร์บอน ผลการทดลองพบว่าวิธีการสังเคราะห์ตัวเร่งปฏิกิริยา และชนิดของสารเพิ่มเสถียรภาพที่ใช้ในการสังเคราะห์ส่งผลต่อปริมาณโลหะในองค์ประกอบ ขนาดอนุภาค และพื้นที่การเกิดปฏิกิริยาเคมีไฟฟ้าของตัวเร่งปฏิกิริยา สำหรับการสังเคราะห์ตัวเร่งปฏิกิริยา Ni_{core} – $PtRu_{shell}$ บนตัวรองรับคาร์บอน ตัวแปรที่เกี่ยวข้องในการสังเคราะห์ได้ศึกษาโดยการออกแบบการทดลองแบบ FCC – 2^4 ผลการศึกษาระบุว่า สัดส่วนโดยอะตอมของแพลทินัมต่อรูทิเนียม สัดส่วนโดยโมลของสารตั้งต้นนิกเกิลต่อสารเพิ่มเสถียรภาพพีวีพี อุณหภูมิรีดักชันสำหรับขั้นตอนของการเกิดชั้นเปลือกโลหะผสมแพลทินัมรูทิเนียม และอันตรกิริยาระหว่างสัดส่วนโดยโมลของสารตั้งต้นนิกเกิลต่อสารเพิ่มเสถียรภาพพีวีพีและอุณหภูมิรีดักชันสำหรับขั้นตอนการเกิดชั้นเปลือกโลหะผสมแพลทินัมรูทิเนียม มีผลต่อพื้นที่การเกิดปฏิกิริยาเคมีไฟฟ้าของตัวเร่งปฏิกิริยาที่สังเคราะห์ได้ นอกจากนี้ การปรับสภาพอนุภาคโลหะที่เป็นแกนด้วยความร้อนก่อนเติมชั้นโลหะผสมสามารถปรับปรุงกัมมันตภาพของตัวเร่งปฏิกิริยา Ni_{core} – $PtRu_{shell}$ บนตัวรองรับคาร์บอนได้ การศึกษาความทนทานของตัวเร่งปฏิกิริยา Ni_{core} – $PtRu_{shell}$ บนตัวรองรับคาร์บอนด้วยเทคนิคโพเทนเชียลไซคลิงแสดงให้เห็นเสถียรภาพที่สูงกว่าเมื่อเทียบกับตัวเร่งปฏิกิริยาทางการค้าแพลทินัมบนตัวรองรับคาร์บอน

ภาควิชา.....เคมีเทคนิค.....ลายมือชื่อนิสิต.....

สาขาวิชา.....เคมีเทคนิค.....ลายมือชื่อ อ.ที่ปรึกษาวิทยานิพนธ์หลัก.....

ปีการศึกษา.....2555.....ลายมือชื่อ อ.ที่ปรึกษาวิทยานิพนธ์ร่วม.....

5173888523: MAJOR CHEMICAL TECHNOLOGY
KEYWORDS: CORE – SHELL CATALYST / Ni CORE / PtRu ALLOY / MODIFIED POLYOL / PEM FUEL CELL

SAOWALUCK BHLAPIBUL: PREPARATION OF Ni_{core} – Pt $ALLOY_{shell}$ CATALYSTS FOR PEM FUEL CELL. ADVISOR: ASSOC. PROF. PORNPOTE PIUMSOMBOON, Ph.D., CO-ADVISOR: ASSOC. PROF. KEJVALEE PRUKSATHORN, Dr. de l'INPT, 120 pp.

The effort to develop the PEM fuel cell electrocatalyst by lowering the precious metal loading in the composition has been extensively addressed. The carbon supported core – shell structure catalyst structure is considered to be the interesting alternative for improving the catalyst properties and stability. In the preliminary stage of this work, the preparation of Ni_{core} – Pt_{shell}/C was studied. The results suggested that the synthesis method and type of stabilizer used in the synthesis process had an effect on the metal content in the composition, particle size and the EAS of the catalyst. For the synthesis of Ni_{core} – $PtRu_{shell}$/C catalyst with modified polyol method, the parameters concerning in the synthesis were investigated by FCC – 2^4 experimental design. The results indicated that the atomic ratio of platinum to ruthenium, the mole ratio of Ni precursor to the PVP stabilizer, the reduction temperature for the PtRu alloy shell formation step and the interaction between the mole ratio of Ni precursor to the PVP stabilizer and the mole ratio of Ni precursor to the PVP stabilizer affected the EAS of the synthetic catalyst. In addition, heat treatment of the Ni core particle before adding PtRu alloy shell layer could improve the activity of the Ni_{core} – $PtRu_{shell}$/C. The durability study of the heat – treated Ni_{core} – $PtRu_{shell}$/C by potential cycling technique showed the higher stability compared to the commercial Pt/C.

Department: …...Chemical Technology….Student's signature…….……
Field of Study: ...Chemical Technology….Advisor's signature……
Academic Year: ……...2012…….....Co – advisor's signature…….……

ACKNOWLEDGEMENTS

I would not possible achieve my doctoral degree without the wisdom and valuable experience from my advisor, Assoc. Prof. Dr. Pornpote Piumsomboon, and my co –advisor, Assoc. Prof. Dr. Kejvalee Pruksathorn. I am more grateful for their favor, supervision and encouragement.

I also would like to acknowledge Assoc. Prof. Dr. Somkiat Ngamprasertsith, Assoc. Prof. Dr. Mali Hunsom, Dr. Kunakorn Poochinda, Prof. Dr. Orawon Chailapakul and Assoc. Prof. Dr. Supaporn Therdthianwong for serving as chairman and members of the dissertation committee, respectively.

Many thanks to scientists, supporting staffs, technicians and the members of Fuel Cell Laboratory, Department of Chemical Technology for their kind support during my work period.

I would like to express my sincere thanks to Prof. Yong Gun – Shul for his great suggestion and inspiration for my research work. Also, I would like to thank for their kindness of the inorganic material laboratory members, department of chemical and biomolecular engineering for providing me every conveniences during 3 months in Yonsei University, Seoul, Republic of Korea.

I gratefully acknowledge Office of the Higher Education Commission Thailand for providing me the strategic scholarships fellowships frontier research networks and the research fund through the Higher Education Research Promotion and National Research University Project of Thailand (EN276B and CU56 – EN05) throughout my study period.

Many thanks for their encouragement and many supports from Dr. Benjapon Chalermsinsuwan and Dr.Sasithron Sunphorka. They are always there to brighten my day.

I would like to express my appreciation to Mr. Rungroj Chanchairoek, for always being by my side and supporting me in every way.

Finally, I would like to express my deep gratitude to my mom and my family for their love, support and encouragement throughout my Ph.D. program.

CONTENT

PAGE

PAGE

PAGE

PAGE

LIST OF TABLES

TABLE PAGE

TABLE PAGE

LIST OF FIGURES

FIGURE PAGE

FIGURE PAGE

FIGURE PAGE

FIGURE PAGE

CHAPTER I

INTRODUCTION

1.1 Motivation

Proton exchange membrane (PEM) fuel cell is a very attractive technology for application in vehicle and other mobile purposes because of its compactness, higher efficiency than combustion and non – emission. The advantages of PEM fuel cell are the low temperature operation leading to faster start up from ambient condition and immediately response to the change in the demand for power [1]. The important technical barrier for PEM fuel cell operation is the durability of membrane electrode assembly (MEA) under the wide range of operating conditions such as dynamic load cycling, start up/shut down and freeze/ thaw condition. Based on the present data, the degradation of MEA may cause by: (i) the activation loss of electrocatalyst; (ii) the corrosion of catalyst support and (iii) the degradation of the polymer electrolyte membrane. Among these roots, the activation loss of the electrocatalyst is said to be the most significant [2]. The challenges to improve the electrocatalyst in respect of increasing the catalyst activity and to reduce the precious metal in respect of reducing the cost of PEM fuel cell are the motivations to develop the promising electrocatalyst. A core – shell structure catalyst which is usually composed of transition metal as a core and precious/ alloy metal as a shell may be one of the choices for improving its performance. With this structure, the increasing of surface area to volume ratio could be obtained. Also, the near surface alloy (NSA) effect, in which the underlying metal and alloys layer affects the binding enthalpies, can enhance the selectivity and catalytic activity [3].

1.2 Objectives of this study

1. To study preparation methods and the effect of parameters on the preparation of Ni_{core} – Pt $alloy_{shell}$ catalyst for PEM fuel cell.

2. To investigate the ability of prepared catalyst to catalyze the oxygen reduction reaction in PEM fuel cell.

3. To study the stability of prepared catalyst during the oxygen reduction reaction.

1.3 Scope of the dissertation

1. Investigate the appropriate preparation method of Ni_{core} – Pt_{shell}/C catalyst by comparing between the conventional method and the modified polyol method.

2. Study the effect of stabilizers using in the preparation of Ni_{core} – Pt_{shell}/C catalyst by the modified polyol method.

3. Examine the effect of parameters on the preparation of Ni_{core} – $PtRu_{shell}$ /C catalyst by the modified polyol method namely; the mole ratio of Ni precursor and stabilizer, the atomic ratio of Pt and Ru, the reduction temperature and the reduction time for the formation of PtRu alloy layer. The FCC – 2^4 factorial design is introduced to indicate the significant parameters and the optimal condition for catalyst synthesis.

4. Study the removal of stabilizer from Ni core nanoparticles by heat treatment and investigate the characteristic of the synthetic Ni_{core} – $PtRu_{shell}$ /C prepared with the heat treatment Ni core nanoparticles.

5. Characterize the prepared catalyst both the physical and electrochemical properties by the analytical instruments such as

- Scanning Electron Microscope/Energy Dispersive X-ray spectrometer (SEM/EDX) for examination the elements content and the element mapping of the prepared catalyst.

- X-ray Diffractometer (XRD) for analysis the crystalline structure, the particle size and the lattice parameter.

- The potentiostat/ galvanostat instrument by the Cyclic Voltammetry (CV) and Linear Sweep Voltammetry (LSV) techniques which are used to investigate the electrochemical active surface area (EAS) and the limiting current density in the oxygen reduction reaction, respectively.

6. Conduct the performance test of the optimal condition catalyst in 5 cm^2 electrode area of single PEM fuel cell.

7. Examine the durability of prepared catalyst by potential cycling and chronoamperometry technique.

1.4 Anticipated benefits

1. To obtain the optimal condition for synthesizing the $Ni_{core} - PtRu_{shell}/C$ catalyst for the oxygen reduction reaction in PEM fuel cell.

2. To obtain the stabilized $Ni_{core} - PtRu_{shell}/C$ catalyst for the oxygen reduction reaction in PEM fuel cell.

1.5 Format of the dissertation

This dissertation was formatted in the chapter form. Motivation, objectives and scope of the research work were presented in Chapter I. Some important theories and the gathering of relevant literatures were provided in Chapter II. Details of chemicals, materials and experimental procedures were given in Chapter III. The physical and electrochemical characterization techniques of the synthetic catalysts were also mentioned in this chapter.

Chapter IV was summarized the results and discussion of this research work namely;

- The preliminary study of $Ni_{core} - Pt_{shell}/C$ catalyst by comparing the preparation methods between the conventional and the modified polyol method.
- The effect of stabilizers on the properties of $Ni_{core} - Pt_{shell}$ catalyst preparing by the modified polyol method.
- The FCC – 2^4 factorial design study for the synthesis of $Ni_{core} - PtRu_{shell}/C$ by the modified polyol method.

Moreover, the studying of heat treatment Ni core nanoparticles before applying PtRu shell layer was presented in Chapter V. The physical and the electrochemical properties of the synthetic $Ni_{core} - PtRu_{shell}$ /C catalyst using the heat – treated Ni core nanoparticle were shown here. This chapter also revealed the PEM single cell performance test and the durability of this synthetic catalyst.

Finally, the important conclusion from this research and recommendations for the future work were given in Chapter VI.

CHAPTER II

THEORY AND LITERATURES REVIEW

2.1 Fuel Cell [4, 5]

Nowadays, fuel cells are the promising technology for the environmental friendly aspect. The mechanism of fuel cell in generating the DC electricity is converting chemical energy of the reactants directly into electricity and heat. Generally, the configuration of a fuel cell composes of an electrolyte layer contacted with the porous anode and cathode. The fuel and the oxidant are fed continuously to the anode and the cathode, respectively. Then, the electric current is produced from the electrochemical reaction which occurred at the electrodes.

Both Fuel cell and battery are electrochemical devices which generate the electricity from the electrochemical reaction. But the different characteristic is that battery is the energy storage with the fuel and oxidant built onboard and has limited lifetime. Fuel cells, on the contrary, have the outside storage of fuel and the oxidant and have a capability to generate the electricity as long as the fuels and the oxidant are fed to the electrodes. The schematic comparison of battery and fuel cell is shown in Figure 2.1

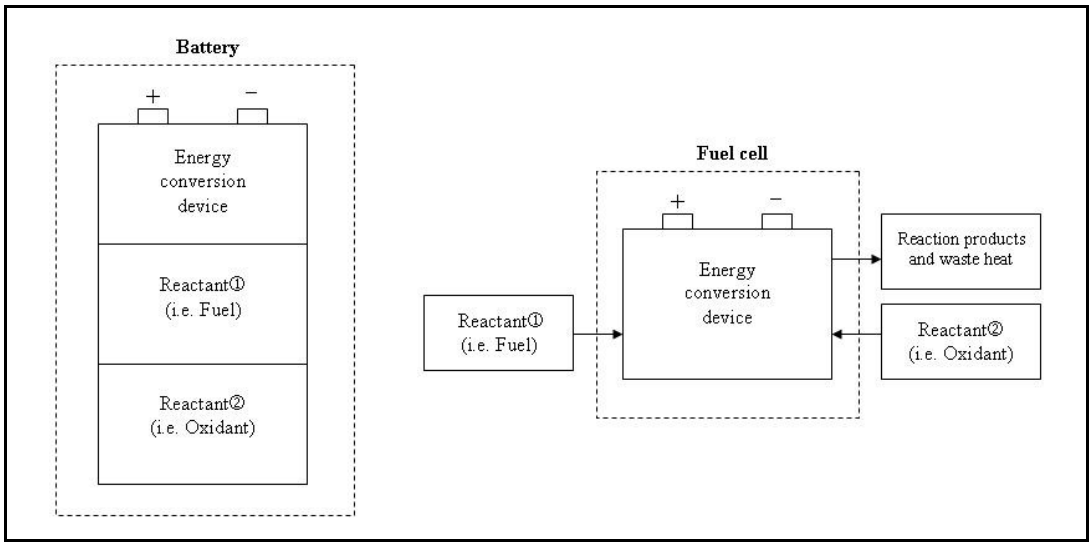

Figure 2.1 The schematic comparison of battery and fuel [5]

Fuel cells are said to have many advantages such as

- A high operating efficiency which is not a function of the system size.
- Various types of the fuel sources.
- Near – Zero greenhouse emission and silence

Types of fuel cells can be classified by the electrolyte used since the electrolyte defines the properties of fuel cell such as the operating principle, the design and also the material used for cell components. The operational characteristics and the application of each type of fuel cells are summarized in Table 2.1

Table 2.1 Summary for different types of fuel cell [1]

Fuel cell type	**Mobile ion**	**Operating temperature (^oC)**	**Applications**
Alkaline (AFC)	OH^-	50 – 200	Used in space vehicles.
Proton exchange membrane (PEMFC)	H^+	30 – 100	Vehicles and mobile applications, lower power CHP systems.
Direct methanol (DMFC)	H^+	20 – 90	Suitable for portable electronic systems of low power, running for long time.
Phosphoric acid (PAFC)	H^+	~220	Large numbers of 200kW CHP systems in use.
Molten carbonate (MCFC)	CO_3^{2-}	~650	Suitable for medium to large scale CHP system, up to MW capacity.
Solid oxide (SOFC)	O^{2-}	500 – 1000	Suitable for all sizes of CHP systems, 2kW to multi-MW.

2.2 Proton exchange membrane fuel cell [1]

As mentioned before, PEM fuel cell is one type of fuel cells that converts the chemical energy of the hydrogen and oxygen redox reaction to electrical energy. The main physical components of PEM fuel cell is composed of an electrolyte layer or proton exchange membrane which each side in contact with a catalyst coated on porous gas diffusion layer. This sandwich – liked component is also call membrane electrode assembly or MEA. Following the gas diffusion layer is a flow – field plate or bipolar plate, which is served as a unit for supplying the reactant gases via flow channel and usually makes from graphite. The details of PEM fuel cell components are shown in Figure 2.2.

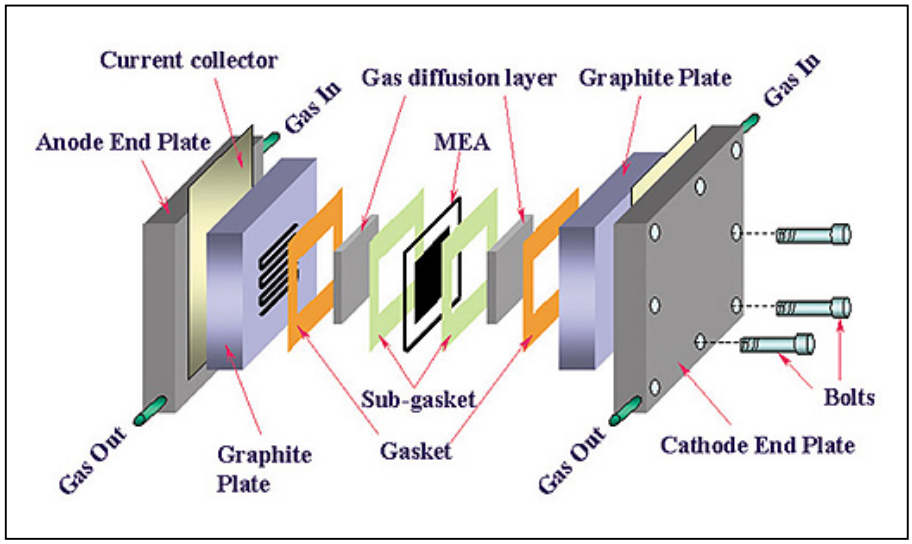

Figure 2.2 Structure of single Proton Exchange Membrane Fuel Cell (PEMFC) with the detail of its components [6]

The fuel gas and oxidant for PEM fuel cells are H_2 and O_2. For the mechanism of PEM fuel cells, as shown in Figure 2.3. H_2 and O_2 from the outer sources are fed into flow – field channel of the anode and cathode sides, respectively.

This means that fuel cell can produce the electrical energy as long as fuel gas and oxidant being fed. When the H_2 gas reaches the catalyst surface, the oxidation of H_2 occurs to liberate protons and electrons. Protons are transferred to cathode side via the proton exchange membrane and electrons travels through the external loading to the cathode. At the cathode side, protons, electrons and oxygen atoms are reunited to form water molecules as explained in equation 2.1 – 2.3 below.

Anode reaction: $H_2 \rightarrow 2H^+ + 2e^-$ $E^0 = 0.00$ V/SHE (2.1)

Cathode reaction: $1/2O_2 + 2H^+ + 2e^- \rightarrow H_2O$ $E^0 = 1.229$ V/SHE (2.2)

Overall reaction: $H_2 + 1/2O_2 \rightarrow H_2O$ $E^0 = 1.229$ V/SHE (2.3)

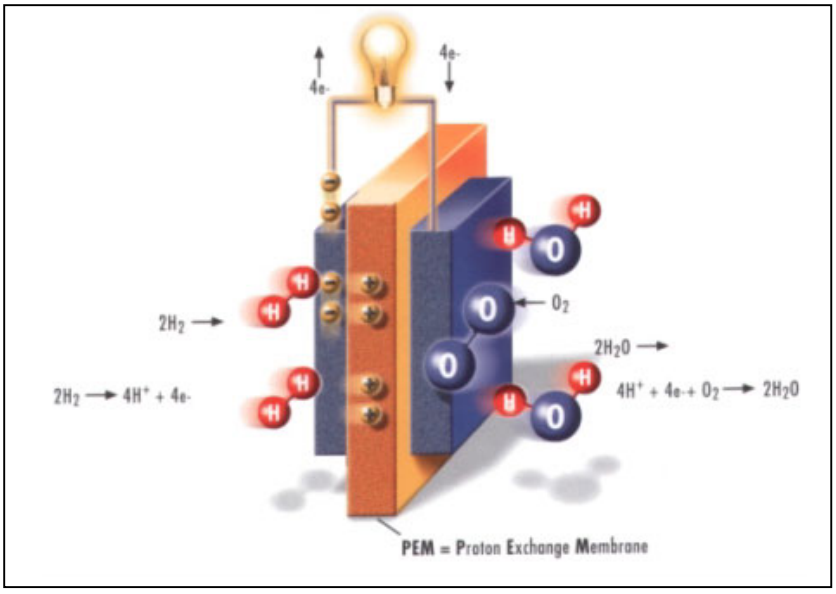

Figure 2.3 Mechanism of PEMFC [7]

Since single PEM fuel cell consists of only one anode and one cathode, the resistances that occur in the single cell system might reduce the operating potential to be less than 1V. This voltage is inadequate for vehicle or even small

portable power device. Thus, several cells must be assembled to form a fuel cell stack which can be either in parallel and series type. The ordinary PEM fuel cell stack is presented in Figure 2.4. From the figure, every single cell is electrically connected with each other by using a bipolar plate which also serves as a gas barrier that separates the H_2 gas and O_2 gas of adjacent cells.

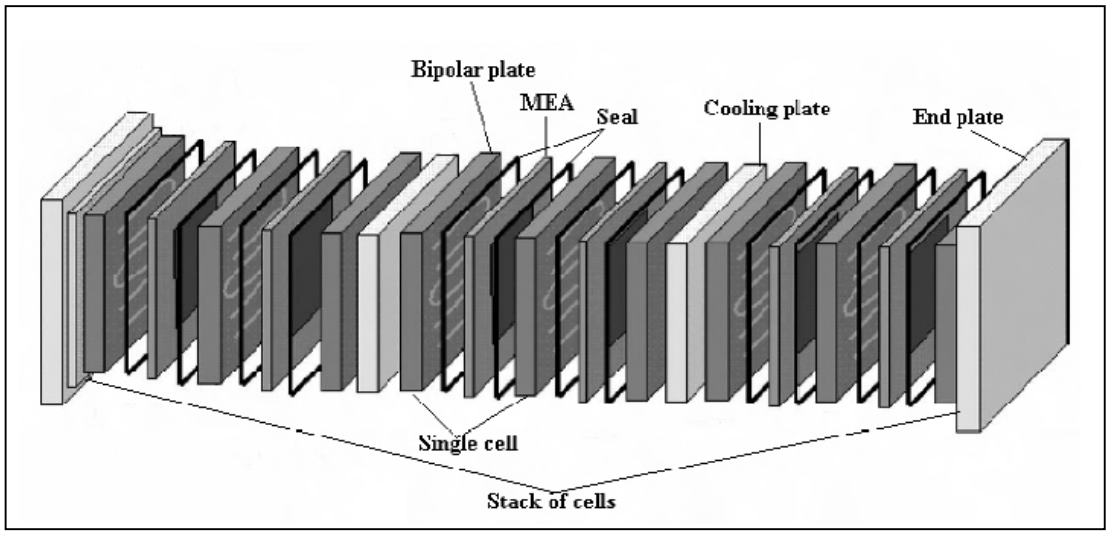

Figure 2.4 PEM Fuel Cell stack [8]

Because of PEM fuel cell generating a wide range of electric power, they can be applied with any application as shown in Table 2.2

Table 2.2 PEM fuel cells application categorized by their power level generations [8]

Level of power	Applications
> 1 MW	Local distributed power station.
100 kW – 1 MW	Large transportation vehicles such as naval ships, submarines and buses; small portable power station; small stationary power station.
10 kW – 100 kW	Transportation vehicles such as cars and mid- size buses; backup power for mid – size communication station; small power station.
1 kW – 10 kW	Transportation vehicles such as motorcycles, utility vehicles, cars, yacht; various portable power devices used for field working, underwater platform; backup power; uninterruptible power, residential power system.
100W – 1 kW	Simple riding devices such as bicycles, scooters and wheelchairs; backup power; power for exhibition or demo; UPS for small devices, terminals and computers.
10W – 100W	Portable power such as for emergency working power supply and military equipment; battery replacements; lighting; signal light power.
< 10 W	Small portable power devices; cell phone.

2.3 Membrane electrode assembly (MEA) and its components [8]

The key of fuel cell for generating electricity are the electrochemical reactions on membrane electrode assembly (MEA). MEA is composed of three main parts which connect like a sandwich structure as showed in Figure 2.5, namely

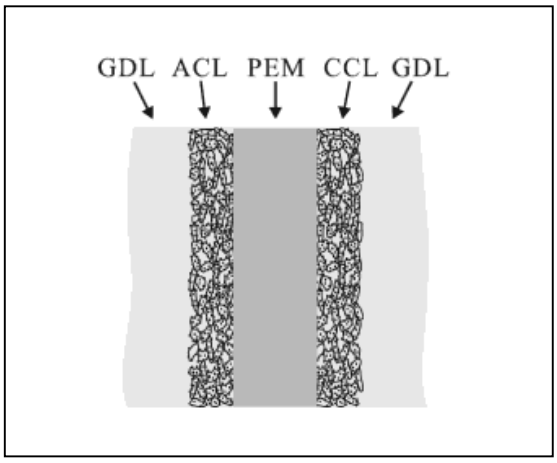

Figure 2.5 Illustration of membrane electrode assembly (MEA) structure. GDL – gas diffusion layer; ACL – anode catalyst layer; CCL – cathode catalyst layer; PEM - proton exchange membrane [8].

- Gas diffusion layer (GDL)

GDL was prepared from a porous carbon paper or carbon cloth, usually 1000 μm thick. The function of GDL are to provide the mechanical support, be an electrical pathway for electrons, transfer water away from the electrodes and certainly disperse fuel gases. With the porous structure of the GDL, the fuel gases can spread out and contact with the entire surface of catalyst and membrane.

- Membrane

The main roles of the membrane in fuel cell are to transport protons from the anode to the cathode and prevent the mixing of fuel gas and oxidant. So the ideal membrane should have excellent proton conductivity, strength and flexibility,

chemical and thermal conductivity, low gas permeability, low water drag, low cost and good availability. Until now, the membrane that is proved to be superior in performance and durability is Nafion® membrane.

The structure of Nafion® membrane is composed of aliphatic perfluorinated backbone with ether – linked side chains ending in sulfonate cation exchange sites as shown in Figure 2.6. In water absorbing state, the proton conducting network is formed in the membrane. The proton conductivity of membrane increases as a function of the content of water swelling in membrane up to a point. As the water content increases further, the conductivity is decreased.

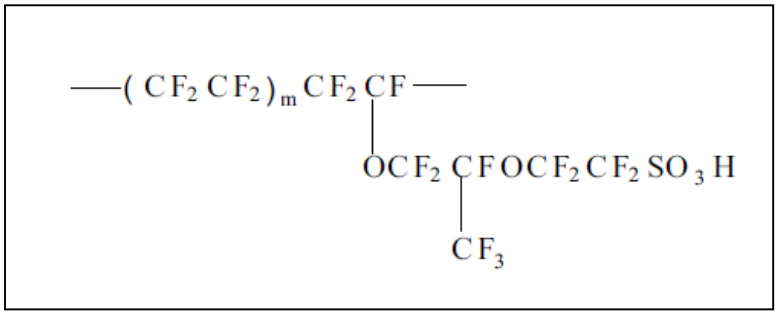

Figure 2.6 The structure of Nafion® membrane [8]

- Catalyst layer (CL)

Because of the slow reaction rate at normal condition, catalyst is applied for both anode and cathode sides. For hydrogen/ oxygen (air) PEM fuel cell, Pt/C is normally used for both anode and cathode because of its high catalytic activity.

The optimal catalyst layer is needed to catalyze the desired reaction with high rate. However, the amount of catalyst for required power output should be minimal. The requirements which should be considered are large three – phase interface in the catalyst layer as illustrated in Figure 2.7, efficient protons transport, well dispersion of reactant and product gas and easy to remove the water product.

Also, the continuous of electron transfer pathway between the reaction sites on catalysts and current collector should be regarded.

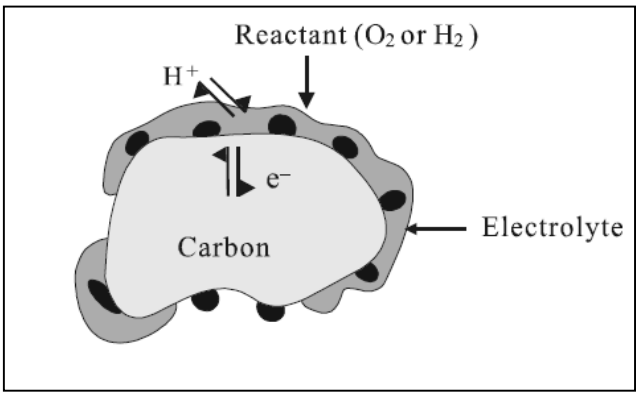

Figure2.7 Three-phase interface formed in the catalyst layer [8].

For creating the catalyst layer, the well uniformed catalyst ink should be prepared. Normally, catalyst ink usually obtains from the mixing of (1) the ionic conductor such as perfluorosulfonate acid (PFSA) ionomer to provide the pathway of protons to transfer (2) metal catalyst supported on a conducting material like carbon (3) a water repelling substance such as PTFE. Every particular factor should be optimized to provide the excellent overall performance of a catalyst layer.

The different coating methods for creating the catalyst layers in MEAs can be divided into 2 modes as presented in Figure 2.8. The traditional mode is to apply the catalyst ink onto the GDL. The examples of the techniques in this mode are

- *Spraying technique*: the catalyst ink is repeatedly sprayed on the carbon cloth or carbon paper. After spraying each catalyst layer, the carbon cloth is heated to evaporate the solvent to prevent the catalyst ink components from re – dissolving in the next spraying.

- *Electrodeposition*: the metal catalyst is deposited at conducting sites of the carbon cloth or carbon paper to create the catalyst layer.

Besides, the other one is to apply the catalyst ink directly to the membrane, also called catalyst coated membrane (CCM). There are several techniques used in this mode, for instance,

- *Catalyst decal transfer*: the catalyst ink is directly sprayed onto the substrate such as Mylar film [9] and transferred to membrane by hot pressing. A very thin catalyst layer is left on the membrane after peeling the substrate away.

- *Printing*: the catalyst ink is prepared with a special formula for applying with a minor modification of commercial inkjet printer. The membrane, after treatment process, is attached with a cellulose acetate sheet and fed through the printer using the original paper feed plate. In the printing process, the electrode dimensions, thickness and shape are controlled by computer software [10].

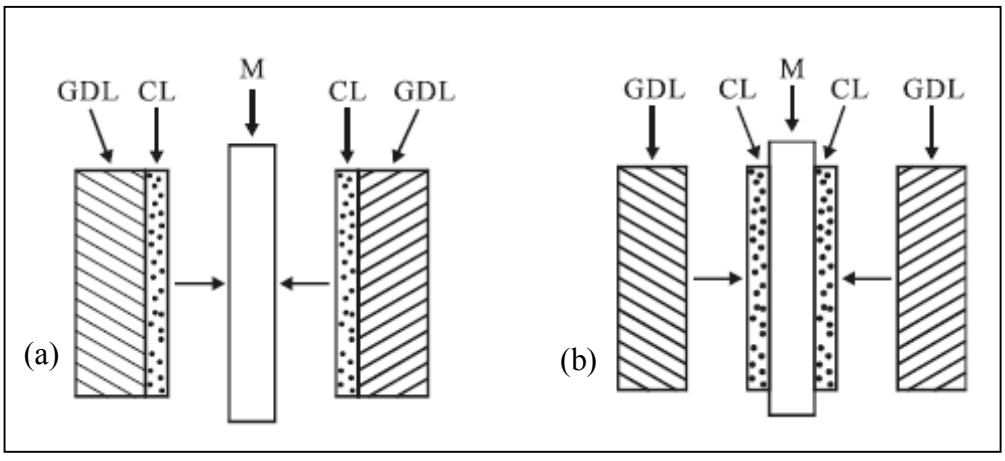

Figure 2.8 Construction of MEAs for (a) the catalyst layer on GDL and (b) the catalyst layer on membrane [8].

2.4 Platinum - based alloying catalyst [8]

One of the challenges in PEM fuel cell commercialization is to reduce the platinum loading of the electrocatalyst. Platinum- based alloying with other transition metal is the interesting approach to lower the platinum consumption. Unexpectedly, platinum-based alloying is not only achieving the platinum reduction target but some properties of this platinum alloy also push the catalytic activity. The alloying effects are generally considered as the structural effect, the inhibition of absorbed hydroxide species effect and the electronic effect.

The development of Pt – based catalyst depends on the application in the MEA. In the anode side, the kinetic of hydrogen oxidation reaction (HOR) is very fast on pure platinum surface with the exchange current density about 10^{-3} Acm^{-2}. But the critical problem for anode electrode with pure platinum catalyst is the poisoning from the contaminants in hydrogen stream, especially carbon monoxide (CO). Therefore, mostly researches emphasis on the improvement of CO tolerance catalyst.

For cathode side, as mainly discussion in this research work, there is the limitation in oxygen reduction reaction (ORR) kinetics. The ORR exchange current density on pure platinum surface is only 10^{-10} Acm^{-2} which about 5-7 order of magnitude slower than HOR under normal condition. Thus, the developing of ORR catalyst generally focuses on the accelerating of ORR kinetics to reach a practical level in PEM fuel cell. Normally, there are many factors, such as the O_2 adsorption energy, the dissociation energy of the O – O bond and the binding energy of OH on the platinum surface, that strongly affect the catalytic activity toward ORR. To obtain the Pt-based alloy with the improvement of ORR kinetics, the theoretical calculation of such O_2 and OH binding energy on several metals have proceeded. This calculation can predict which PtM (M = transition metal e.g. Ni, Co, Ru, etc.) should have higher catalyst activity toward ORR and the trend of oxygen reduction activity as a function of the O_2 binding energy in some metals is shown in Figure 2.9

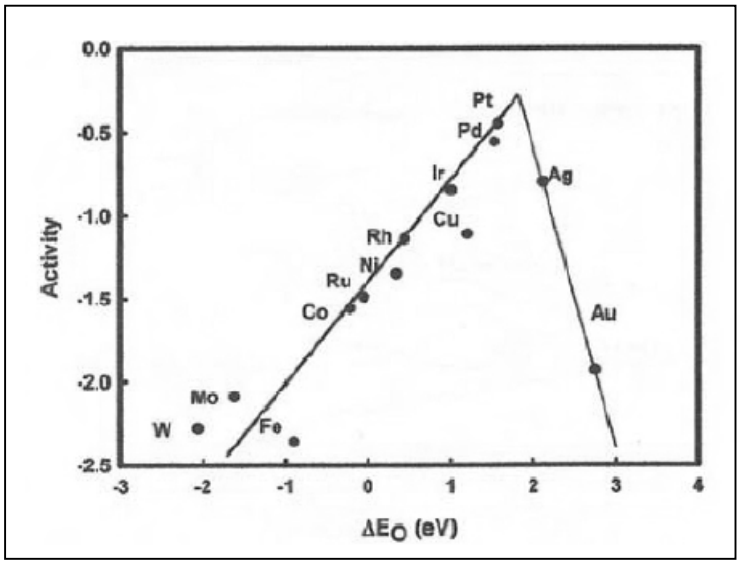

Figure 2.9 Plot of oxygen reduction activity as a function of oxygen binding energy in several metals [8].

The extensive study of binary and ternary Pt- based alloy catalyst has been carried out. Because of their lower material cost, many transition metals are chosen to create the Pt alloy and investigate the properties of the obtained catalyst.

For example, the carbon supported $Pt_{25}Cu_{75}$ and $Pt_{20}Cu_{20}Co_{60}$ were synthesized by an impregnation/freeze drying method followed by annealing under H_2 atmosphere. Comparing to Pt/C, these prepared binary and ternary alloy catalysts were able to retain the mass activity and reduced the electrochemical active surface area (EAS) loss after they were performed the oxygen reduction (ORR) activity and catalyst durability tests. The data from short – term durability testing in liquid electrolyte environment showed that cobalt was the appropriate component that benefited by enhancing the stability compared with the binary PtCu alloy [11].

For a high exchange current density transition metal in oxygen reduction reaction, palladium (Pd) was also demonstrated the remarkably characteristic as a Pt – Pd bimetallic electrocatalyst. In the preparation step, the impregnation of Pd was conducted in a basic condition using $NaBH_4$ as a reducing agent on Vulcan XC72 support. After the monometallic Pd/C was formed, the

electroless deposition of Pt was carried out to partial encapsulate the Pd particle. The result revealed that, the performance in oxygen reduction reaction of this catalyst was equal or lower than commercial catalyst. However, from potential cycling test, Pt – Pd/C catalyst produced noticeably less H_2O_2 byproduct which would help to reduce ionomer degradation resulting from the oxidation by H_2O_2 [12].

In aspect of enduring cathode catalyst, Pt- based alloys have been expected to be the promising material. The PtCo/C catalyst was synthesized and evaluated the durability with the potential cycling method. A 25 cm^2 active area of MEA was prepared for PEM fuel cell and the cell operation condition were at 65^oC and 101 kPa (absolute). In the potential cycling test, the voltage will be fluctuated between 0.87 and 1.2 V versus RHE with a time step 30 second for each voltage. The test was continued for 2400 cycles and was evaluated after every 400 cycles. The result showed that within 2400 cycles, the PtCo/C catalyst enhanced the cell performance over Pt/C catalyst in comparison. However, there was the dissolution of cobalt but this phenomenon did not affect the membrane conductance and did not reduce the cell voltage [13].

Apart from cathode side of PEM fuel cell, bimetallic alloy catalyst is very useful for enhancing the durability of the anodic electrocatalyst in case of CO contaminated fuel. At this time, the study of PtRu alloy electrocatalyst preparation is widely interesting because of its promising CO – tolerant property. From the study of Camara et al. [14], for instance, the carbon supported PtRu alloy catalyst was prepared from chemical reduction method which an atomic Pt:Ru ratio of 1:1. After that, the prepared catalyst was entered 2 steps thermal treatment process at 200^oC in the oxidant environment (air) for 1 h and then under a H_2 atmosphere for 1 h at various temperatures. It was revealed that with the increase of the second step heat treatment temperature, the particle size and the conversion of ruthenium into the alloyed metal were increased. Also, the performance of hydrogen oxidation reaction in the presence of 100 ppm CO was improved as a linear function of the second step heat treatment temperature.

2.5 Polyol synthesis

The metal nanoparticles can be prepared by the method of using the temperature – dependent reducing ability of liquid polyol or diol in the presence of a stabilizing agent. Liquid polyols such as ethylene glycol and propylene glycol are generally used in this polyol synthesis. The hydrogen – bonding in the chemical structure made this liquid polyol be able to dissolve ionic inorganic compounds. Then, a mild reducing property of this polyol provides the ability to reduce metal precursors to metals or complexes of metals at room or moderate temperature. Besides, the polyol molecules act as protective agents by adsorbing on the metal particles to prevent the agglomeration of metal particles.

The temperature – dependent reducing potential of liquid polyol is verified to be a convenient, multipurpose and low cost route for synthesis of metal nanostructure with narrow size distribution. The metal nanostructure synthesis typically occurs as the following scheme; (i) the metal salts are dissolved with a suitable amount of sodium hydroxide in the liquid polyol; (ii) the nucleating agent, if required, is added into the solution; (iii) the solution is heated and the precipitation occurs *in situ* in an intermediate phase (metal alkoxide hydroxide); (iv) at higher temperature, the precipitates degenerate and liberate the cationic species in the solution; (v) metal cations are reduced by the polyol; (vi) nucleation and growth of the metal nanoparticles are further generated in the solution [15,16].

In case of using 1, 2 propanediol (1, 2 PDO) as a polyol solvent, the mechanism of polyol reduction can be described similarly to the reduction mechanism formulated elsewhere [17] as shown in the equations below.

$$CH_3 - HCOH - CH_2OH \rightarrow CH_3CH_2CHO + H_2O \quad (2.4)$$

$$M^{2+} + 2CH_3CH_2CHO + 2OH^- \rightarrow M + CH_3CH_2CO - COCH_2CH_3 + 2H_2O \quad (2.5)$$

The polyol synthesis has the major advantage of simply monitoring the reaction kinetic by changing the experimental parameters. Therefore, the modification

of polyol method is introduced to the synthesis of some metal nanoparticles and investigates the effect of varying the synthesis parameters.

Couto et al. [18] synthesized nickel nanoparticles in ethylene glycol using $NaBH_4$ as a reducing agent. Polyvinylpyrrolidone (PVP) was used as a stabilizer and the weight ratio of Ni precursor to PVP was also varied. The reaction temperature was 140^{o}C and the reaction time was 2 h. In this case, the result showed that the nickel particle size was decreased in proportion to the increasing of PVP amount. The average nickel particle size is 3.8 nm and the particle size of non – PVP nickel was 7.7 nm.

The carbon support adding sequence also impacted the properties of synthetic Pt/C. As reported in the study of Qi and co-workers, carbon supported Pt nanoparticles were synthesized via a polyol method using ethylene glycol as a polyol solvent. The synthesis temperature was 140^{o}C and the reaction time was 3 h. HCl was used as a precipitation promoter. The particle size of Pt/C prepared by adding carbon support after the reduction of Pt metal by ethylene glycol was found to be a function of Pt precursor concentration. However, for the Pt/C prepared by adding carbon support before the Pt reduction, the particle size was not depended on the Pt precursor concentration and the average particle size was 3.5 nm. This phenomenon occurred especially for the carbon support which contained large amount of micropores [19].

Park et al. [20] performed the experiment of copper nanoparticle synthesis with diethylene glycol solvent and PVP (molecular weight 40,000) as a capping agent. The reaction temperature was varied from 140 – 200 ^{o}C and the effect of the injection rate of copper precursor solution into the reaction medium was also investigated between 2 to 8 ml/min. The reducing agent used in this synthesis was sodium phosphinate monohydrate. From XRD analysis, the result showed face – centered cubic structure of pure copper particles. However, some particles contained the amorphous layer of copper oxide and chemisorbed PVP on the surface as revealed by XPS and HR-TEM analysis. The reaction temperature and the injection rate played an important role in controlling the particle size distribution and the particle size, respectively.

The concentration of sodium hydroxide in the polyol reaction also affects the particles size and structure of final nanoparticle. Bai et al. [20] investigated the effect of alkalinity on the synthesis of nickel particles. Based on the results, the purity and morphology of Ni particle were found to depend on the alkalinity which related to the concentration of NaOH. For the NaOH concentration below 0.3M, pure nickel particle could not be obtained. When the concentration was controlled between 0.4 and 0.5M, the nickel particle structure was dominated by polyhedra structure. And the flower – like clusters of nanoflakes were formed with the 0.6M NaOH concentration. It can be reported that the high concentration of NaOH resulting in rapid reduction and disordered aggregation of nickel particle in the early state of the reaction.

Polymer stabilizer also influences the obtained nanoparticle as the investigation of Zhang et al. [21]. The effect of modifying agent on the synthesis of nanostructure Ni in 1,2 propanediol was studied. The modifiers used in this experiment were polyethylene glycols (PEG) and sodium dodecyl sulfate (SDS). It can be reported that XRD pattern of synthesized Ni nanocrystal showed the major characteristic peak of pure Ni metal. It means that there were no nickel oxides or other crystalline materials formed under the experiment condition. Shapes and particle size of synthesis Ni nanoparticles were found depending on the type of modifier used either single modifier or composite modifier. For PEG, the obtained crystal shape was either triangular nanoprism crystal or dodecahedron crystal depending on the molecular weight of PEG. In case of SDS, the fabricated Ni nanoparticle is dodecahedron crystal.

Besides, the polyol method can be applied for the metal alloy synthesis. For example, CoPt nanoparticle was synthesized via modified polyol method using octyl ether and PVP as a capping agent. In this method, Co precursor and Pt precursor were co – reduction at 260^{o}C synthesis temperature for 1 h under Ar atmosphere. After drying, the obtained CoPt alloy was annealed at 600◦C for 1.5 h in the N_2/H_2 atmosphere. The average particle size was 5.3 nm with high crystallinity

face – centered cubic structure. The particle size distribution of CoPt alloy from TEM analysis also showed narrow distribution [22].

For the other alloy synthesis, the observation of the effect of Ni/Pd molar ratio on the properties of NiPd alloy nanoparticle was accomplished via modified polyol method. Ethylene glycol solvent and PVP stabilizer were used in this reaction and the condition for synthesis was 3 h refluxing at 197^{o}C under inert gas atmosphere. The XRD results revealed that the different Ni/Pd molar ratio did not affect the crystalline structure. All NiPd nanoparticle samples gave the face – centered cubic structure. As the Ni content increased, the diffraction peak was shifted to high angle and nearly the pure Ni diffraction pattern. Also, the particle size was decreased with the increasing of Ni amount due to the influence of Ni on the extraction of the lattice parameter [23].

PtRu alloy can also be synthesized by modified polyol method. Lee et al. [24] investigated the effect of post – treatment condition on the properties of modified polyol synthesis PtRu alloy nanoparticle. The polyol solvent used in this method was ethylene glycol. The reaction condition was refluxing at 160^{o}C for 5 h in Ar atmosphere and cooled down to room temperature. To increase the metal loading on the carbon support, H_2SO_4 was added to the reaction solution under the vigorous stirring after 30 min of carbon support adding. Then the temperature of solution was increased to 70^{o}C for 1h. The obtained catalyst was 60%wt PtRu loading on carbon support. The three different post – treatment conditions in tube furnace were 10% H_2/Ar at room temperature, 10% H_2/Ar at 160^{o}C and air at 160^{o}C. Among these three conditions, the PtRu nanoparticle under 10% H_2/Ar at room temperature showed the highest methanol oxidation reaction activity. This mild condition resulted in the reduction of the particle agglomeration and also the phase separation between Pt and Ru.

2.6 Core – shell structure catalyst

Due to its unique physical and surface - chemical properties, core – shell nanostructure is attractive and technically important. Core – shell nanostructure consists of nanoparticle core uniformly covered by a layer of another material shell. The physical and chemical properties of core – shell nanostructure depend strongly on its particle size, component and the structure of the core and the shell, especially at its interface. The interface of core – shell nanostructure is very important because its sharpness; the degree of lattice and chemical gradient are significant to the transfer of electron and electron coupling. Normally, the correlation among various metals or oxides in core – shell nanostructure often exhibits distinctive behaviors as compared to that inherent to the individual components. In general, these behaviors contain tunable or tailorable optical properties and enhanced catalytic activity. The common synthetic method to create core – shell nanostructure involves a combination of several wet – synthetic methods such as solid – state inorganic synthesis, sol – gel process and hydrothermal synthesis. The main idea of multi - step reaction is relevant to the growth of core materials followed by a suitable approach to coat the shell over the core material. During these multi – step reaction, there is a necessity to passivate the intermediate and final nanoparticle to prevent aggregation either by electrostatic covalent or steric interaction [25].

Zeng et al. [26] examined the electronic effect of Au core on the catalysis of Pt in the carbon supported Au core – Pt shell nanoparticles. The synthesis of this experiment was accomplished by the seed- meditate growth method of the Ag core - Pt shell nanoparticle followed by the displacement reaction of Ag core with Au core. The particle size of prepared catalyst examined by TEM was approximate 4 - 10 nm. Based on the results, the CO stripping peak from cyclic voltammograms of prepared catalyst in 0.5 M H_2SO_4 solution was located at more negative potential than that of Pt/C catalyst. It was suggested that the underlying Au core enhanced the electron transfer from Au to Pt atom resulting in enhanced oxygen adsorption. The oxygen presence on the catalyst surface created the active oxygen – containing species which facilitated the removal of adsorbed CO molecules.

Zhao et al. [27] studied the characteristic of Co core – PtRu alloy shell nanoparticles catalyst supported on multiwalled carbon nanotubes (MWCNTs) for methanol oxidation. The catalyst was prepared by using a surface displacement reaction. A two – step reduction method was employed with $NaBH_4$ – NaOH as a nucleating agent and hydrazine hydrate as a reducing agent, respectively. The adding of hydrazine hydrate was used to control the reduction speed of Co^{2+} and gave the narrow size distribution. The particle size of Co core and PtRu alloy shell in this experiment were 30 nm and 3.4 nm measured by high resolution – TEM. The cyclic voltammetry in the mixed solution of 0.5M H_2SO_4 and 1M CH_3OH under half – cell condition was performed. The result showed a negative shift of methanol oxidation potential of Co core – PtRu alloy shell / MWCNTs compared to that of commercial PtRu alloy/ C catalyst. It means that methanol was easy to be oxidized on PtRu alloy surface due to the high utilization of PtRu alloy layer on the surface of Co core.

Kristain et al. [28] studied the effect of Pt shell thickness on the activity of carbon supported Au core – Pt shell catalyst by varying the precursor Pt/Au mole ratio in the constant amount of Au seeds. It can be observed that core – shell catalyst improved electrochemical active surface area than Pt/C because of the Pt dispersion improvement. The electrocatalytic activities tested in the mixed solution of 0.5M H_2SO_4 and 1M CH_3OH revealed that Pt/Au ratio of 2:1 and 1:1 were two or three times better than Pt/C. However, the higher mole ratio gave almost the same or slightly lower activities compared to that of Pt/C. For the Pt/Au ratio of 1:2, the lower activity was observed due to the incomplete coverage of Au core with Pt shell layer.

Wei et al. [29] examined the characteristic of the Cu core – Pt shell nanoparticles prepared by two steps of electrodeposition of Cu and partial replacement of deposited Cu by Pt. To prevent the deposited nanoparticle Cu from reacting with dissolved oxygen in the solution, thiourea was added as an inhibitor. Compared with commercial Pt/C, the Cu core – Pt shell catalyst exhibited the better activity for oxygen reduction reaction even though the lower Pt loading of Cu core – Pt shell. The stability of the Cu core – Pt shell was also investigated. It could be reported that the hydrogen adsorption/ desorption area in the cyclic voltammetry

profiles of the 10^{th} and 100^{th} cycle were hardly changed which implied that this prepared core – shell catalyst was reasonably stable.

Lee et al. [30] prepared the carbon supported Co core – Pt shell catalyst by thermal decomposition of dicobalt octacarbinyl and the reduction of platinum acetylacetonate. The kinetics of oxygen reduction reaction (ORR) of prepared catalyst was also investigated. Based on the results, the good dispersion of Co core – Pt shell on the surface of supported carbon was found and the average particle size was 4.12 nm. by TEM. For the electrochemical properties, the current density and mass activity of ORR at overpotential of 0.1V were higher than that of Pt/C catalyst. Moreover, Co core – Pt shell catalyst was observed to have a higher exchange current density compared to Pt/C with implicit that the fast ORR kinetic would be occurred on Co core – Pt shell rather than Pt/C.

Wu et al. [31] studied the characteristic of carbon supported PtPd alloy core – Pt shell prepared by two steps colloidal method. From TEM measurement, the active components were highly dispersed on the carbon support with a narrow size distribution and its average particle size was 4.8 nm. Result also indicated that the electrochemical active area of PtPd alloy core – Pt shell/C was 6% higher than that of the Pt/C. The highly dispersion of Pt on the PtPd core and the strong interaction between the outer Pt shell and the inner PtPd core resulting in high activity toward the anodic oxidation of methanol as well as the reduction of oxygen. The hydrogen – air single cell test of MEA prepared by PtPd core - Pt shell for anode and commercial Pt catalyst for cathode gave over 80% higher current density at 0.65V cell voltage than that of commercial Pt/C MEA.

Ma et al. [32] conducted the synthesis of Au core – Pt shell supported on carbon for oxygen reduction reaction by seed mediate method. It can be reported that the Au core – Pt shell nanoparticle were dispersed homogenously as small and uniform spots on the surface of the carbon support with the average particle size about 5.7 nm. The weight ratio between Pt and Au such as 4:2, 3:2, 2:2 and 2:3 were observed. The Au core – Pt shell/C with Pt: Au = 3:2 expressed better metal mass –

specific activity and ORR activity due to the increase of utilization of Pt in the core shell structure.

Zhao et al. [33] investigated the characteristic of Ni core – Pd shell supported on multiwalled carbon nanotubes (MWCNTs) in alkaline media. The core – shell structure catalyst was prepared by the co – reduction of Ni^{2+} and $PdCl_4^{2-}$ in the sodium dodecyl sulfate (SDS) as the capping and structure – directing agent. It could be observed that metal nanoparticles showed very well uniform dispersion on the surface of MWCNTs and the particle size evaluated by TEM was about 6 – 8 nm. It also indicated that the electrochemical active surface area, specific activity for the electro – oxidation of methanol and electrochemical stability of the Ni core – Pd shell/MWNTs catalyst were much higher than that of PdNi alloy and Pd nanoparticles supported on MWNTs.

2.7 Durability study in PEM fuel cell [8, 34]

Even though a PEM fuel cell has many benefits such as a zero emission power source and higher efficiency than internal combustion engines, on the other hand, the system lifetime and cost for implementation still undergo technical advancement. In order to compete against the conventional power source, the standard criteria for the development of PEM fuel cell system are needed. Several government sections and energy development organizations make an effort to establish the technical targets for PEM fuel cell application. For instant, Tables 2.3, 2.4 and 2.5 below are the long – term technical targets categorized by application and components such as membrane electrode assemblies and electrocatalysts for transportation purpose, respectively, prepared by the office of energy efficiency and renewable energy, US department of energy, setting for the hydrogen, fuel cells and infrastructure technologies program.

Table 2.3 United State department of energy (DOE), Office of Energy Efficiency and Renewable Energy, long –term targets categorized by application [34].

Application	Durability			
	Efficiency	(Hours)	Cost,2010	Cost,2015
Transportation	60%	5,000	$45/kW	$30/kW
Stationary	40%	40,000	$750/kW[1]	-
Consumer Electronics (<50W)	-	5,000	$3/kW	-
Auxiliary power unit (3-30kW)	40%	35,000	$400/kW	$400/kW

[1]*Milestone delayed from 2010 to 2011 due to appropriations shortfall and congressionally directed activities.*

Table 2.4 United State department of energy (DOE), Office of Energy Efficiency and Renewable Energy, technical targets for membrane electrode assemblies (MEAs) [34].

Characteristic	**Units**	**2005 Status**	**2010**	**2015**
Cost	$/kW	60	10	5
Durability with cycling				
At operating temp of ≤ 80°C	Hours	>2,000	5,000	5,000
At operating temp of > 80°C	Hours	N/A	2,000	5,000
End of life (EOL) power density	% BOL	95	90	95

Table 2.5 United State department of energy (DOE), Office of Energy Efficiency and Renewable Energy, targets for electrocatalysts using in transportation purpose [34].

Characteristic	Units	2005 Status		Stack Targets	
		Cell	Stack	2010	2015
Cost	$/kW	9	55	5	3
Durability with cycling					
Operating temp ≤ 80°C	Hours	>2,000	~2,000	5,000	5,000
Operating temp > 80°C	Hours	N/A	N/A	2,000	5,000
Electrochemical area loss	%	90	90	<40	<40
Electrocatalyst loss	mV after 100 hours at 1.2V	>30	N/A	<30	<30

To achieve all of the technical goals, the intensively understanding of the degradation mechanism in PEM fuel cell components is needed. All the components have to be individually examined their degradation mechanism and durability accompanying by the function they serve in PEM fuel cell operation.

2.8 Degradation of membrane electrode assembly (MEA)

Membrane electrode assembly is the key component of PEM fuel cells where the electrochemical reactions, which are hydrogen oxidation reaction (HOR) and oxygen reduction reaction (ORR), take place to generate the electricity. However, the other unfavorable side reactions also occur and restrict the fuel cell lifetime. These reactions are [34]

i. The dissolution and re- deposition of Pt ion on the other Pt particles;
ii. The dissolution and diffusion into the membrane to develop Pt band;
iii. The corrosion of carbon support at high potential resulting in the agglomeration of Pt;
iv. The formation of harmful chemical to membrane for example hydrogen peroxide (H_2O_2), hydrogen peroxyl radical (•OOH) and hydroxyl radical (•OH); and
v. The reversible and irreversible adsorption of contaminants on the active site of catalyst.

All of these side reactions directly affect the long term performance of fuel cell since they lead to the electrochemical active surface area and activity loss and the increasing of membrane/ionomer resistance and the mass –transport resistance in catalyst layer.

Table 2.6 presents the summary of the contributing factors which result in PEM fuel cell performance loss and the typical examination techniques.

Table 2.6 Summary of the contributing factors for PEM fuel cell performance loss and the typical examination techniques [34].

Type of loss observed	Some possible contributors and typical diagnostic tests		
	Anode diffusion media or catalyst layer	Membrane	Cathode diffusion media or catalyst layer
Catalyst activity Performance loss nearly independent of current density	**Possible causes** • Loss of catalyst area by sintering or dissolution • Contamination by adsorption* **Diagnostics** • Cyclic voltammogram of anode		**Possible causes** • Loss of catalyst area by sintering or dissolution • Contamination by adsorption* • Pt oxide formation* **Diagnostics** • Cyclic voltammogram of cathode • Tafel measurement
Ohmic (ionic or electronic) Performance loss proportional to current density	**Possible causes** • Dryout of ionomer* • Contamination by foreign cations* • Increased contact resistance, intra- or interlayer **Diagnostics** • Electrochemical H_2 pump • Current interrupt • Impedance measurement plus model	**Possible causes** • Dryout of membrane* • Contamination by foreign cations* **Diagnostics** • Impedance measurement of ionic resistance • Electrochemical H_2 pump • Current interrupt	**Possible causes** • Dryout of ionomer* • Contamination by foreign cations* • Increased contact resistance, intra- or interlayer **Diagnostics** • Electrochemical H_2 pump • Current interrupt • Impedance measurement plus mode

Table 2.6 *(cont.)*

Type of loss observed	Some possible contributors and typical diagnostic tests		
	Anode diffusion media or catalyst layer	Membrane	Cathode diffusion media or catalyst layer
Reactant mass transfer Performance loss exponential with current density	**Possible causes** • Flooding of diffusion media or catalyst layer* • Reactant channel blockage* • Carbon oxidation **Diagnostics** • Voltage gain, H_2 vs. dilute H_2 • Compare H_2/N_2 with H_2/He • Voltage vs. H_2 utilization • Reactant pressure drop • Impedance measurement plus model		**Possible causes** • Flooding of diffusion media or catalyst layer* • Reactant channel blockage* • Carbon oxidation **Diagnostics** • Voltage gain, O_2 vs. air • Dilute O_2 IV curve • H_2/O_2 IV curve • Voltage vs. O_2 utilization • H_2/Helox IV curve • Reactant pressure drop • Impedance measurement plus model

**Often substantially reversible.*

As shown in Table 2.6, there are many possible factors that initiate the performance loss in PEM fuel cell operation. Hence, the study of performance loss of PEM fuel cell in various operating conditions and the factors that affect the catalyst stability are extensively considered.

In the work of Ornelas et al. [35], the preliminary screening of the Pt supported on the different commercial carbon support catalysts was done. Four accelerated methods were nominated for identifying the stability which were; (i) half – cell operation at high potential in oxygen atmosphere for a week, (ii) potential cycling between 0.6 and 1.2 V/RHE for investigating the sintering of Pt, (iii) half – cell operating at a constant 1.2 V/RHE for 24 h to examine the carbon corrosion and (iv) the investigation of performance alteration resulting from the operation of catalyst at 130^{o}C, 24 h. The gas – diffusion electrode, the Pt – grid and a saturated Hg/$HgSO_4$ were served as working, counter and reference electrode, respectively. The result showed that Pt sintering occurred in every carbon supported Pt catalysts in potential cycling test. The increasing in particle size resulted in the 50% decreasing of electrochemical active surface area (ECSA) and also loss of catalyst activity. The corrosion test for carbon supports revealed that the loss of ECSA was smaller comparing to the result of Pt corrosion test.

The influence of PEM fuel cell operating temperature on the degeneration of Pt/C cathode catalyst was demonstrated in the work of Bi and Fuller. The 25 cm^2 PEM single cell was assembled with commercial MEA and moistened at open circuit potential, 80^{o}C for 2 h. Then, this cell was continually operated at 50, 200, 500, 800 and 1,000 mA/cm^2 for 1 h at each current density with 100% relative humidity. After completing all conditions, the potential cycling test was applied with a square wave between 0.87 and 1.2V/RHE and a time step for each potential was 30s.The cycling test was continued until complete 7000 cycles. The effect of operating temperature was observed during the potential cycling by varying cell temperature to 40^{o}C, 60^{o}C and 80^{o}C, respectively with a different MEA at each temperature. The fuel and oxidizing reactant used in this study were ultrapure hydrogen gas and air. The result revealed that the higher operating temperature, the

more speed up of the decreasing rate of the cell performance and the ECSA. At 80^{o}C operating temperature, the severe undergoing of carbon corrosion was observed in the MEA and the Pt strip was also found in the membrane [36].

For core – shell structure catalyst, the difference in core material and core size were correspondingly affected the durability of catalyst. Inaba et al. [37], investigated the stability of Pd_{core} - Pt_{shell}/C and Au_{core} – Pt_{shell}/C catalysts. Both core – shell catalysts were prepared by the under potential deposition (UPD) of Cu method. The durability test was performed in 0.1M $HClO_4$ solution using catalyst loaded glassy carbon disc, Pt wire and the RHE as a working, counter and reference electrode, respectively. In this test, the square – wave potential cycling was applied between 0.6 V (3 s) and 1 V (3 s) at 60^{o}C and observed the reducing of the ECSA. The result showed that, for catalyst using Au as a core material, smaller core size provides the higher durability. While Pd core material, the higher durability came from the larger core size.

Not only metal but some of conducting polymers were chosen as an alternative for shell material and the investigation of the catalyst stability was done as well. The electrocatalyst Pt/C – polyaniline (PANI) core – shell catalyst was synthesized by direct polymerization of PANI layer on the carbon supported Pt catalyst. In this case, a thin PANI layer favorably adsorbed on the carbon surface via π - π conjugation of PANI and the carbon support. The result revealed that the PANI shell layer could protect the surface of carbon support from the acidic environment. The improvement of ORR activity and stability of Pt/C – PANI core – shell catalyst was on account of the weak adsorption of oxygenated species on a surface of Pt. In addition, the increasing of ORR activity intensely depended on the PANI shell thickness. The durability study was conducted by accelerated stress tests (AST) in a single cell for 5,000 cycles. After finishing the AST test, the current density at 0.6V of Pt/C-PANI catalyst decreased only 24% while 86% decreasing of current density was observed in Pt/C [38].

A catalyst support is also the one of the key components that influences the stability of catalyst. At high potential, the corrosion of the carbon support occurs and results in the detachment of Pt particles and loss of electrochemical active surface area (EAS). Many efforts are made to investigate the novel enduring catalyst support in PEM fuel cell operating environment. Titanium dioxide (TiO_2) is one of the choices because of its stability in acidic and oxidative environments and good mechanical resistance. The stability study of TiO_2 as a catalyst support was done by Huang et al. [39]. $PtPd/TiO_2$ catalyst with 60 wt% metal loading was synthesized by chemical reduction method. The accelerated durability test (ADT) using half – cell condition was employed for investigating the catalyst stability and durability. The test condition was continued cycling between 0.6 - 1.4 V in 0.5M H_2SO_4 for 1500 cycles at 50 mV/s scan rate. The ADT investigation for Pt/TiO_2 and Pt/C were also made for comparison. The results revealed that ORR activity at 0.85V of the $PtPd/TiO_2$ ($3.05mA/cm^2$) catalyst was similar to Pt/C ($3.18\ mA/cm^2$) and higher than that of Pt/TiO_2 ($2.30mA/cm^2$). After 1500 cycles of ADT testing, Pt/TiO_2 and $PtPd/TiO_2$ gave the smaller loss in EAS (40% and 50% loss, respectively) while 95% of EAS loss was observed in Pt/C. Moreover, the $PtPd/TiO_2$ showed the higher ORR activity ($1.79\ mA/cm^2$) than Pt/C ($0.44\ mA/cm^2$) after ADT testing. These results indicated that using TiO_2 as a catalyst support could improve the stability and durability of the cathode catalyst.

Apart from searching the promising catalyst support, the modification of conventional carbon support properties for more enduring in the PEM fuel cell environment is in demand. Chen et al. [40] studied the stability of N – doped carbon nanotubes (CNTs) supported Pt catalyst. The ethylene glycol reduction method was used to synthesize Pt/ N-doped CNTs with 30wt% metal loading. To evaluate the stability of the modified catalyst support, the accelerated durability test (ADT) was performed. The test condition was repeatedly cycled in the potential range of 0.6 – 1.2V for 4,000 cycles. with 50mV/s scanning rate. The 0.5M H_2SO_4 electrolyte was saturated with O_2. The results showed that the electrochemical active surface area (EAS) and the stability of Pt/ N- doped CNTs supported catalyst was increased. Compare to the conventional Pt/C catalyst, after 4000 cycles of ADT test, the EAS of

Pt/C catalyst was only 4.6% from the initial value while the EAS of Pt/N-doped CNTs catalyst was 42.5% remain from the beginning.

However, for preliminary evaluation the catalyst durability, the short period durability test for catalyst study usually conducts in half-cell experiment. Many methodologies were proposed in order to receive the informative durability data of the promising catalysts and the examples were summarized in Table 2.7.

Table 2.7 The examples of short period durability test for electrocatalyst conducting with half – cell experiment (three-electrode configuration)

catalyst	Short period durability test				reference
	Electrochemical method	Testing solution	Testing condition	Indication	
Pt/C	Potential cycling by cyclic voltammetry	0.5M H_2SO_4 with exposed to air, 25^oC	Held at 0.45 V for 60 s then potential cycling at (a) 0.0–1.0 V/SHE (b) 0.0–1.4 V/SHE 300 cycles and 100 mV/s	Change in ESA and the total of dissolved Pt nanoparticles	[41]
Pt/CNT_s	Potential cycling by cyclic voltammetry	O_2 saturated 0.5M H_2SO_4 , 25^oC	Potential cycling at 0.6 – 1.2 V/SHE, 4000 cycles and 50 mV/s	Change in ESA at every 1000 cycles by full-scale cyclic voltammetry at 0.05 and 1.2 V/SHE in N_2 saturated 0.5 M H_2SO_4	[40]
Pt and Pt-Ni/C	Potential cycling by cyclic voltammetry	O_2 – free 0.5M H_2SO_4	Potential cycling at 0.5 – 1.0 V/RHE, 1000 cycles and 20 mV/s	The steady state current density by chronoamperometry test at 0.8V/RHE for 3600 s.	[42]

Table 2.7 *(cont.)*

catalyst	Short period durability test				reference
	Electrochemical method	Testing solution	Testing condition	Indication	
Pt-Pd/C	Potential cycling test by cyclic voltammetry	N_2 saturated 0.5M H_2SO_4	Potential cycling at 0.6 V - 1.2 V/SHE, 500 cycles and 50 mV/s	Change in ESA at every 100 cycles	[43]
Pt-Co/C	Chronoamperometry	O_2 saturated 0.5M H_2SO_4	at the constant potential of 0.6 V/SCE for 20h	Change in ORR reduction current	[44]

.

CHAPTER III

EXPERIMENTAL AND CHARACTERIZATION

3.1 Materials

Chemicals for catalyst synthesis

Nickel (II) acetate ($Ni(Ac)_2$, Carlo Erba), Sodium hydroxide (NaOH, Carlo Erba), Oleic acid (Panreac), Polyvinylpyrrolidone (PVP with average mw ~ 10,000 , Aldrich), 1,2 propanediol (1,2 PDO, Unilab), Sodium borohydride ($NaBH_4$, Labchem) , Hexachloroplatinic acid (H_2PtCl_6, Fluka), Ruthenium chloride ($RuCl_3$, Aldrich), Ethanol (C_2H_5OH, Merck) and Carbon powder (Vulcan® XC-72, Cabot), Air (Zero grade , Praxair) .

Chemicals for fabricating MEA and MEA performance test

Deionized water, Sulfuric acid (98% H_2SO_4, QReC), Nitric acid (65% HNO_3, QReC), Hydrogen peroxide (30% H_2O_2, Carlo Erba), Polytetrafluoroethane (PTFE; 60 wt%, Aldrich), 2 – propanol (Fisher scientific), 1,2 dimethylether (DME, Fluka), Nafion® perfluorinated resin solution (5wt% in lower aliphatic alcohols and water, Aldrich), Nafion® 115 membrane (Electrochem), carbon cloth (E –TEK), Hydrogen gas (99.999% H_2, Praxair), Oxygen gas (99.999% O_2, Praxair), Nitrogen gas (99.99% N_2, Praxair)

3.2 Laboratory instruments

3.2.1 Hot plate and stirrer (Ceramag midi, IKA)

3.2.2 Spray gun (GP-50, Sparmax)

3.2.3 Oven (UFB 500 , Memmert)

3.2.4 Vacuum Oven (VD23, Binder)

3.2.5 Ultrasonic water bath (NXPC-1505P, Koda)

3.2.6 Shaker water bath (SBD-50, Heto)

3.2.7 Centrifuge (Handi-spin 15k, Seward)

3.2.8 Cylinder Furnace with temperature control (In – house fabrication)

3.2.9 Compression mould (model LP20, Labtech engineering)

3.2.10 PEM single cell hardware (working area 5 cm^2, Electrochem)

3.3 Catalyst preparation

3.3.1 Preparation of acid – treated carbon support

Before using Vulcan XC-72 (herein Vulcan) as a carbon support for the synthetic catalysts, Vulcan was treated to remove all impurities. The treatment solution was prepared from the mixing of 12 M. H_2SO_4 and 12 M. HNO_3 with the volume ratio of 1:1. Then a certain amount of Vulcan was added with the mixed acid solution in the closed container which the ratio 70:30 by volume of the carbon to the mixed acid solution. Then, the mixed acid – Vulcan was shaken for 8 h and kept in a chemical fume hood with unfold to the atmosphere until completed 24 h from adding of mixed acid solution. The treated Vulcan was separated by filtration and washed several times with deionized water until the pH of the washing water was neutral. The filtrated Vulcan was dried overnight at 120^oC and ready to use.

3.3.2 Synthesis of the carbon supported Ni_{core} – Pt_{shell} catalyst with conventional method

Core – shell catalysts in section 3.3.2 and 3.3.3 were prepared following the condition shown in the Table 3.1

Table 3.1 The synthesis condition for carbon supported $Ni_{core} – Pt_{shell}$ catalyst

Parameter	Condition
weight ratio of Ni precursor : stabilizer	1:5
Atomic ratio of Ni : Pt	2:1
Weight ratio of active metal : catalyst support	20 : 80

To obtain the core – shell structure catalyst with conventional chemical reduction method, the step by step reduction was introduced to the synthesis. In this research, deionized water was used as a solvent and the reaction temperature was set to 60^{o}C. Firstly, 0.0747 g nickel (II) acetate, 0.6 g NaOH and 0.374 g PVP were dissolved in 50 ml of deionized water in a 250 ml three – neck round bottom flask. Then the solution was kept stirring under the N_2 atmosphere for 30 min. Later, 10 ml of 0.2 M $NaBH_4$ solution was added drop by drop into the reaction flask and continually stirred for 1 h to generate the Ni core nanoparticles. Next, the formation of Pt shell was allowed by adding 3.102 ml of 0.0195M H_2PtCl_6 (in deionized water) solution and following by 10 ml of 0.2 M $NaBH_4$ (in deionized water) solution to set off the reduction of Pt NPs on the surface of Ni core NPs. Finally, 0.1176 g of the treated Vulcan was totally added into the reaction flask under the vigorous stirring. The desired catalyst powder was separated by centrifugation and washed with deionzied water several times until observed the clear washing solution. Then, the catalyst was dried in a vacuum oven at 100^{o}C for 3 h.

3.3.3 Synthesis of the carbon supported $Ni_{core} – Pt_{shell}$ catalyst with a partial support of polyol method (denoted as modified polyol method)

The partial support of polyol method was modified to synthesize a core – shell structure catalyst as described elsewhere [45]. Concisely, 0.0747g nickel (II) acetate, 0.6 g NaOH and 0.374 g PVP (or 0.42ml in case of using Oleic acid stabilizer) was dissolved in 50 ml of 1,2 PDO in a 250 ml three – neck round bottom flask. The solution was then heated to 118^{o}C and kept at 118^{o}C for 20 min. Next, the solution was heated to 138^{o}C under a N_2 atmosphere. Subsequently, 10 ml of 0.2 M $NaBH_4$ (in 1,2 PDO) solution was added into the reaction flask and continually stirred for 1 h to allow the formation of Ni core NPs. Next 3.102 ml of 0.0195 M H_2PtCl_6 (in 1,2 PDO) solution was gradually added to the reaction solution and stirred for 1 h to allow the complete reduction of Pt particles on the Ni core nanoparticles surface. Finally, 0.1776 g Vulcan was added under vigorous stirring. The preferred catalyst powder was separated by centrifugation and washed with ethanol several times until observing the clear washing solution. Then, the catalyst was dried in a vacuum oven at 70^{o}C for 3 h.

3.3.4 The carbon supported Ni_{core} – $PtRu_{shell}$ catalyst synthesis with faced – centered central composite 2^4 experimental design

The carbon supported Ni_{core} – $PtRu_{shell}$ catalysts were synthesized via a modified polyol method as described in section 3.3.3 using PVP as a stabilizer. The interesting parameters that might affect the properties of the obtained catalyst were selected including the atomic ratio of platinum to ruthenium, the mole ratio of Ni precursor (Nickel acetate) to stabilizer (PVP), the reducing temperature and the reduction time in the step of PtRu alloy shell formation. The faced – centered central composite 2^4 experimental design was introduced to this experiment to screen some significant parameters and achieve the optimal condition. The two levels and the center point for each parameter were summarized in Table 3.2 as a condition for catalyst synthesis.

Table 3.2 The experiment conditions for FCC - 2^4 experimental design of the carbon supported Ni_{core} – $PtRu_{shell}$ catalyst synthesis via a modified polyol method[*,**].

Experimental Number	Parameter (coded value)			
	A	**B**	**C**	**D**
1	1:0.5 (-)	1:1 (-)	138 (-)	60 (-)
2	1:1 (+)	1:1 (-)	138 (-)	60 (-)
3	1:0.5 (-)	10:1 (+)	138 (-)	60 (-)
4	1:1 (+)	10:1 (+)	138 (-)	60 (-)
5	1:0.5 (-)	1:1 (-)	180 (+)	60 (-)
6	1:1 (+)	1:1 (-)	180 (+)	60 (-)
7	1:0.5 (-)	10:1 (+)	180 (+)	60 (-)
8	1:1 (+)	10:1 (+)	180 (+)	60 (-)
9	1:0.5 (-)	1:1 (-)	138 (-)	180 (+)

Table 3.2 *(cont.)*

Experimental Number	Parameter (coded value)			
	A	**B**	**C**	**D**
10	1:1 (+)	1:1 (-)	138 (-)	180 (+)
11	1:0.5 (-)	10:1 (+)	138 (-)	180 (+)
12	1:1 (+)	10:1 (+)	138 (-)	180 (+)
13	1:0.5 (-)	1:1 (-)	180 (+)	180 (+)
14	1:1 (+)	1:1 (-)	180 (+)	180 (+)
15	1:0.5 (-)	10:1 (+)	180 (+)	180 (+)
16	1:1 (+)	10:1 (+)	180 (+)	180 (+)
17	1:1 (+)	5:1 (0)	159 (0)	120 (0)
18	1:0.5 (-)	5:1 (0)	159 (0)	120 (0)
19	1:0.75 (0)	10:1 (+)	159 (0)	120 (0)

Table 3.2 *(cont.)*

Experimental Number	Parameter (coded value)			
	A	**B**	**C**	**D**
20	1:0.75 (0)	1:1 (-)	159 (0)	120 (0)
21	1:0.75 (0)	5:1 (0)	180 (+)	120 (0)
22	1:0.75 (0)	5:1 (0)	138 (-)	120 (0)
23	1:0.75 (0)	5:1 (0)	159 (0)	180 (+)
24	1:0.75 (0)	5:1 (0)	159 (0)	60 (-)
25	1:0.75 (0)	5:1 (0)	159 (0)	120 (0)

***** A: the atomic ratio of platinum to ruthenium, B: the mole ratio of Ni precursor to the stabilizer, C: the reduction temperature (^{o}C) and D: the reduction time (min) for the formation of PtRu shell step.

** (+) sign, (-) sign, and (0) were denoted as the coded value of the high value, the low value and the medium point of the studied parameters, respectively.

All the 25 experiments were randomly conducted and replicated. The electrochemical active surface area (EAS) was observed as the response. And all of responses were statistically analyzed by Design Expert program.

3.3.5 Catalyst preparation for studying the heat – treated Ni nanoparticles as a core metal (Chapter V)

3.3.5.1 Synthesis of the carbon supported Ni nanoparticles

In this section, the carbon supported Ni nanoparticles were synthesized following the procedure described in section 3.3.3 with 3 wt% Ni loading on carbon support. But after finishing the reduction of Ni nanoparticle, the acid treated carbon support was added immediately under vigorous stirring instead of Pt precursor. The separation of carbon supported Ni powder was done by centrifugation. Finally, this powder was washed with ethanol for several times and dried at 70^{o}C for 3 h under the vacuum condition.

3.3.5.2 The heat treatment of Ni core nanoparticles [46].

After finishing the synthesis, the carbon supported Ni nanoparticles were heated at 300^{o}C for 3 h under the air condition following by 300^{o}C for 1 h under H_2 atmosphere. Then the sample was cool down naturally before collecting.

3.3.5.3 Synthesis of the carbon supported Ni_{core} – Pt_{shell} catalyst by applying Pt shell on the heat – treated Ni/C nanoparticles with modified polyol method.

Using the polyol method to prepare the Pt layer on the heat – treated Ni/C nanoparticles, the procedure was similar to section 3.3.3 which will be described next. 0.5 g of carbon supported Ni nanoparticles after heat treatment were dispersed in 20 ml 1,2 PDO for 30 min in a 250 ml three – neck round bottom flask under the vigorous stirring. Then, the mixing solution was heated to 118^{o}C and the solution of 0.6 g of NaOH in 20 ml 1,2 PDO was added and keep stirring for 30 min. After that, the calculated amount of 0.0195 M H_2PtCl_6 (in 1,2 PDO) solution was gradually added into the reaction solution and constantly stirred for 1 h. After separating the powder catalyst by centrifugation, the catalyst was washed with ethanol for several times and dried in a vacuum oven at 70^{o}C for 3 h.

3.3.5.4 Synthesis of the carbon supported Ni_{core} – $PtRu_{shell}$ catalyst by applying PtRu shell on the heat – treated Ni core nanoparticles with sodium borohydride ($NaBH_4$) reducing agent [47].

In this section, Ni_{core} – $PtRu_{shell}$/C was prepared following the condition in Table 3.3. 0.5 g of carbon supported Ni nanoparticles after heat treatment was dispersed in the mixed solution of 2.5 ml 2 - propanol and 2.5 ml deionized water by ultrasonication for 20 min. Then, the calculated amount of the mixed solution of 0.0195 M H_2PtCl_6 and 0.015 M $RuCl_3$ was added and continuously ultrasonicated for 30 min. After that, the pH of solution was adjusted approximately to 9 by 0.5 M NaOH solution. The reduction of Pt – Ru alloy was initiated by gradual adding 0.15 M $NaBH_4$ solution under continuing ultrasonication at 70^{o}C for 2h. After collecting the catalyst powder by centrifugation and washing with deionized water for several times, the catalyst was dried at 110^{o}C for 20 h.

Table 3.3 The synthesis condition for carbon supported Ni_{core} – Pt_{shell} catalyst

Parameter	Condition
weight ratio of Ni precursor : stabilizer	1:5
Atomic ratio of Ni : PtRu	1:10
Atomic ratio of Pt : Ru	1:0.5
Weight ratio of active metal : catalyst support	20 : 80

3.4 MEA preparation

3.4.1 Membrane treatment

Nafion® 115 membrane (herein membrane) was used in this work with pretreatment as the following steps in the shaker water bath at 80°C. Firstly, the membrane was soaked in a beaker of 0.03 wt% of H_2O_2 solution for 1 h. Then, the membrane was washed and soaked in DI water for 1 h. Next, the membrane was soaked in 0.5 M H_2SO_4 for 1 h. After that the membrane was washed and soaked in DI water for 1 h and repeated this step for more 2 times to ensure the cleaning process. The pretreated membrane was finally kept in a DI water container.

3.4.2 Preparation of the gas diffusion layer

The carbon ink for preparing the diffusion layer was prepared by mixing 1 ml of de-ionized water and 2.668 μl of polytetrafluoroethane (PTFE; 60 wt%, Aldrich), and then sonicated for 30 min at room temperature. Next, 2 ml of 2 – propanol (Fisher scientific) was added to the mixed solution and sonicated for 30 min following by the addition of 0.038 g of acid – treated carbon black (Vulcan® XC-72). The mixed suspension was continually sonicated for 2 h to attain the carbon ink, which was then coated on a 5 cm^2 carbon cloth (E –TEK) by brushing and drying at 70°C for 3 min to remove the excess solvent. The brushing-drying step was repeated as above until the theoretical loading of carbon black on the carbon cloth was 2 mg/cm^2. Then, the brushed carbon cloth was dried at 300°C for 1 h to finish the preparation of the diffusion layer.

3.4.3 Preparation of catalyst layer and MEA assembly

In order to prepare the catalyst layer for the electrochemical characterization, the catalyst ink was prepared by mixing 0.125 g of the catalyst in 2 ml of 1,2 dimethylether and ultrasonicated for 30 min. After that, 0.142 ml of Nafion solution was added and the ink was continually ultrasonicated for 2 h. The catalyst layer was created by directly spraying on the prepared gas diffusion layer

using a spray gun until the complete the calculated metal loading level. The obtained electrocatalyst layer was then dried at 80 ^{o}C for 30 min before used.

To prepare a 5 cm^2 MEA for PEM single cell performance test, The catalyst layer and the catalyst ink were prepared as described below.

For catalyst ink, 0.1 g of catalyst was mixed with 0.4 g deionized water. Then 0.8 g of Nafion solution was added following by adding 1.2 g 2-propanol. After that, the mixing solution was 3 min ultrasonicated and 5 min stirred under the ice condition. The step of ultrasonication following by stirring was repeated for 5 cycles and keeping stirring until using. Catalyst coated membrane (CCM) technique was introduced to made catalyst layer. To make the 5 cm^2 active area, the Nafion® 115 membrane was stretched in the acrylic frame with leave the space for 5 cm^2 active area. Then, the catalyst ink was directly sprayed using a spray gun on the membrane until the complete the calculated metal loading level and the catalyst coated membrane was dried at 60^{o}C for 1 h.

In order to fabricate the MEA, two pieces of the prepared gas diffusion layer (section 3.4.2) were dropped with 5 μl of Nafion solution at all their corners and assembled on each side of prepared catalyst coated membrane by compression mould. The compressing condition was at 137^{o}C, 65 kg/cm^2, 2.5 min for hot pressing and 2.5 min for cool pressing.

3.5 Catalyst Characterization

3.5.1 Physical characterization

3.5.1.1 Scanning electron microscopy with energy dispersive X-ray spectroscopy (SEM/EDX)

The elements content of the prepared catalyst were measured by the scanning electron microscopy with energy dispersive X – ray on a JEOL JSM – 6400 scanning microscope. And the element mapping was also performed to examine the dispersion of the core metal and the shell metal on a surface carbon support.

3.5.1.2 X – ray diffraction (XRD)

The crystalline structure of the prepared catalyst was characterized by X – ray diffraction technique on a Bruker AXS – D8 Advance machine using Cu Kα radiation. The diffraction patterns were collected between 30^o and 80^o at the scanning rate of 1^o/min.

3.5.1.3 Transmission electron microscopy (TEM)

The morphology and the particle size of the synthetic catalysts particle were investigated by transmission electron microscopy (TEM) on a JEM – 2100F (UHR) transmission electron microscope (ultra high resolution) (at the faculty of engineer, Yonsei university, Seoul, Republic of Korea).

3.5.2 Electrochemical characterization

To measure the electrochemical properties of the prepared catalysts, the three electrode configuration was set with the sprayed synthetic catalyst on a carbon cloth as the working electrode, a Pt grid as the counter electrode and a Ag/AgCl electrode as the reference electrode. All the electrochemical characterizations were carried out by the potentiostat/ galvanostat (AUTOLAB – PG STATO 30) at room temperature.

3.5.2.1 Cyclic voltammetry (CV)

The electrochemical active surface area (EAS) was measured in a N_2 saturated 0.5 M H_2SO_4 solution which used as the electrolyte. The scan potential was varied from 1.2 to -0.54 V vs. Ag/AgCl with a constant sweep rate at 20 mV/s. The voltammogram was reproducible until the 15 scans completed.

In case of examination the durability of the synthetic catalyst, the potential cycling was performed by CV. The voltammogram of working electrode was continueously scanned to complete 1000 scans in the potential range of (-0.54) – 1.0 V vs. Ag/AgCl and 20 mV/s scanning rate.

All data from cyclic voltammogram were processed by GPEs program.

3.5.2.2 Linear sweep voltammogram (LSV)

The activity towards the ORR was measured by a linear sweep voltammogram (LSV) with a rotating disk electrode (RDE). The LSV measurement was conducted in a 0.5 M H_2SO_4 electrolyte with continuous O_2 bubbling and a constant rotating rate of 2000 rpm. The scan potential was varied from 0.8 to (-0.2) V vs. Ag/AgCl at a constant scan rate of 20 mV/s

To examine the electron pathway of the synthetic catalyst, the RDE rotating rate was varied from 500 to 2000 rpm with the scan potential range of 0.8 – (-0.2) V vs. Ag/AgCl at a constant scan rate of 20 mV/s in a saturated O_2 0.5 M H_2SO_4 electrolyte.

3.5.2.3 Chronoamperometry

The activity and stability of synthetic catalysts was evaluated by chronoamperometric technique. This examination was conducted before and after the potential cycling by CV measurement. The working electrode was held over a period of 1 h at a constant potential 0.6 V vs. Ag/AgCl in a saturated O_2 0.5 M H_2SO_4 electrolyte.

3.6 PEM single cell performance test

The assembled MEA and the 5 cm^2 active area PEM single cell hardware (as shown in Figure 3.1) were fabricated with 40 lb_f/in^2 moment torque. The performance test was performed at the PEM fuel cell test station at the atmospheric pressure with 60^oC, 65^oC and 60^oC for cell, anode humidifier and cathode humidifier temperature, respectively. The flow rate of both H_2 and O_2 were 100 sccm. The PEM single cell was break in for 4 h at 0.3 V before evaluating the cell performance. The diagram for PEM single cell test station was given in Figure 3.2.

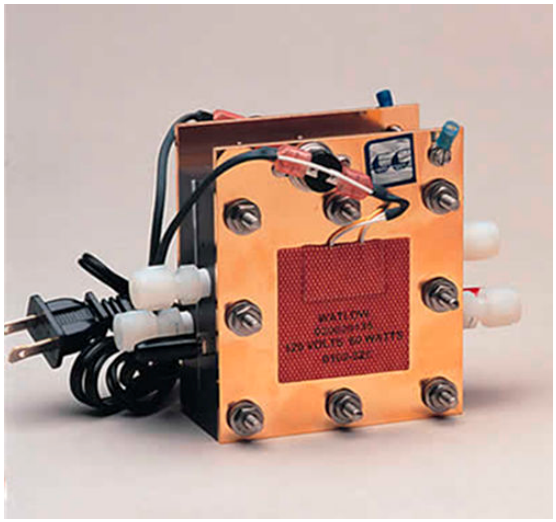

Figure 3.1 PEM single cell hardware for MEA performance test [48].

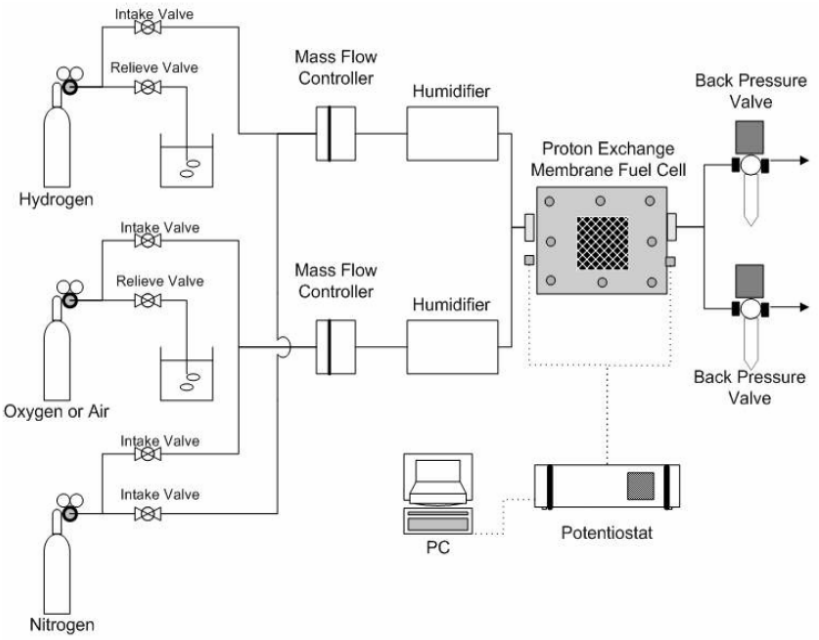

Figure 3.2 The diagram for PEM single cell fuel cell test station [49].

CHAPTER IV

RESULTS AND DISCUSSION

As mentioned in chapter II, the core – shell structure is very attracting because of its novel arrangement and its advantages. In this chapter, the study of the suitable methodology for preparing carbon supported $Ni_{core} - Pt_{shell}$ ($Ni_{core} - Pt_{shell}/C$) catalyst was presented. The parameters that might influence the properties of this prepared catalyst such as type of stabilizer, weight ratio of Ni (core metal) precursor to stabilizer, atomic ratio of Pt to Ru (for generating PtRu alloy shell layer), temperature and time for PtRu shell reduction as prepared by polyol method were counted into the investigation. All the results were discussed respectively.

4.1 The preliminary study of $Ni_{core} - Pt_{shell}/C$ catalyst: comparison of the preparation method

In order to prepare core – shell structure catalyst, the step by step reduction, namely, the reduction of core metal (usually transition metal) first then following by the reduction of shell metal (normally precious metal), was used. However, to obtain the desired properties of the synthetic catalyst, type of metal precursor, reducing agents and the reaction medium should be considered due to their significant effects [50]. In this preliminary study, the synthesis of $Ni_{core} - Pt_{shell}/C$ nanoparticle catalyst was compared between the using $NaBH_4$ as a reducing agent for both steps of core and shell metal (denoted as a conventional method) and the using of a partial support from the polyol method only in the step of Pt shell reduction (denoted as a modified polyol method). The experimental results were shown following.

4.1.1 Physical characterization

To explore the difference in the issue of the solvent using and reducing agent in the step of Pt shell reduction, these two methods, a conventional and a modified polyol method, are definitely different in the reduction temperature. The reaction temperature for a conventional method was approximately 60^{o}C. On the other hand, a modified polyol method needs to proceed the reaction with much higher temperature due to this process required the decomposition of polyol solvent.

Then, to compare the potential of each method, especially in the Pt shell reduction, SEM/EDX technique was introduced to detect the elements content in the catalysts. The EDX spectra presented in Figure 4.1 (a) and Figure 4.1 (b) revealed the element content of $Ni_{core} - Pt_{shell}/C$ catalysts formed with a conventional method and a modified polyol method, respectively. For clearly illustration, the element contents were summarized in Figure 4.2. It could be seen that the atomic ratio of Ni to Pt from modified polyol method was 2.55 which was quite similar to the preset condition. Whereas this ratio from the conventional method was 1.71 which is lower than the preset condition. Because both of preparation methods using the same reducing agent, $NaBH_4$, in the step of Ni reduction, the smaller content of Ni metal appeared in the conventional method may be due to the lower reducing temperature. These might result in the lower kinetic of nickel reduction mechanism [51, 52]. When considering the Pt metal content, it was shown that the modified polyol method had the lower potential in Pt reduction comparing to $NaBH_4$ reducing agent since the smaller amount of Pt metal was found [53].

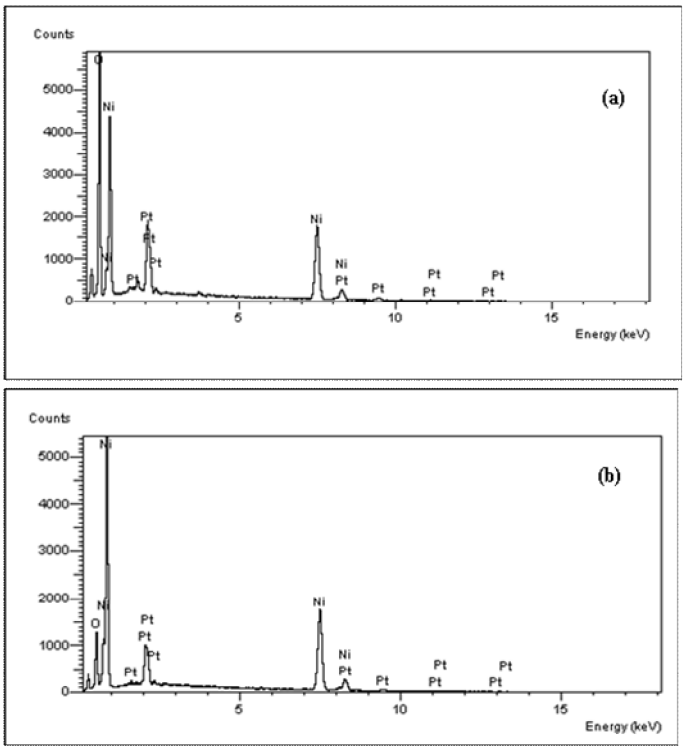

Figure 4.1 SEM/EDX spectra of Ni_{core} – Pt_{shell}/C catalysts synthesized via either (a) conventional method or (b) modified polyol method.

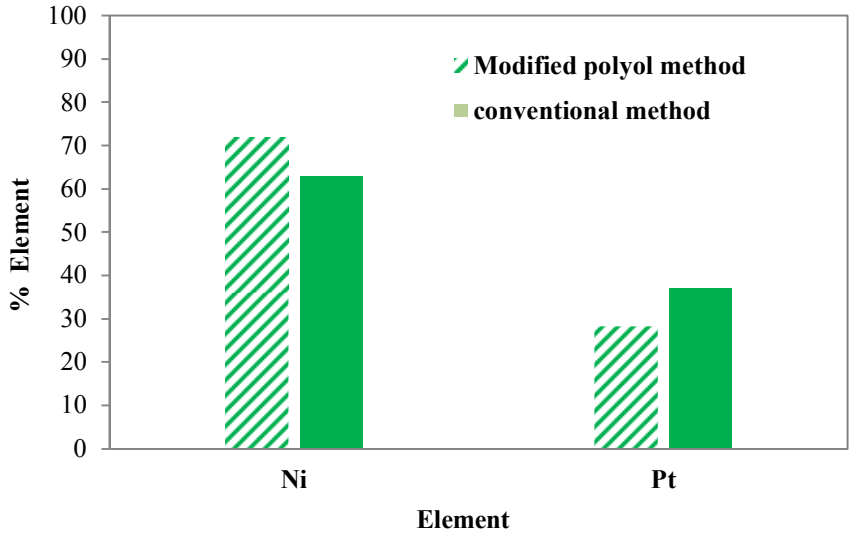

Figure 4.2 The elements content in synthetic Ni_{core} – Pt_{shell}/C catalysts synthesized via either the conventional method or the modified polyol method, as analyzed by SEM/EDX.

When focusing on the dispersion of Pt on Ni the catalyst surface, as verified by EDX mapping technique in Figure 4.3, there was no difference in the dispersion of the Pt on the catalyst surface. However, the dispersion of Ni on surface of a modified polyol method catalyst was observed to be more densely than that of a conventional method catalyst. This result was consistent with the element content shown in Figure 4.2.

To characterize the crystalline structure and the related properties of the synthetic catalysts, XRD technique was chosen to verify the alteration that might occur from the different preparation method. Figure 4.4 showed the XRD patterns of the synthesized $Ni_{core} - Pt_{shell}/C$ catalysts from a conventional method and a modified polyol method in the step of Pt shell formation. It could be seen that the two diffraction patterns were obviously different. For $Ni_{core} - Pt_{shell}/C$ catalysts prepared by a conventional method, with face – centered cubic (FCC) crystalline, the diffraction peak near 39.96, 46.56 and 68.86 quite close to the characteristic peaks of pure crystalline Pt at 2θ values of 39.9 [111], 46.2 [200] and 67.9 [220] [54]. On the other hand, the pattern of $Ni_{core} - Pt_{shell}/C$ catalyst taken from a modified polyol method contained the characteristic peak of Ni at 2θ values of 44.60 [111], 51.28 [Ni 200] and 76.24 [Ni 220] with face – centered cubic (FCC) crystalline [54]. However, from SEM/EDS analysis, there was the evidence of Pt appeared on the surface of synthetic catalyst. It could be suggested that Pt might form a very thin shell layer with amorphous structure at the outer surface of Ni nanoparticle [45].

The average crystallite size and the lattice parameter were calculated from these two patterns corresponding with the Scherer's equations [33] and the Bragg's law [55] (appendix A), respectively and the results were summarized in Table 4.1. As shown in the table, the average crystallite size calculated from the diffraction peak of the plane [200] of a modified polyol method catalyst (4.07 nm) was 1.16–fold larger than that of catalyst particle formed by a conventional method (3.51 nm). The larger crystallite size of the modified polyol catalyst might attribute to the lift of synthesis temperature (~138^{o}C) causing the growth of small nanoparticles to the larger size [51].

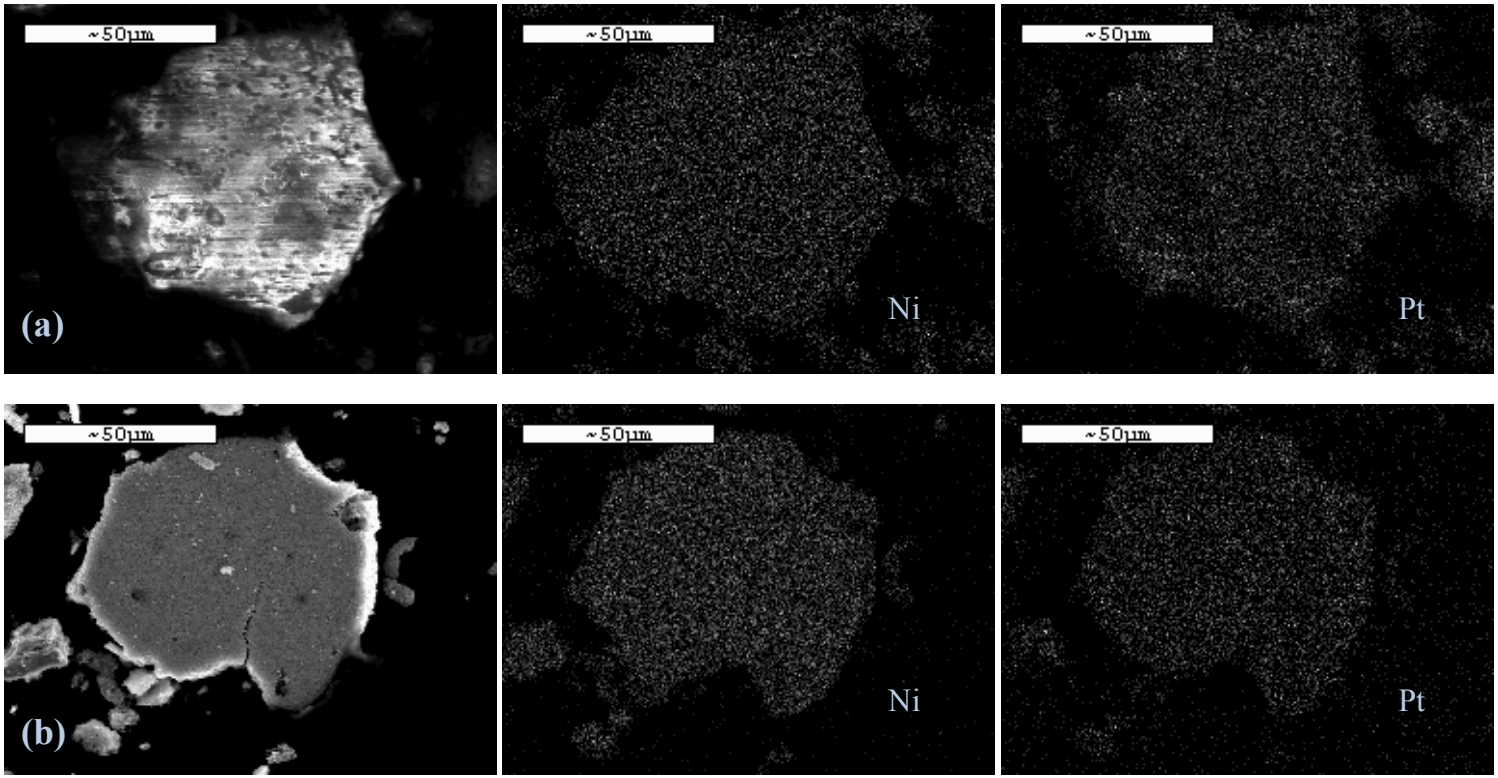

Figure 4.3 SEM/EDX elemental mapping images of the $Ni_{core} – Pt_{shell}/C$ catalysts formed with either (a) conventional method or (b) modified polyol method.

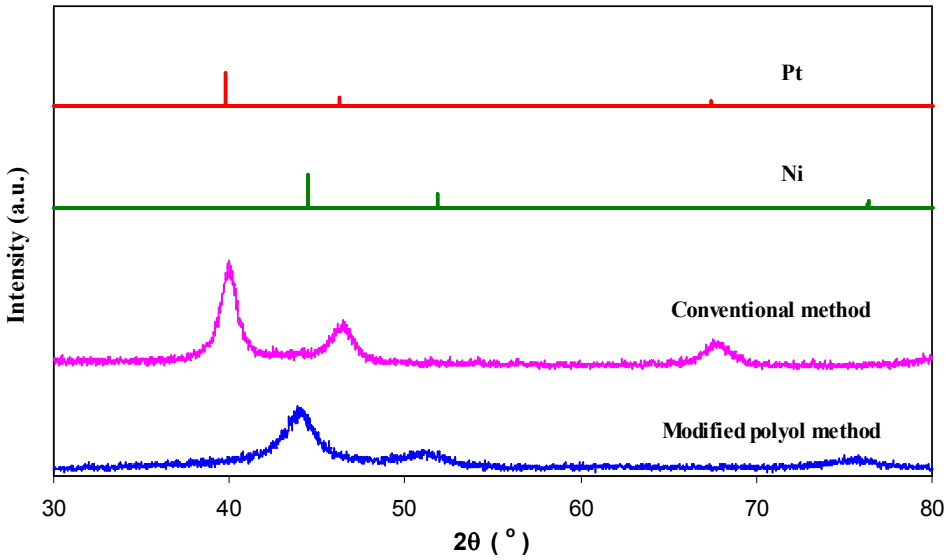

Figure 4.4 XRD patterns of Pt metal, Ni metal and synthetic $Ni_{core} - Pt_{shell}/C$ catalysts prepared by either conventional method or modified polyol method.

Table 4.1 Physical properties of $Ni_{core} - Pt_{shell}/C$ catalysts prepared with different preparation methods

Preparation method	Properties of synthetic $Ni_{core} - Pt_{shell}$ /C catalyst	
	Calculated crystallite size (nm)	Lattice parameter (nm)
Conventional	3.51	0.3979
Modified polyol	4.07	0.3528

The estimated lattice parameter (appendix A) from XRD pattern was revealed that the alloying between nickel and platinum did not occur in these core – shell structure synthetic catalysts. Since the lattice parameter of the modified polyol method catalyst showed the similar value (0.3528 nm) to the reported one of pure nickel metal (0.3520 nm). While the conventional method core – shell catalyst also displayed a slightly higher lattice parameter (0.3979 nm) compared with the reported value of pure platinum metal (0.3920 nm).

4.1.2 Electrochemical characterization

The report of the electrochemical properties of these synthetic Ni_{core} – Pt_{shell}/C catalysts is presented in this section. Since the catalyst is designed to be employed at the cathode area of the PEM fuel cell, the electrochemical active surface area (EAS) and the activity toward the oxygen reduction reaction (ORR) of the catalysts are the key to be determined.

To check the difference of the catalyst surface before and after applying Pt shell, the synthetic Ni_{core} – Pt_{shell}/C with modified polyol method was chosen to be investigated the alteration of electrochemical property before and after applying Pt shell layer. Then, the synthesis of the carbon supported Pt (Pt/C) by polyol method and the carbon supported Ni (Ni/C) with polyol solvent and $NaBH_4$ reducing agent were done for comparison. The experiments were conducted by the cyclic voltammetry in N_2 saturated 0.5 M H_2SO_4 electrolyte and their cyclic voltammograms were shown in Figure 4.5. From this figure, the cyclic voltammogram of Ni/C did not show any adsorption and desorption peak of hydrogen molecule. Only hydrogen evolution and oxygen evolution occurred on the surface of Ni/C [8]. While the cyclic votammograms of both Pt/C and modified polyol method Ni_{core} – Pt_{shell}/C displayed the similarity in the peak positions of hydrogen adsorption/desorption. It could be implied that there was the Pt layer formed on the surface of Ni nanoparticles after applying Pt shell process.

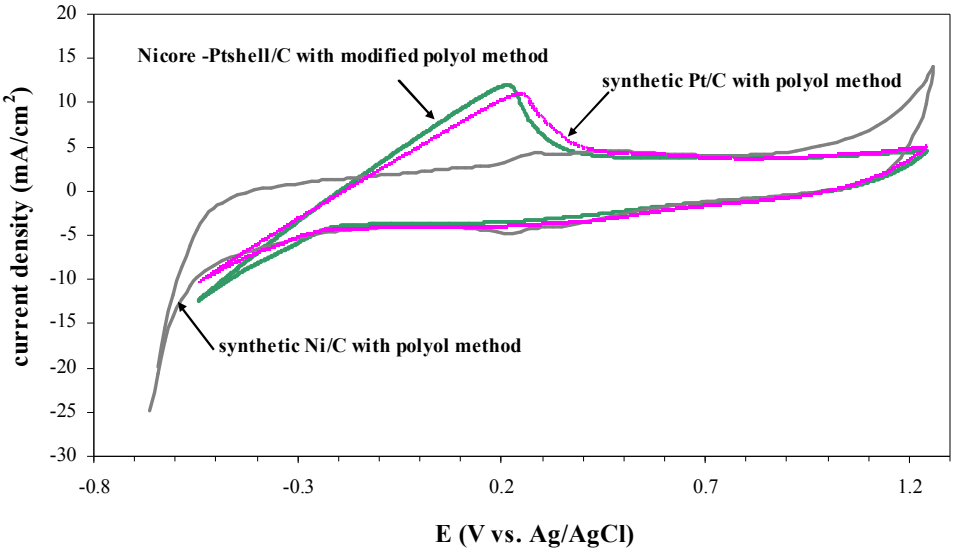

Figure 4.5 Cyclic voltammograms of the Ni_{core} – Pt_{shell}/C catalyst prepared by modified polyol method, synthetic Ni/C and synthetic Pt/C with 0.3 mg metal/cm^2 loading on each electrode, and assayed in a N_2 saturated 0.5 M H_2SO_4 electrolyte, at a scan rate of 20 mV/s and a scan range of (-0.64) – 1.2 V vs. Ag/AgCl.

For the CV measurement of the synthetic Ni_{core} – Pt_{shell}/C with the conventional method and the modified polyol method, the cyclic voltammograms of the synthetic catalysts were shown in figure 4.6 (a) and (b), respectively. When considering the stability within the 10 scans, the coincidence of the entire ten scans was appeared in the case of the modified polyol method catalyst. While in the case of the conventional method catalyst, the shift of voltammogram was observed. This could be clarified with regard to the wetting behavior at the electrode surface and saturation of the Nafion layer that covered the electrocatalyst particle [56].

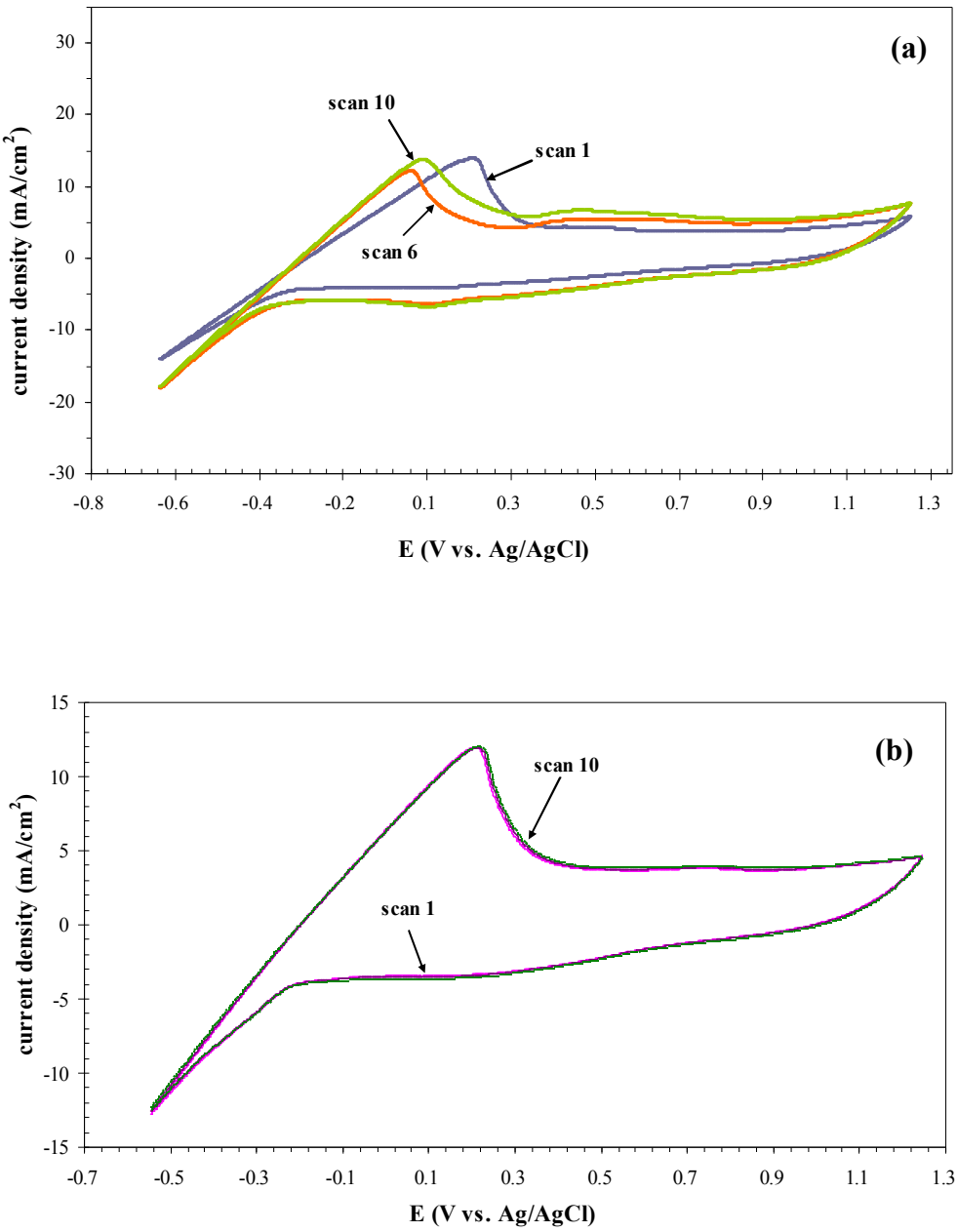

Figure 4.6 Cyclic voltammograms of the $Ni_{core} - Pt_{shell}/C$ catalysts (0.3 mg metal/cm^2 loading) prepared by either (a) conventional method or (b) modified polyol method, and assayed in a N_2 saturated 0.5 M H_2SO_4 electrolyte, at a scan rate of 20 mV/s and a scan range of (-0.54) – 1.2 V vs. Ag/AgCl.

From the cyclic voltammograms, the calculated area under the H_2 desorption peak in terms of coulomb was converted to the EAS (appendix B) and tabulated in Table 4.2. At 10 cycles of scanning, the EAS of the conventional method and the modified polyol method catalysts were 130.2 and 110.9 m^2/g Pt, respectively. These calculating results were in accordance with the calculated crystallite sizes of the respective synthetic catalysts, where the smaller crystallite size offers a higher EAS.

To preliminarily study the behavior of oxygen reduction reaction (ORR) occurring inside the porous catalyst layer, the kinetic parameters such as the exchange current density and the limiting current density were indicated [8]. In this research, the limiting current density was chosen to evaluate the ORR activity of two different preparation methods catalyst. With the aim of receiving the limiting current density, the linear sweep voltammetry in oxygen saturated 0.5M H_sSO_4 was carried out as demonstrated in Figure 4.7.

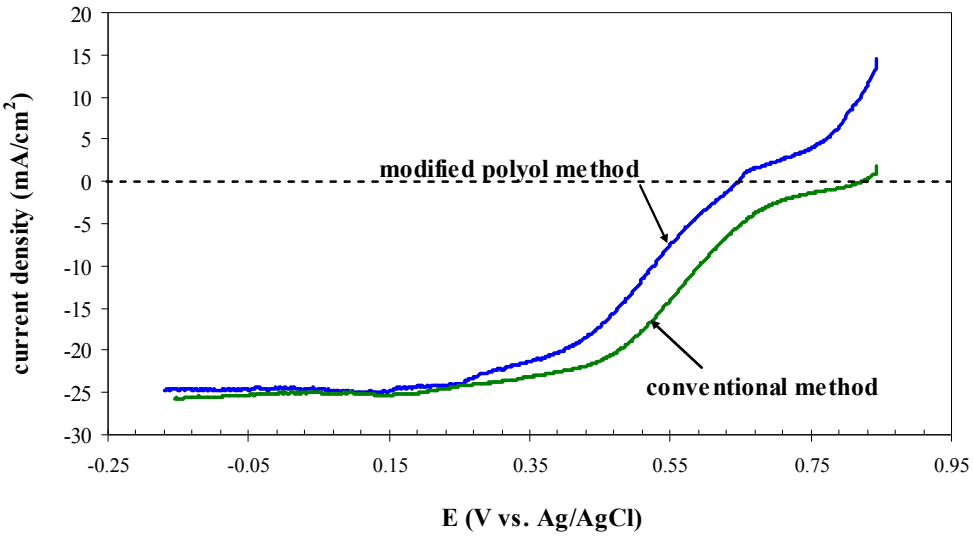

Figure 4.7 Linear sweep voltammogram of the synthetic $Ni_{core} - Pt_{shell}/C$ catalyst synthesized via either conventional method or modified polyol method and assayed in a constant O_2 bubbling 0.5 M H_2SO_4 electrolyte at a rotating rate of 2000 rpm, a scan rate of 20 mV/s and a scan range of (-0.2) – 0.8 V vs. Ag/AgCl.

From this figure, at the low potential range (0.15 to -0.2 V vs. Ag/AgCl) which is considered to be the mass transfer region, the limiting current density was evaluated as shown in Table 4.2. It could be observed that there was a slightly difference of the limiting current density between Ni_{core} – Pt_{shell}/C catalyst synthesized via the conventional method (25.6 mA/cm^2) and modified polyol method (24.5 mA/cm^2). However, when focusing on the onset potential which defined as a potential that the cathodic current (reduction reaction) begins to be observed on the linear voltammetry curve [57], the conventional method catalyst exhibited a slightly positive shift of the onset potential compare to that of the modified polyol method catalyst. It might be noted that the conventional method catalyst provided a catalyst with more favorable in oxygen reduction than the modified polyol method [58].

Table 4.2 Electrochemical properties of Ni_{core} – Pt_{shell} catalysts prepared with different preparation methods.

Preparation method	Properties of synthetic Ni_{core} – Pt_{shell} /C catalyst	
	Electrochemical active surface area (EAS, m^2/g Pt)	Limiting current density (mA/cm^2)
Conventional	130.2	25.6
Modified polyol	110.9	24.5

4.2 Effect of polymer stabilizer on the properties of synthetic $Ni_{core} - Pt_{shell}/C$ catalyst

In the synthesis of metal nanoparticle, to control the particle size, the polymer stabilizers used in the synthesis process has the important role to control the particle size owing to their effect on the growth process of the nanoparticle. Also, the interaction of polymer stabilizer and the metal particle might vary considerably depending on the surface chemistry of metal, the polymer used, the solvent used in the reaction and the reaction temperature [59]. Since, there is the report about the morphology and particle size of the core particle on the properties of synthetic core – shell structure catalyst [37], in this work, type of polymer stabilizer used in the step of nickel core preparation was investigated. Oleic acid and polyvinylpyrrolidone (PVP, mw ~10,000) which being different in the chemical structure (linear chain polymer and linear chain with aromatic branch polymer, respectively) were chosen for this study.

4.2.1 Physical characterization

Figure 4.8 (a) and (b) represent the spectrum of the synthetic $Ni_{core} - Pt_{shell}/C$ with PVP and oleic acid stabilizer, respectively which analyzed by SEM/EDX technique. For explicit illustration, the composition and the quantity of the synthetic $Ni_{core} - Pt_{shell}/C$ with different stabilizers were summarized in Figure 4.9. It could be noted that only $Ni_{core} - Pt_{shell}/C$ with PVP stabilizer gave the atomic ratio of Ni: Pt (2.55:1) close to the nominal ratio (2:1). Also, using different types of the stabilizer might affect the Ni content in the composition of catalyst. The higher amount of Ni could be observed in the catalyst using PVP stabilizer. This might contribute to the PVP monolayer which formed on the surface of Ni nanoparticle after reducing process and prevented further aggregation and the surface oxidation of Ni nanoparticle [21].

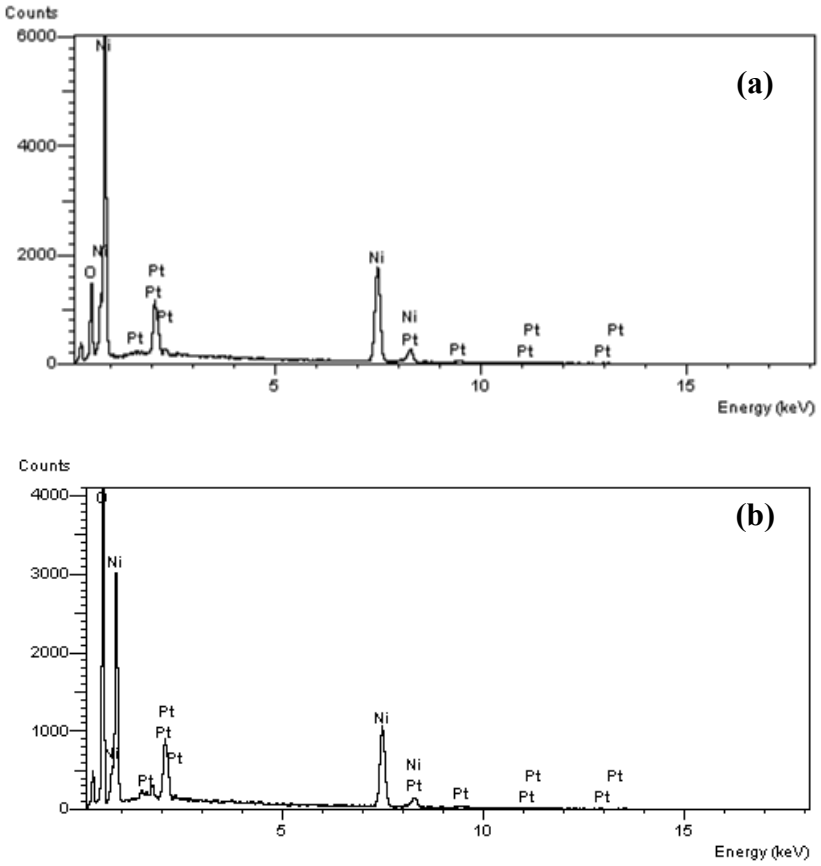

Figure 4.8 SEM/EDX spectrums of Ni_{core} – Pt_{shell} catalysts with (a) PVP and (b) oleic acid stabilizers.

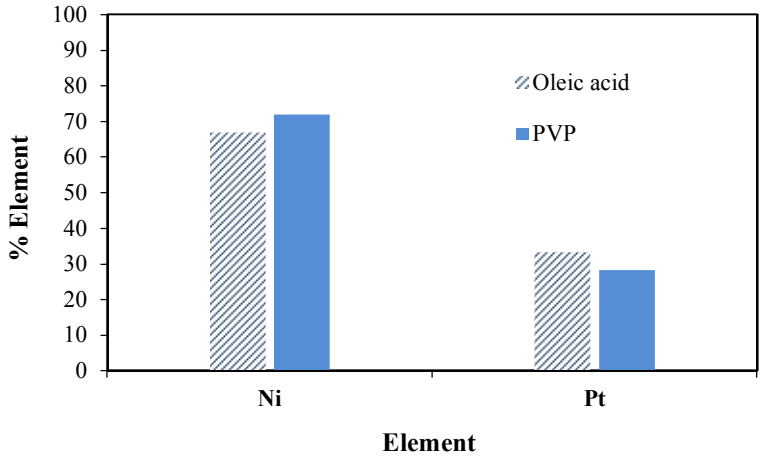

Figure 4.9 The element content in synthetic Ni_{core} – Pt_{shell} catalysts with different stabilizers by SEM/EDX analysis.

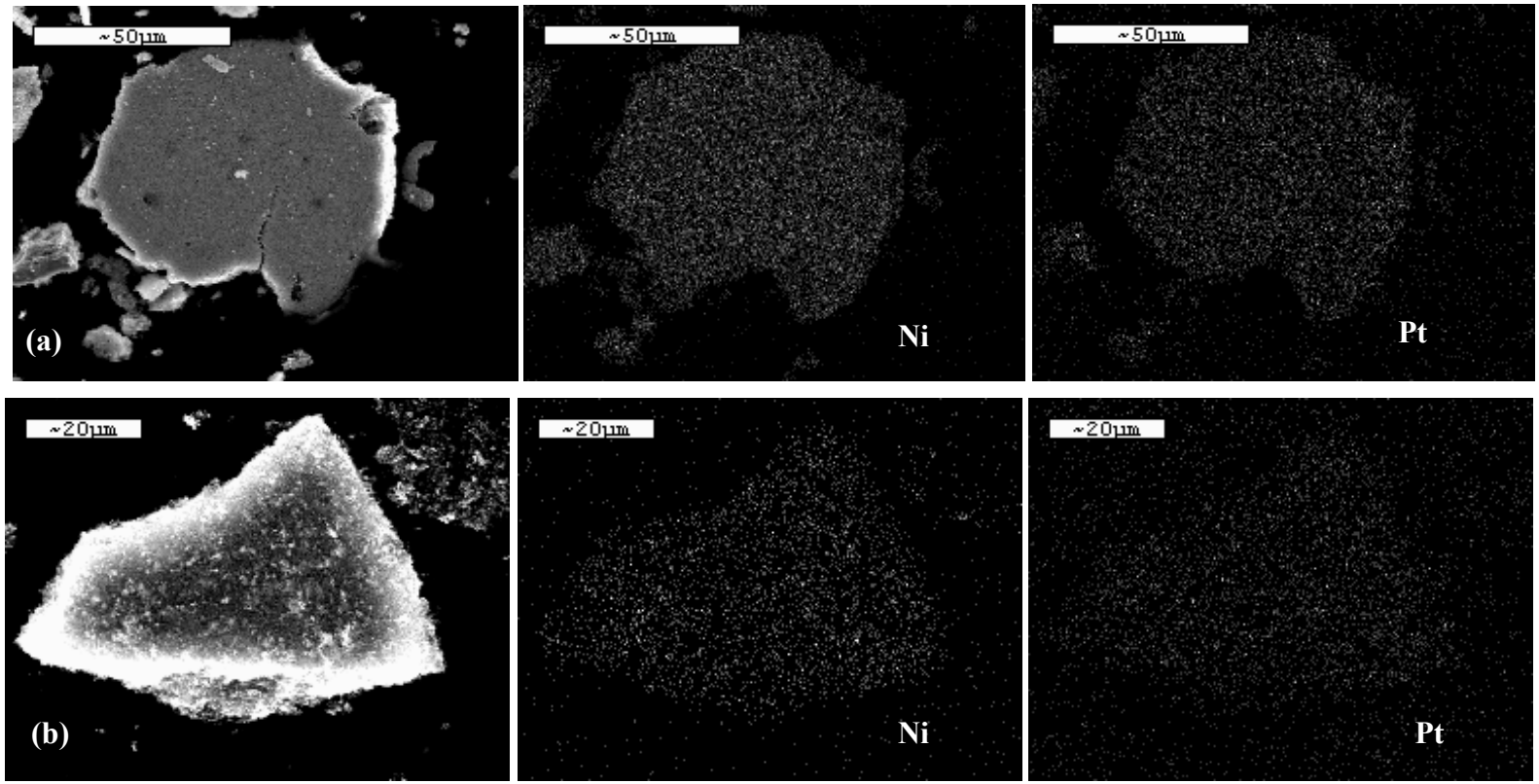

Figure 4.10 SEM/EDX elemental mapping of $Ni_{core} - Pt_{shell}$ catalysts with (a) PVP and (b) oleic acid stabilizers.

From EDX mapping technique as seen in Figure 4.10, the massive dispersion of both Ni and Pt on the surface of $Ni_{core} - Pt_{shell}$ catalysts with PVP was observed. This result was consistent with the element content shown in Figure 4.9. However, the well dispersion of Ni and Pt on the catalyst surface was appeared for catalyst using either PVP or oleic acid stabilizer.

The crystalline structures of the $Ni_{core} - Pt_{shell}$ catalysts with different stabilizer were characterized by XRD technique and the XRD pattern were compared in Figure 4.11. It could be observed that only three main Ni particle characteristic peaks with face – centered cubic (FCC) crystalline appeared in the XRD pattern of $Ni_{core} - Pt_{shell}$ catalysts either with PVP or oleic acid stabilizer. The 2θ values corresponding to [111], [200] and [220] planes, for the catalyst with PVP as the stabilizer, contained 44.60, 51.28 and 76.24, respectively. For that with oleic acid as the stabilizer, the characteristic peak included 44.50, 51.85 and 76.37 correlating with crystalline plane [111], [200] and [220], respectively. Moreover, the crystalline characteristic of Pt at 2θ values of 39.9 [111], 46.2 [200], 67.9 [220] did not show in both mentioned patterns. The alloy formation between Ni and Pt did not occur in this case since there was no shift of the characteristic peak of these synthetic nanoparticles to Pt character. However, the SEM/EDX analysis indicated the presence of Pt particle on the catalyst surface for both formed with PVP and oleic stabilizer. It might be suggested to be owing to the very thin shell layer with an amorphous Pt structure at the surface of Ni nanoparticles and this result conformed to the previous study of $Ni_{core} - Pt_{shell}$ catalyst preparation by the polyol process [45].

The average crystallite size and the lattice parameter of synthetic catalysts can be calculated from the XRD diffraction peaks following the Scherer's equation [33] and the Bragg's law [55] (appendix A), respectively. From the calculating results tabulated in Table 4.3, when using PVP as a stabilizer, the average crystallite size was 4.07 nm which was similar to the reported of Ni nanoparticle preparing by polyol method with PVP stabilizer at the same Ni precursor to PVP ratio [18]. Whereas using oleic acid as a stabilizer inclined to have a larger crystallite size (5.11 nm). This result can be explained by the fact that PVP might have a higher ability to covering the Ni surface than oleic acid and thus, preventing the

agglomeration of the high surface energy nanoparticle by strongly adsorbing on the growth sites. Besides, the thorough covering the Ni nanoparticles surface might occur in the case of using PVP and then hindered the growth of nanoparticles by precluding the diffusion of the new atoms from the surrounding solution to the growing nanoparticle surface [59, 60, 61].

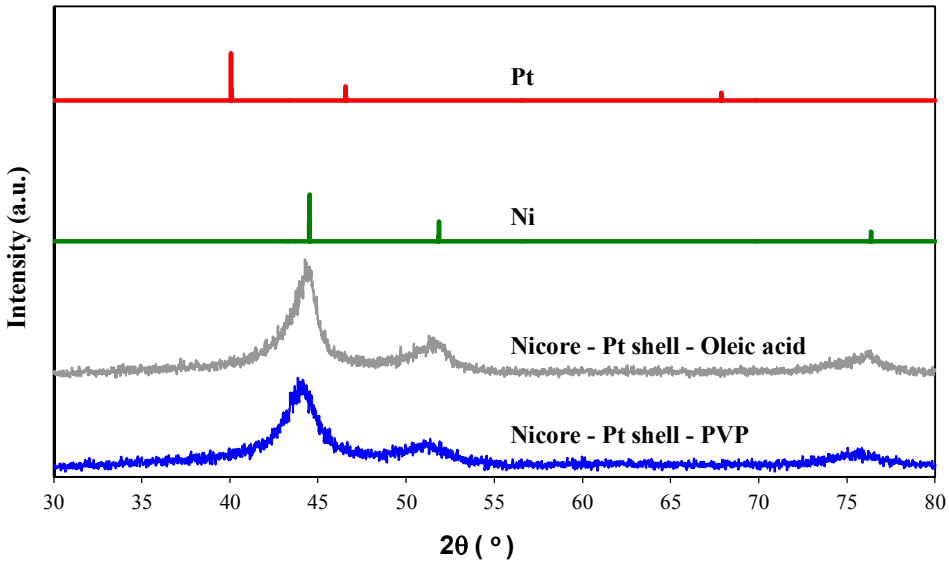

Figure 4.11 X – ray diffraction patterns of synthetic Ni_{core} – Pt_{shell}/C catalysts prepared by using different stabilizers.

Table 4.3 Physical properties of Ni_{core} – Pt_{shell}/C catalysts prepared with different stabilizers.

Stabilizer	Properties of synthetic Ni_{core} – Pt_{shell} /C catalyst	
	Calculated crystallite size (nm)	Lattice parameter (nm)
PVP	4.07	0.3545
Oleic acid	5.11	0.3524

However, the observed diffraction peak of plane [111] of Ni_{core} – Pt_{shell}/C catalyst preparing with oleic acid stabilizer expressed asymmetric peak. It might be due to the overlap between the diffraction pattern of PtNi alloy and Ni metal.

The calculated lattice parameter from XRD patterns (appendix A) of both Ni_{core} – Pt_{shell}/C catalyst prepared with PVP and oleic stabilizer confirmed that there was no alloy material formed between Ni and Pt. Their calculated values for PVP and oleic acid stabilizer catalyst were 0.3545 and 0.3524 nm, respectively which similar to the reported value of pure nickel metal (0.3520 nm).

4.2.2 Electrochemical characterization

In this section the electrochemical properties analyzed by cyclic voltammetry and linear sweep voltammetry were presented. For cyclic voltammetry analysis, the Ni_{core} – Pt_{shell}/C catalyst either formed with PVP or oleic acid stabilizer were measured in the saturated N_2 0.5 M H_2SO_4 electrolyte and the voltammogram were shown in Figure 4.12. The position of hydrogen desorption peak in Figure 4.12(a) and (b) exhibited the similar potential. Within the 10 scans, the catalyst using PVP as a stabilizer exhibited an overlaying voltammogram whereas the catalyst using oleic acid stabilizer displayed the tendency of coincidence after the sixth scan. This could be clarified with regard to the wetting behavior at the electrode surface and saturation of the Nafion layer that covered the electrocatalyst particle [56]. Thus, it could be implied that stabilizer using in the catalyst synthesis would affect the steady state approach the in cyclic voltammetry measurement.

The electrochemical active surface area (EAS) at 10 scanning cycles of the Ni_{core} – Pt_{shell}/C catalyst prepared by using PVP and oleic acid stabilizer were calculated (appendix B) and summarized in Table 4.4. It could be seen that PVP stabilizer catalyst provided the higher calculated EAS (110.9 m^2/g Pt) than that of oleic acid stabilizer catalyst (92.9 m^2/g Pt). This result was consistent with the

calculated crystallite sizes of the respective synthesis catalyst, where the smaller crystallite size would give a higher EAS.

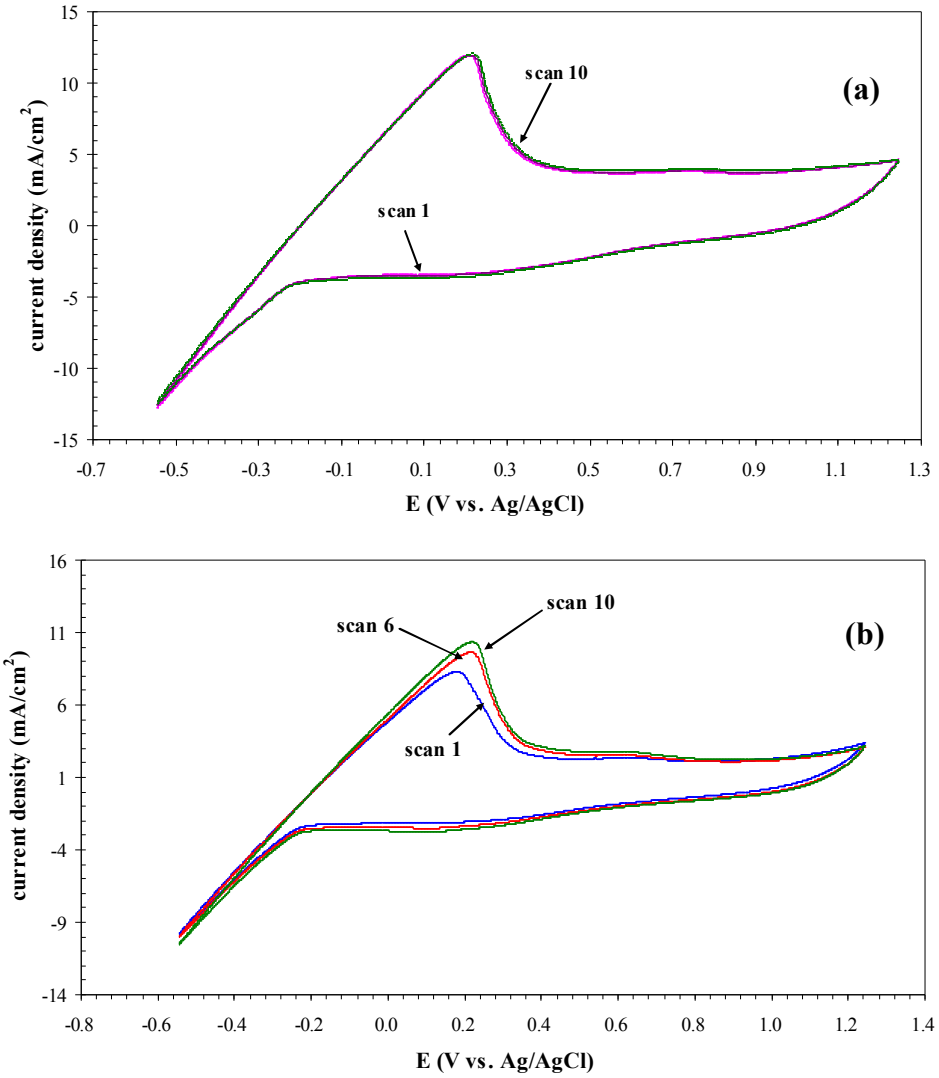

Figure 4.12 Cyclic voltammogram of $Ni_{core} - Pt_{shell}/C$ with (a) PVP stabilizer (b) oleic acid stabilizer in the saturated N_2 0.5M H_2SO_4 solution, at a scan rate 20 mV/s, and a scan range (-0.54) – 1.2 V vs. Ag/AgCl and 0.3 mg metal/cm^2 loading.

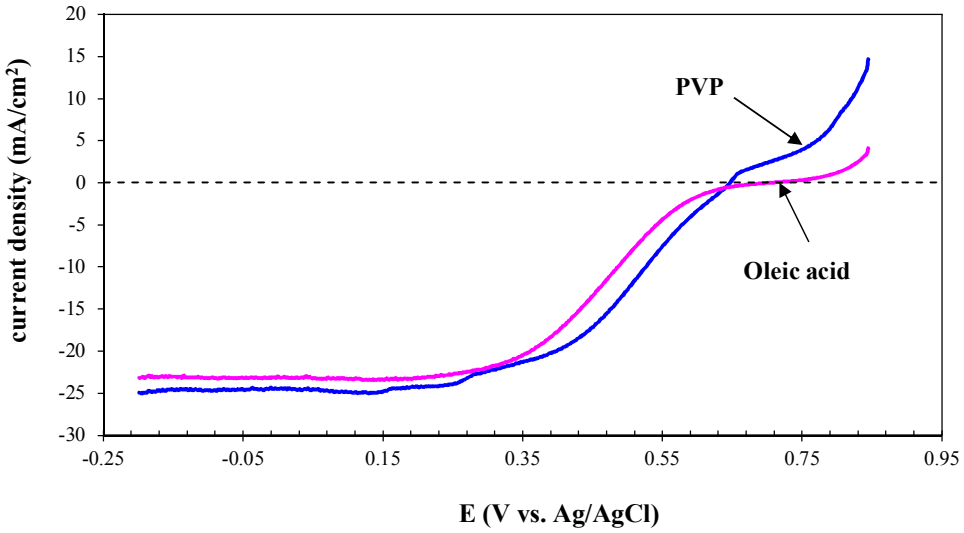

Figure 4.13 Linear sweep voltammogram of synthetic Ni_{core} – Pt_{shell} catalyst with different stabilizers in the continued O_2 bubbling 0.5M H_2SO_4 at rotating rate of 2000 rpm, at a scan rate of 20 mV/s. and a scan range (-0.2) – 0.8 V vs. Ag/AgCl.

Table 4.4 Electrochemical properties of Ni_{core} – Pt_{shell} catalysts prepared with different preparation methods

Stabilizer	Properties of synthetic Ni_{core} – Pt_{shell} /C catalyst	
	Electrochemical active surface area (EAS, m^2/g Pt)	Limiting current density (mA/cm^2)
PVP	110.9	24.5
Oleic acid	92.9	23.1

Although the calculated crystallite size of the synthetic $Ni_{core} – Pt_{shell}$ /C catalyst both formed with PVP and oleic acid stabilizer was found to be larger than the synthesized PtNi alloy supported on Vulcan XC 72 (2.2 nm), the calculated EAS of the synthetic core – shell structure catalysts were higher. Besides, the metal loading of $Ni_{core} – Pt_{shell}$ /C catalyst (20 wt%) was lower than that of PtNi alloy (65% metal) catalyst [62]. Thus, this result might verify that the core – shell structure could improve the electrochemical activity of the precious metal (in this case, Pt) on the core metal surface [25].

To investigate the activity toward the ORR of the prepared catalysts, the linear sweep voltammetry in oxygen saturated 0.5M H_2SO_4 was conducted and the voltammograms were demonstrated in Figure 4.13. In the mass transfer region (0.15 to (-0.2) V vs. Ag/AgCl), it revealed the slightly difference in the limiting current density of the catalyst formed with PVP stabilizer (24.5 mA/cm^2) and that of the catalyst formed with oleic acid stabilizer (23.1 mA/cm^2) as summarized in Table 4.4. However, the observed onset potential on the voltammetry curve of the catalyst formed with oleic acid stabilizer expressed the slightly higher positive value than that of catalyst formed with PVP stabilizer. It might be concluded that using oleic acid stabilizer yielded more favorable ORR catalyst than using PVP stabilizer.

4.3 The Face Centered Composite (FCC) – 2^4 factorial design experiment for the synthesis of Ni_{core} –$PtRu_{shell}$/C by the modified polyol method

The 2^k factorial design is well known to be useful for the preliminary state of the experiment. It is extensively applied for screening the important factor when there are many factors to be examined [63]. In this part, the parameters concerning the synthesis of the Ni_{core} - $PtRu_{shell}$/C catalyst, such as, the atomic ratio of Pt to Ru (factor A), the mole ratio of Ni precursor to PVP stabilizer (factor B), the reduction temperature (factor C) and the reduction time for the formation of PtRu alloy layer (factor D) were counted into the full 2^4 experimental design with the EAS as the observed response. Besides, to optimize the synthesis process, the application

of face – centered composite design (FCC) was implemented to the experimental work. The two levels of all factors and the central point were shown in Table 4.5.

Table 4.5 The experimental variables in coded and actual units for the FCC – 2^4 experimental design.

Factors	Variables	Low (-)	Medium (0)	High (+)	Unit
A	The atomic ratio of platinum to ruthenium	1:0.5	1:0.75	1:1	-
B	The mole ratio of Ni precursor to the PVP stabilizer	1:1	5:1	10:1	-
C	The reduction temperature for the PtRu alloy shell formation	138	159	180	^{o}C
D	The reduction time for the PtRu alloy shell formation	60	120	180	min

4.3.1 Effect of the synthesis parameters

After finishing the preparation the catalyst layer on the GDL substrate, not all of the catalysts are effective due to many factors such as the electrical separation of the catalyst particles [64]. Thus, the EAS is one of the important parameters and should be the observed response of FCC – 2^4 experimental design for assessing the catalyst layer formed with each synthetic condition. EAS of the each synthetic catalyst can be determined from the hydrogen desorption region of the cyclic voltammogram following the calculation method in the appendix B. Table 4.6 presents the EAS as the observed response for the FCC - 2^4 factorial design of the synthetic Ni_{core} –$PtRu_{shell}$/C synthesis**.** These EAS were calculated associating with 25 CV scanning cycles.

Table 4.6 The observed responses (EAS, m^2/ g Pt) of the FCC - 2^4 factorial design of the synthetic Ni_{core} –$PtRu_{shell}$/C synthesis

Experimental	Parameters (Coded value)				EAS (m^2/g Pt)
	A	B	C	D	
1	(-)	(-)	(-)	(-)	157.75 ± 9.33
2	(+)	(-)	(-)	(-)	133.68 ± 2.92
3	(-)	(+)	(-)	(-)	180.21 ± 0.27
4	(+)	(+)	(-)	(-)	172.22 ± 1.71
5	(-)	(-)	(+)	(-)	0 ± 0.00
6	(+)	(-)	(+)	(-)	0 ± 0.00
7	(-)	(+)	(+)	(-)	109.00 ± 0.3
8	(+)	(+)	(+)	(-)	0 ± 0.00
9	(-)	(-)	(-)	(+)	169.51 ± 0.35
10	(+)	(-)	(-)	(+)	111.16 ± 3.46
11	(-)	(+)	(-)	(+)	146.07 ± 1.94
12	(+)	(+)	(-)	(+)	104.39 ± 17.22
13	(-)	(-)	(+)	(+)	0 ± 0.00
14	(+)	(-)	(+)	(+)	0 ± 0.00
15	(-)	(+)	(+)	(+)	100.18 ± 3.35
16	(+)	(+)	(+)	(+)	75.07 ± 2.16

Table 4.6 ***(Cont.)***

Experimental	Parameters (Coded value)				EAS (m^2/g Pt)
	A	B	C	D	
17	(-)	(0)	(0)	(0)	105.68 ± 0.66
18	(+)	(0)	(0)	(0)	0 ± 0.00
19	(0)	(-)	(0)	(0)	137.17 ± 3.43
20	(0)	(+)	(0)	(0)	0 ± 0.00
21	(0)	(0)	(-)	(0)	135.31 ± 0.59
22	(0)	(0)	(+)	(0)	0 ± 0.00
23	(0)	(0)	(0)	(-)	95.93 ± 6.30
24	(0)	(0)	(0)	(+)	83.34 ± 6.20
25	(0)	(0)	(0)	(0)	211.33 ± 0.53

From Table 4.6, it can be seen that the EAS of some experiments expressed zero value. These results could be due to the cyclic voltammograms of these experimental conditions did not show the hydrogen adsorption/ desorption peak. Only the hydrogen evolution peak and oxygen evolution peak could be observed in these voltammograms. Thus, the EAS could not be determined.

Since the EAS of the synthetic catalyst is mainly influenced by the particle size of the electrocatalyst which the smaller particle size supposed to have a larger active surface area [8], the physical characterization of some experimental conditions were done and presented jointly with the EAS in Table 4.7

Table 4.7 Physical and electrochemical properties for some experiments of FCC – 2^4 factorial design of Ni_{core} –$PtRu_{shell}$/C synthesis

Exp. No.	parameter				Synthetic Ni_{core} –$PtRu_{shell}$/C properties			
	A	B	C	D	EAS (m^2 / g Pt)	Crystallite size (nm)	% Element from SEM/EDX	
							Pt	Ru
1	1:0.5	1:1	138	60	157.7	3.6	1.29	0.67
2	1:1	1:1	138	60	133.7	3.9	1.94	1.39
4	1:1	10:1	138	60	172.2	2.8	0.77	1.11
12	1:1	10:1	138	180	104.4	5.1	1.3	1.27
16	1:1	10:1	180	180	75.10	9.9	1.22	1.17

For the effect of the atomic ratio of platinum to ruthenium, from table 4.7, considering experimental number 1 and 2, as the Pt:Ru atomic ratio (A) increases, the crystallite size of the synthetic Ni_{core} –$PtRu_{shell}$/C catalyst was slightly increased. This result might be due to the effect of the concentration of the PtRu alloy precursor. In the nanoparticle synthesis, the increasing of the precursor concentration could result in the raising of the reduction rate. Then, more nucleus of alloy nanoparticles were formed with the high surface energy. And subsequently, the agglomeration of the nanoparticle to form a larger particle would occur in order to reduce the high surface energy and the thermodynamic instability [59]. This result was also consistent with the work conducted by Wang et al. [65] that the particle size of Ni nanoparticle could be monitored by the concentration of the Ni precursor. The larger Ni nanoparticles were formed with the higher concentration of Ni precursor.

In the aspect of the mole ratio of Ni precursor to the PVP stabilizer (B) as seen in the experimental number 2 and 4 of Table 4.7, the increasing of the mole ratio of Ni precursor to PVP stabilizer (or the reducing of PVP stabilizer content)

resulted in the reducing of the synthetic Ni_{core} – $PtRu_{shell}$/C particle size. It could be explained by the fact that in the nanoparticle synthesis with the polymer stabilizer, the diffusion of growth species in the surrounding reaction solution was obstructed from the surface of growing particle by the stabilizer [59]. In this case, PVP was added in this step of Ni core particles formation. Then, PVP stabilizer would cover the Ni surface and served as an inhibitor of the growth process of Ni nanoparticle. Thus, the lower mole ratio of Ni precursor to the PVP stabilizer could yield the smaller Ni particle size. However, in the core – shell structure catalyst, size of the core particle would affect the properties of the obtained catalyst. If the synthetic Ni core particle was too small (from using the lower mole ratio of Ni precursor to the PVP), it might not be suitable for the complete coverage of PtRu alloy shell layer [37]. Then, poor utilization of PtRu alloy (active metal) occurred and might decrease the EAS.

When focusing on the reduction temperature for the PtRu alloy shell formation (C) which can be seen from the experiment number 12 and 16 in Table 4.7, the raising of the reduction temperature for forming the PtRu alloy layer contributed to dramatically increasing in the crystallite size of the synthetic Ni_{core} –$PtRu_{shell}$/C. It could be ascribed to a reaction rate according to the familiar Arrhenius relationship. Then, after increasing the reduction temperature [59, 65, 66], the reduction rate of the Pt and Ru ions were increased and generated more nucleus of PtRu alloy nanoparticles which the high surface energy. So, the aggregation of the nanoparticles occurred so as to reduce the high surface energy of the nanoparticles.

In term of the reduction time for the PtRu alloy shell formation (D)**,** the experimental number 4 and 12 in Table 4.7 revealed that the extension of the reduction time for the PtRu alloy shell formation yielded the larger crystallite size of the synthetic Ni_{core} –$PtRu_{shell}$/C. This result suggested that the increasing of the reduction time in the quite high reaction temperature system like the modified polyol method nanoparticle synthesis could provide the agglomeration of the synthetic nanoparticles which favored to form a larger particle in order to reduce the high surface energy [59].

4.3.2 Statistical analysis of the synthesis parameters

Before the ANOVA analysis, the examination of the plot of residual and the run number of experiment was done. From Figure 4.14, the plot of residual versus run number exhibited the identified pattern which the inequality of the variance (Figure 4.14a). Thus, the log 10 data transformation was introduced to all data and the equality improvement of the plot versus run number was shown in Figure 4.14b.

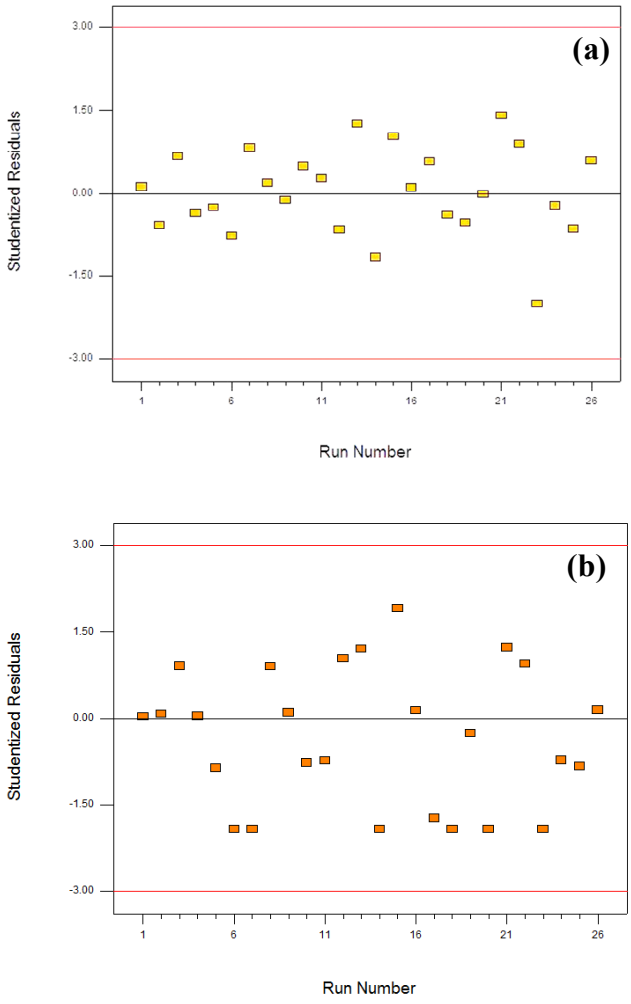

Figure 4.14 The plot of residuals versus run number of the FCC – 2^4 factorial design of Ni_{core} –$PtRu_{shell}$/C synthesis for (a) non – data transformation and (b) following base log 10 data transformation**.**

Then, the analysis of variance (ANOVA) of EAS at a 95% confidence interval was presented in Table 4.8. Based on P-value, any factors or interactions that presented their probability less than 0.05 have a significant influence on response. For the synthetic Ni_{core} –$PtRu_{shell}$/C catalyst, the atomic ratio of platinum to ruthenium (factor A), the mole ratio of Ni precursor to the PVP stabilizer (factor B), the reduction temperature for the PtRu alloy shell formation step (factor C), the interaction between the mole ratio of Ni precursor to the PVP stabilizer and the mole ratio of Ni precursor to the PVP stabilizer (interaction of factor B and C) and the interaction between the squared of the atomic ratio of platinum to ruthenium and the mole ratio of Ni precursor to the PVP stabilizer (interaction of factor A^2 and B) significantly affected the EAS of the synthetic catalyst.

Table 4.8 The analysis of variance (ANOVA) for the FCC - 2^4 factorial design of Ni_{core} – $PtRu_{shell}$/C synthesis following base 10 log data transformation, EAS as a response

Source	Sum of squares	Degree of Freedom	Mean Square	F Value	Prob > F
Model	131.38	18	7.30	3.75	0.0408*
A	12.62	1	12.62	6.48	0.0383*
B	13.20	1	13.20	6.78	0.0352*
C	13.17	1	13.17	6.76	0.0354*
D	1.09	1	1.09	0.56	0.4796
A^2	1.30	1	1.30	0.67	0.4407

* Significant F-values at the 95% confidence level

Table 4.8 *(cont.)*

Source	Sum of squares	Degree of Freedom	Mean Square	F Value	Prob > F
B^2	1.10	1	1.10	0.57	0.4764
C^2	1.11	1	1.11	0.57	0.4745
D^2	7.64	1	7.64	3.92	0.0881
AB	1.61	1	1.61	0.83	0.3936
AC	1.41	1	1.41	0.72	0.4236
AD	1.37	1	1.37	0.70	0.4299
BC	13.76	1	13.76	7.07	0.0325*
BD	1.31	1	1.31	0.67	0.4390
CD	1.69	1	1.69	0.87	0.3828
A^2B	21.85	1	21.85	11.22	0.0123*
A^2C	1.50	1	1.50	0.77	0.4094
AB^2	8.32	1	8.32	4.27	0.0776
ABC	1.72	1	1.72	0.89	0.3780
Residual	13.63	7	1.95		
Cor Total	145	25			

* Significant F-values at the 95% confidence level

From the ANOVA analysis, the regression model in form of the coded factors was generated as shown in the equation (4.1) with the R^2 value of 0.90.

$$\text{Log (EAS)} = 0.75 - 2.51A - 2.57\,B - 2.57\,C + 0.25\,D - 0.71\,A^2 - 0.66\,B^2 - 0.66\,C^2 + 1.73\,D^2 - 0.32\,AB - 0.30\,AC + 0.29\,AD + 0.93\,BC + 0.29\,BD + 0.32\,CD + 3.51\,A^2B + 0.92\,A^2C + 2.16\,AB^2 - 0.33ABC \quad \text{------- (Eq. 4.1)}$$

From the regression model, the optimization for the EAS of the Ni_{core} – $PtRu_{shell}$/C catalyst synthesis via the modified polyol method could be obtained from the response surface analysis. The optimal condition for the maximum EAS was presented in Table 4.9. However, after repeating the optimal condition for several times, the actual value from the experiment did not equal the predicted value. It could be suggested that the observed response of this system expressed a non – linear behavior over the chosen range of each factor.

Table 4.9 The optimal condition for Ni_{core} – $PtRu_{shell}$/C synthesis from response surface analysis

Parameter				**EAS (m^2/g Pt)**	
Atomic ratio of Pt:Ru	Mole ratio of Ni precursor : stabilizer	Reduction temperature for metal alloy shell (^{o}C)	Reduction time of metal alloy shell (min)	**Predicted value**	**Actual value**
1: 0.78	7:1	141.4	61.2	221.31	90.83

To check the assumption, the uni – variate experiments of the mole ratio of Ni precursor to the PVP stabilizer (factor B) and the reduction temperature for the PtRu alloy shell formation step (factor C) were performed for the example. The results presented in Figure 4.15 were conformed to the previous suggestion due to the calculated EAS at 25 scanning cycles showed the fluctuation over the observed ranges.

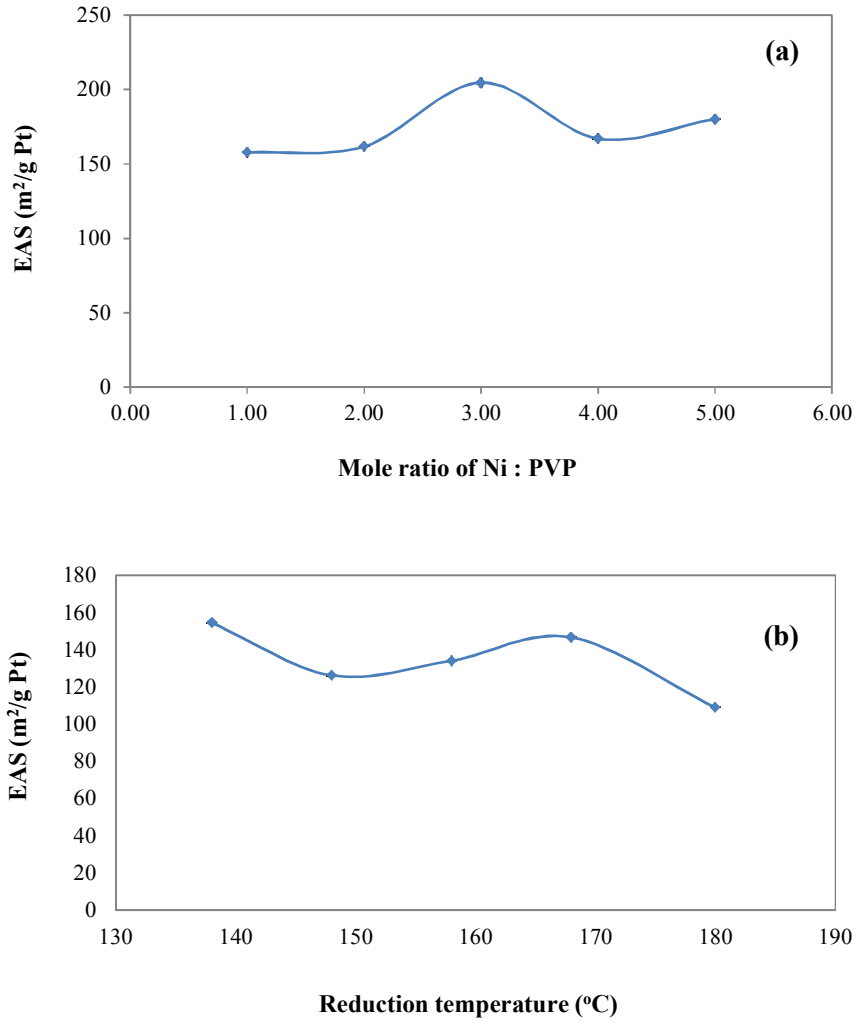

Figure 4.15 Electrochemical active surface area (EAS) as a function of (a) the mole ratio of Ni precursor to the PVP stabilizer (factor B) and (b) the reduction temperature for the PtRu alloy shell formation step (factor C)

However, the performance test of the optimal condition in Table 4.19 was done in order to investigate the activity of the synthetic Ni_{core} – $PtRu_{shell}$/C catalyst. The result showed the very low in the open circuit potential (0.56V). Also the current density was only 30 mA/cm^2 at the potential of 0.3 V and hence, the measurement results could not be shown as the complete polarization curve. The measurement of the impedance spectroscopy analysis for the cathode side, performing after performance test presented in Figure 4.16. The result revealed the very high charge transfer resistance which indicated the poor electrons transfer across the electrode surface.

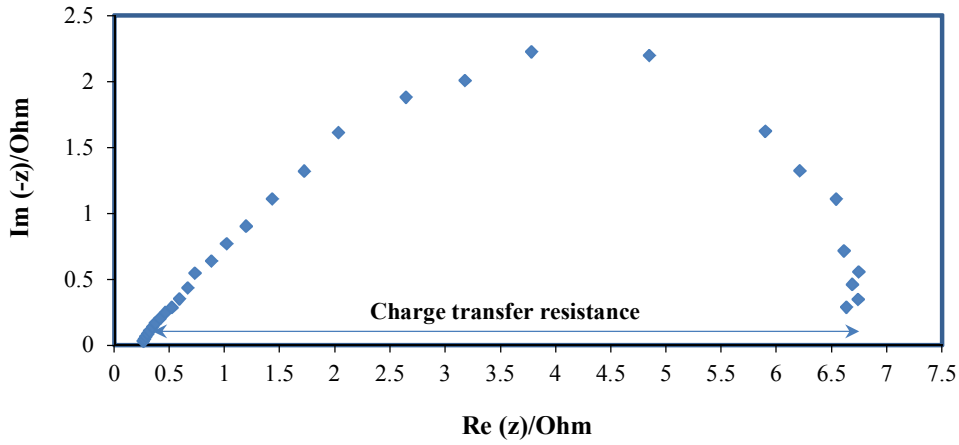

Figure 4.16 Nyquist plot of the synthetic Ni_{core} – $PtRu_{shell}$/C catalyst measuring in PEM single cell.

To overcome this problem, the assumption was established. It was suggested to be due to the incomplete removal of PVP stabilizer from the Ni core surface. This assumption conformed to the study of Long et al. [46]. They found that after removing PVP by heat treatment, the polyol method synthetic Pt nanoparticles expressed the improvement of catalyst activity. Thus, refer to this previous study, the heat treatment process should be introduced to the carbon supported Ni nanoparticles before applying PtRu shell layer which further discussed in Chapter V.

CHAPTER V

THE HEAT TREATMENT OF Ni/C NANOPARTICLES AND THE SYNTHESIS OF THE HEAT – TREATED Ni_{CORE} – $PtRu_{SHELL}$/C CATALYST

In this chapter, the heat treatment of Ni/C nanoparticles was studied. There was the report that only washing with solvent such as acetone, ethanol and hexane in the polyol synthesis of nanoparticles yielded the incomplete stabilizer elimination. This incomplete removal also resulted in the lowering of the catalytic activity [46]. Hence, together with solvent washing, heat treatment was introduced to the Ni core synthesis process before applying the PtRu alloy shell as mentioned in section 3.3.5 of Chapter III. The physical and electrochemical characterization results of the heat treated Ni_{core} – $PtRu_{shell}$/C were presented hereafter.

5.1 Physical characterization

The crystalline structure of carbon supported Ni nanoparticle before and after heat treatment were characterized by XRD as shown in Figure 5.1. It could be seen that the diffraction peak of Ni/C nanoparticle before heat treatment did not show any characteristic peak of Ni. While the diffraction peak of Ni/C nanoparticle after heat treatment near 44.4, 51.6 and 75.6 quite close to the characteristic peaks of pure crystalline Ni at 2θ values of 44.60 [111], 51.28 [200] and 76.24 [220] with face – centered cubic (FCC) crystalline. It could be suggested that the ethanol washing following by heat treatment could remove the excess PVP stabilizer from Ni nanoparticle surface. The calculated lattice parameter associating the crystalline plane [220] was 0.3521 nm with quite close to the reported value of pure Ni (0.3520 nm). However, to decompose PVP, the temperature used in the heat treatment process was quite high (300^{o}C). Thus, it was unavoidable that Ni nanoparticle would be sintered. The calculated particle size from XRD analysis of heat treated Ni/C was found to be 15.36 nm.

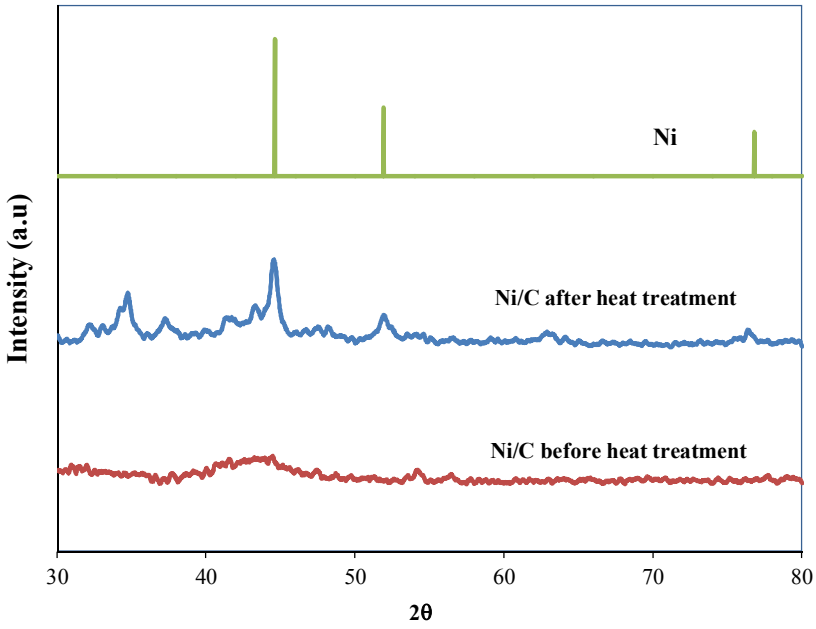

Figure 5.1 XRD pattern of Ni/C particle before and after heat treatment.

After finishing the heat treatment process, shell layer was applied to Ni/C nanoparticles via modified polyol method. In this case, in order to neglect the effect of metal type on the property of the obtained catalyst, Pt was selected as a shell at the beginning of the study. Figure 5.2 (a) and (b) showed the ultra high resolution TEM images of Ni/C nanoparticle after heat treatment and heat – treated $Ni_{core} - Pt_{shell}/C$, respectively. In Figure 5.2 (a), there was the sintering of Ni/C nanoparticle as a large particle. However, after applying Pt shell layer, some small particles could clearly be observed along with some larger particles as seen in Figure 5.2 (b). It could be suggested that using polyol method in reduction of Pt shell layer was not sluggish enough to make Pt as a shell on Ni particle. Thus, some of Pt ions were reduced and deposited on the Vulcan and some were on Ni surface. Besides, high reduction rate would promote Pt nanoparticle to deposit on Pt nanoparticle itself than other metal surface due to the similar crystalline structure [59].

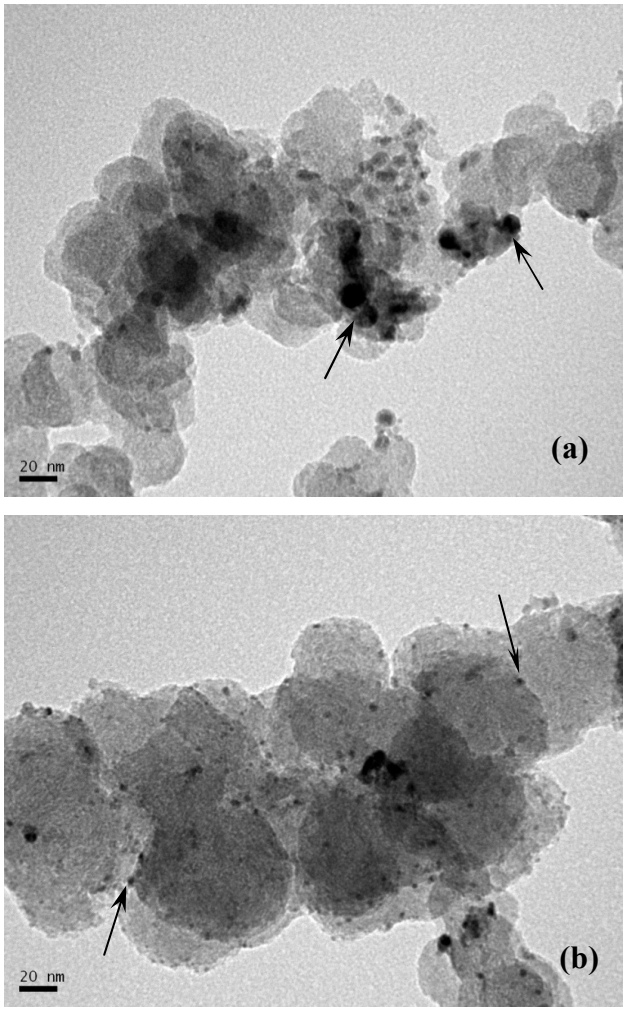

Figure 5.2 Ultra high resolution TEM images of (a) Ni/C nanoparticle after heat treatment and (b) heat – treated $Ni_{core} - Pt_{shell}/C$

Similarly, in the synthesis of $Ni_{core} - PtRu_{shell}$ /C by modified polyol method, it needed to use the high reduction temperature for PtRu alloy formation in order to obtain the uniform composition of PtRu alloy shell [66]. Consequently, it was possible that high reduction temperature would also promote the kinetic rate of PtRu alloy reduction and the separation of PtRu alloy particle from Ni surface might occur. Hence, to prevent the separation of core and shell metal, $NaBH_4$ reducing agent was introduced to the reduction of PtRu alloy instead of modified polyol method. Then,

the reduction rate was controlled by raising the $NaBH_4$ concentration in the reaction solution slowly. In the period of PtRu alloy reduction, the volume of $NaBH_4$ solution was divided equally and added into the reaction at the same interval (7 times within 2 h of reduction time) [47]. For comparison, the carbon supported PtRu catalyst was synthesized with the same methodology with 20%wt metal loading on carbon support.

The obtained heat – treated Ni_{core} – $PtRu_{shell}$ /C catalyst was then characterized by SEM/EDX to check the metal composition and the results were showed in Figure 5.3 (a) and (b). From the quantitative analysis, the atomic ratio of Ni to PtRu alloy was found to be 1: 1.82 which lower than that of the nominal ratio. It seemed that the lowering in the Pt and Ru content also occurred in the case of PtRu/C catalyst with the same reduction method. It might be due to the incomplete reduction of PtRu alloy which occurred for both the carbon supported PtRu alloy and the PtRu shell of the heat treated Ni_{core} – $PtRu_{shell}$/C catalyst. However, the atomic ratio of Pt to Ru of the heat – treated Ni_{core} – $PtRu_{shell}$/C and PtRu/C were found to be 1: 0.56 and 1:0.61, respectively which quite similar to the preset condition.

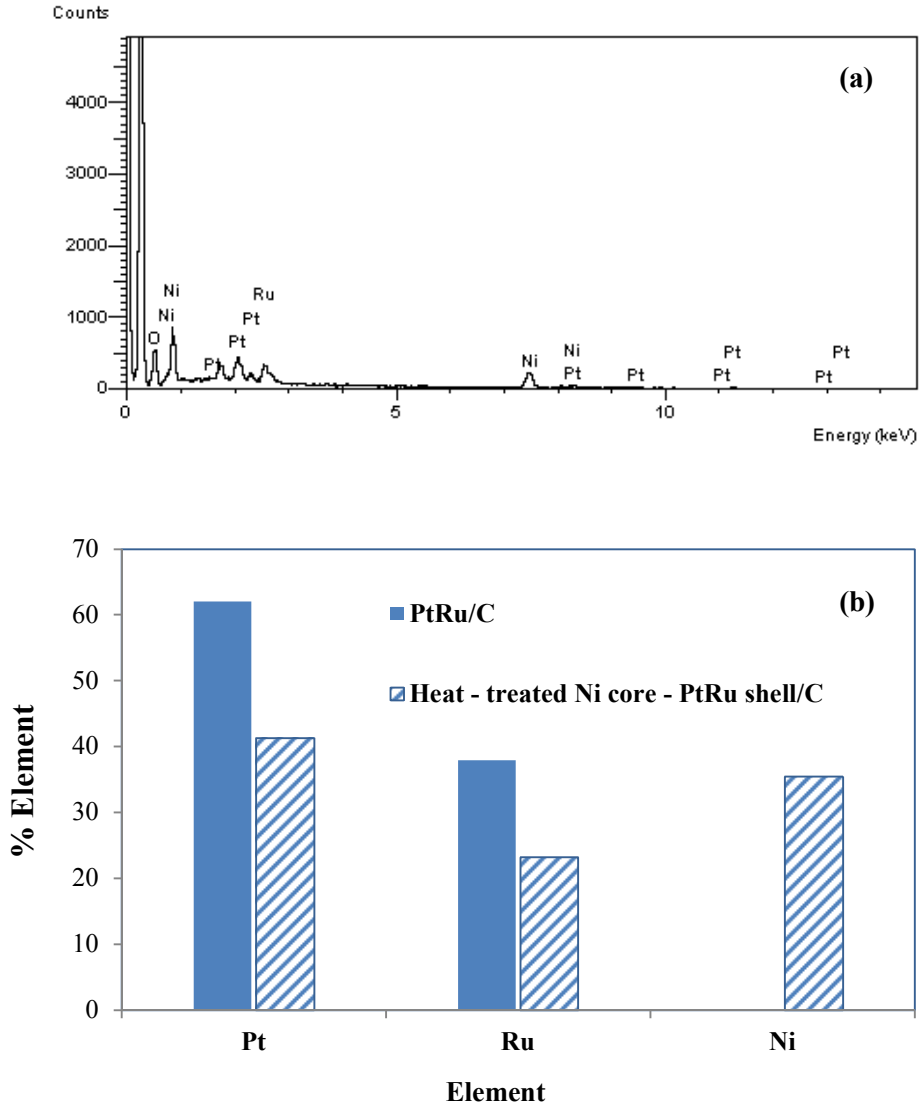

Figure 5.3 (a) SEM/EDX spectra of the synthetic heat treatment Ni_{core} – $PtRu_{shell}$/C catalyst and (b) the comparison of the elements content between the synthetic heat – treated Ni_{core} – $PtRu_{shell}$/C and the synthetic PtRu/C catalyst.

The dispersion of each metal on the heat – treated Ni_{core} – $PtRu_{shell}$/C catalyst surface was verified by EDX mapping technique as seen in Figure 5.4. The mapping images of Ni and Ru were found to have a well dispersion, while some small gatherings of nanoparticles were observed for Pt.

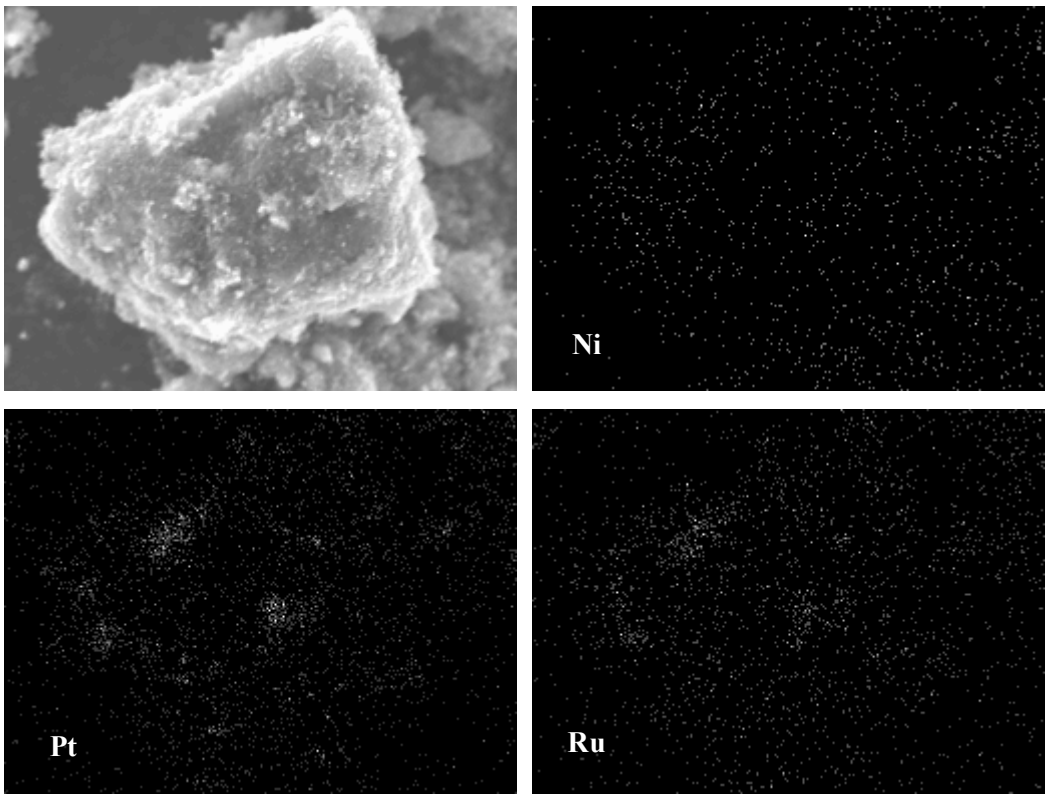

Figure 5.4 SEM/EDX elemental mapping images of the heat – treated Ni_{core} – $PtRu_{shell}$/C catalyst.

The crystalline structure of the heat – treated Ni_{core} – $PtRu_{shell}$/C was determined by XRD analysis as presented in Figure 5.5. The analysis of PtRu/C catalyst was also performed for a comparison. It could be seen that these two diffraction patterns were obviously similar and expressed only three main Pt particle characteristic peaks. The 2θ values corresponding to [111], [200] and [220] planes, for the heat – treated Ni_{core} – $PtRu_{shell}$/C, included 39.76, 45.7 and 67.6, respectively. For that of PtRu/C catalyst, the characteristic peak composed of 39.86, 45.98 and 67.34 associating with crystalline plane [111], [200] and [220], respectively.

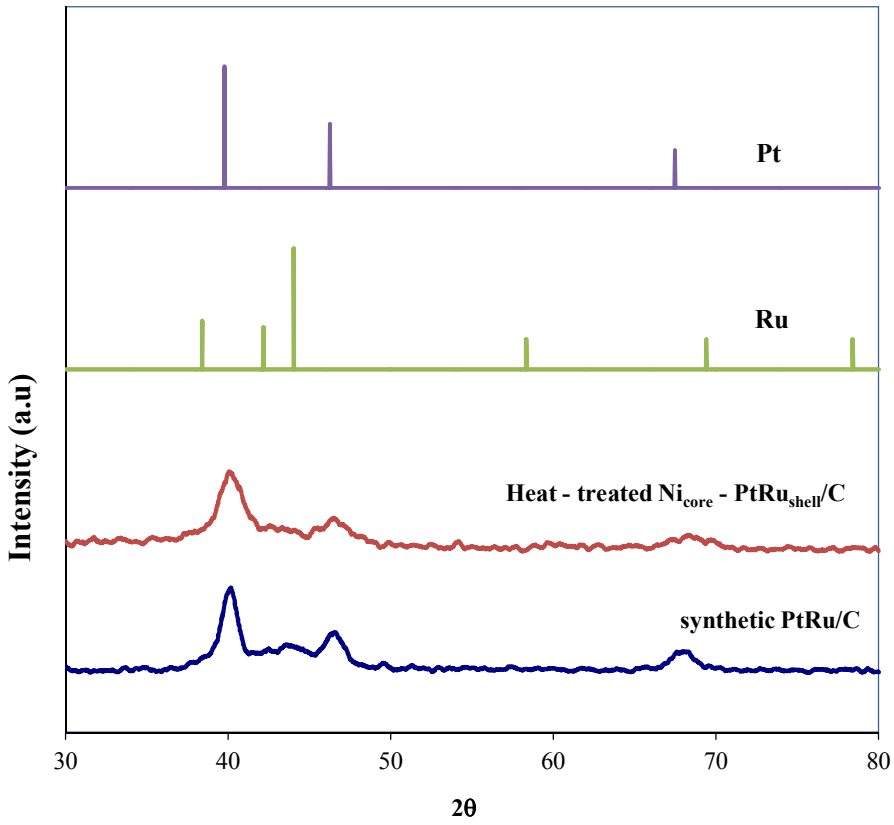

Figure 5.5 XRD pattern of the heat – treated Ni_{core} - $PtRu_{shell}$/C and PtRu/C catalyst.

It was found that there were no characteristic peaks for Ru appearing in the diffraction pattern. It could be explained according to the previous study that Ru presented in the form of Pt – Ru alloy or in the amorphous structure [66].

The average crystallite size and the lattice parameter were calculated from these two diffraction patterns corresponding with the Scherer's equations and the Bragg's law (appendix A), respectively and the results were summarized in Table 5.1. As seen in the table, the average crystallite size calculated from the diffraction peak of the plane [200] of the heat – treated Ni_{core} - $PtRu_{shell}$/C (7.97 nm) was quite equal to that of PtRu/C catalyst (7.17 nm). The calculated crytallite size after applying PtRu shell was decreased comparing to the heat – treated Ni core nanoparticle. It could be suggested by the schematic diagram in Figure 5.6 according to the previous studies [45, 67]. This figure revealed that after applying shell layer, the surface of core nanoparticle would be surrounded by shell metal nanoparticle. Thus, the X- ray

would detect at the surface of the applied shell metal and the calculated particle size from XRD pattern after applying shell layer to be belonging to the PtRu alloy nanoparticles. In this case, the PtRu alloy shell particle size was smaller than heat treatment Ni core nanoparticle.

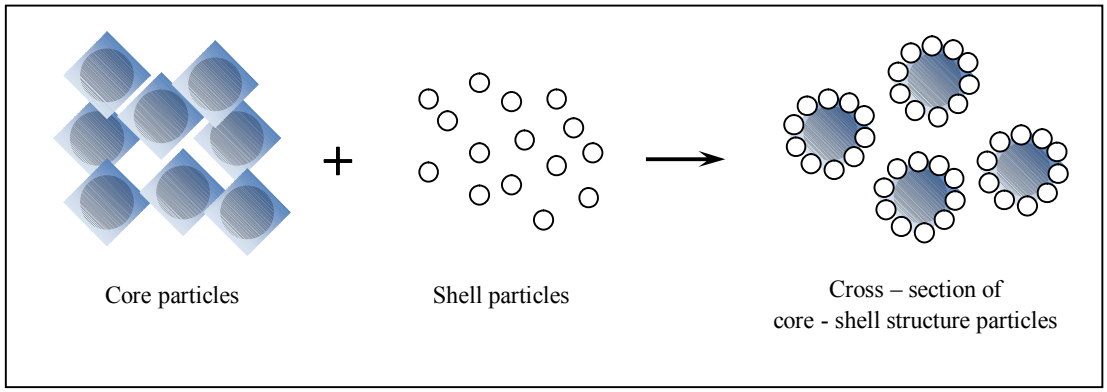

Figure 5.6 Schematic illustration of core – shell structure catalyst formation [68].

Table 5.1 The physical properties of the synthetic nanoparticles for investigation of heat treatment effect.

Synthetic nanoparticles	Properties of synthetic nanoparticles	
	Calculated particle size (nm)	Lattice parameter (nm)
Heat – treated Ni/C (core)	15.36	0.3521
PtRu/C	7.17	0.3880
Heat – treated Ni_{core} – $PtRu_{shell}$/C	7.97	0.3880
Ni (theory)		0.3520
Pt (theory)		0.3920
Ru (theory)		0.2700

As seen in Table 5.1, the estimated lattice parameters associating [220] plane were 0.3880 nm for both heat – treated Ni_{core} – $PtRu_{shell}$/C and PtRu/C catalyst, respectively. These estimated values were slightly lower than the reported value of pure Pt (0.3920 nm). Since the atomic radius of Ru is smaller than that of Pt atom, according to Vegard's law, the consolidation of Ru into the alloyed state will be determined from the decreasing in lattice parameter. The more decreasing in lattice parameter, the more progressive of Pt – Ru alloy forming [68]. Thus, with the decreasing in lattice parameter, it could be confirmed that there was the forming of PtRu alloy in the shell layer of the heat – treated Ni_{core} – $PtRu_{shell}$/C.

5.2 Electrochemical characterization

In this section, the heat – treated Ni_{core} – $PtRu_{shell}$/C was investigated the electrochemical properties, PEM single cell performance test and the durability test by potential cycling technique.

To begin with cyclic voltammetry, this technique was considered to be the surface – sensitive since it analyzed the surface atom electrochemical properties rather than of bulk atoms [31]. For a comparison, the examinations were done for PtRu/C and the heat – treated Ni/C nanoparticles. The cyclic voltammograms in Figure 5.7, after overlaying the PtRu alloy shell, the hydrogen desorption area was obviously observed in the heat – treated Ni_{core} – $PtRu_{shell}$/C catalyst comparing to the heat treatment Ni/C nanoparticle. Moreover, this hydrogen desorption area of the heat – treated Ni_{core} – $PtRu_{shell}$/C catalyst was greater than that of PtRu/C. The electrochemical active surface area (EAS) of the heat – treated Ni_{core} – $Pt_{Rushell}$/C and PtRu/C were calculated and summarized in Table 5.2. It could be seen that the heat – treated Ni_{core} – $PtRu_{shell}$/C catalyst provided the higher calculated EAS (194.34 m^2/g Pt) than that of PtRu/C catalyst (94.11 m^2/g Pt) despite the calculated particle sizes of both catalysts were nearly equal (as seen in Table 5.1). Thus, this result might verify that the core – shell structure could improve the dispersion of precious metal (in this case, PtRu) on the core metal surface [25].

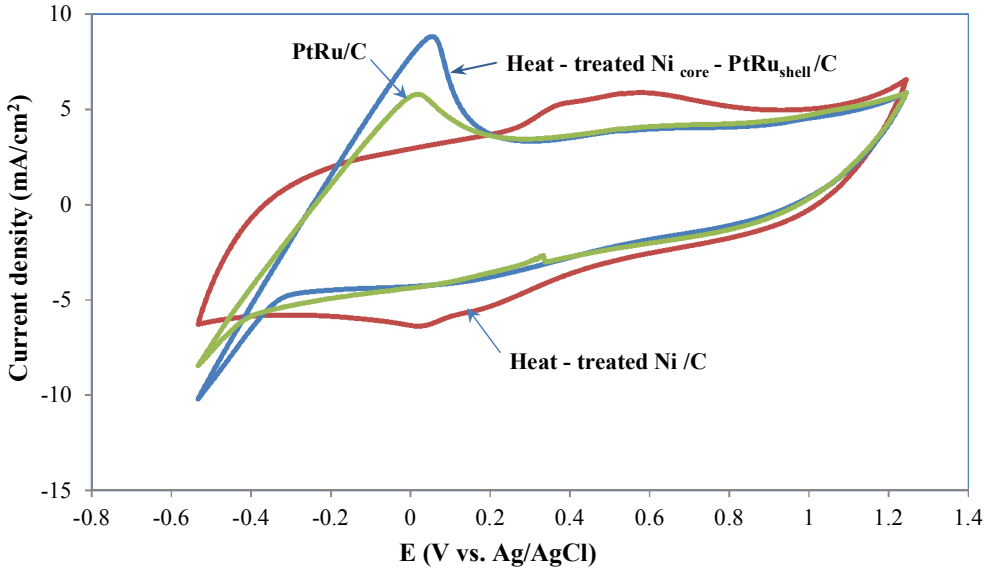

Figure 5.7 Cyclic voltammograms of heat – treated Ni_{core} – $PtRu_{shell}$/C, PtRu/C and heat – treated Ni/C electrode with 0.3 mg metal/cm^2 loading, conducted in a N_2 saturated 0.5 M H_2SO_4 electrolyte, at a scan rate of 20 mV/s and a scan range of (-0.54) – 1.2 V vs. Ag/AgCl.

Table 5.2 Electrochemical properties of the heat – treated Ni_{core} – $PtRu_{shell}$/C and PtRu/C catalyst

catalyst	Properties of synthetic Ni_{core} – Pt_{shell} /C catalyst	
	Electrochemical active surface area (EAS, m^2/g Pt)	Limiting current density (mA/cm^2)
PtRu/C	94.11	16.8
Heat – treated Ni_{core} – $PtRu_{shell}$/C	194.34	15.6

To investigate the activity toward the ORR of the prepared catalysts, the linear sweep voltammetry in O_2 saturated 0.5M H_2SO_4 was performed and the voltammograms were presented in Figure 5.8. In the mass transfer region (0.15 to (-0.2) V vs. Ag/AgCl), it revealed the slightly difference in the limiting current density of the heat – treated Ni_{core} – $PtRu_{shell}$/C (15.6 mA/cm^2) and that of the PtRu/C (16.8 mA/cm^2) as summarized in Table 5.2. However, the observed onset potential on the voltammetry curve of the PtRu/C catalyst expressed the slightly higher positive value than that of the heat – treated Ni_{core} – $PtRu_{shell}$/C which implied that the PtRu/C catalyst was more favorable in ORR.

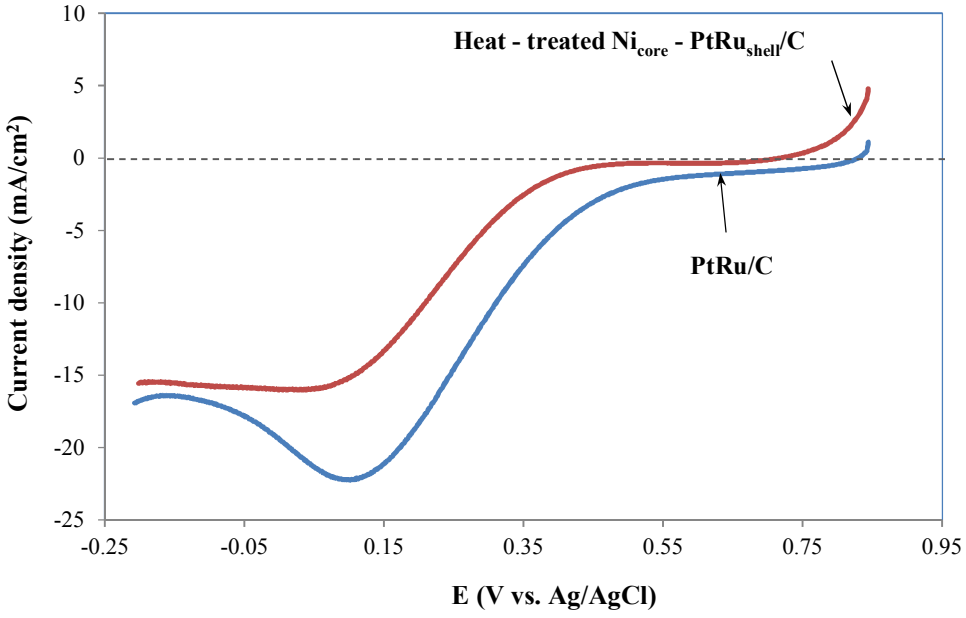

Figure 5.8 Linear sweep voltammogram of the heat – treated Ni_{core} – $PtRu_{shell}$/C and PtRu/C catalyst in the continued O_2 bubbling 0.5M H_2SO_4, at rotating rate of 2000 rpm, at a scan rate of 20 mV/s. and a scan range (-0.2) – 0.8 V vs. Ag/AgCl.

With the purpose of studying the kinetics of oxygen reduction reaction (ORR) of the heat – treated Ni_{core} – $PtRu_{shell}$/C, the linear sweep voltammetry was performed with various rotational speed of the rotating disk electrode (500 – 2000 rpm) as seen in Figure 5.9 (a). To determine the kinetics of ORR, the Levich – Koutecky equation was introduced to the evaluation as shown in equation 5.1

$$\frac{1}{j} = \frac{1}{j_k} + \frac{1}{B\omega^{\frac{1}{2}}} \tag{5.1}$$

Where j is the experimental current density, j_k is the kinetic current density, ω is the rotational speed rate, B is a constant given by equation 5.2.

$$B = 0.62nFD^{\frac{2}{3}}\upsilon^{\frac{-1}{6}}C_{O_2} \tag{5.2}$$

Which n is the number of electrons transferred in the oxygen reduction reaction, F is the Faraday's constant (96,485 C/mol), D is the diffusion coefficient of oxygen in the solution (1.9×10^{-5} cm^2/s), υ is the kinematics viscosity (0.01 cm^2/s) and C is the oxygen concentration in bulk solution (1.1×10^{-6} mol/cm^3).

After selecting current density – potential data in the mixed controlled region, the Levich – Koutecky plot following the Levich – Koutecky equation was done as seen in Figure 5.9 (b). Subsequently, the linear trend line was added for every data set from different potentials in order to determine the slope of linear equation which would be equal to the reciprocal of B value. Then, the number of electrons transferred could be determined and the data were summarized in Table 5.3. The number of electrons transferred was in the range of 3.543 – 4.453 with the average of 3.984 ± 0.38. Thus, the heat – treated Ni_{core} – $PtRu_{shell}$/C had the 4 – electrons pathway dominated.

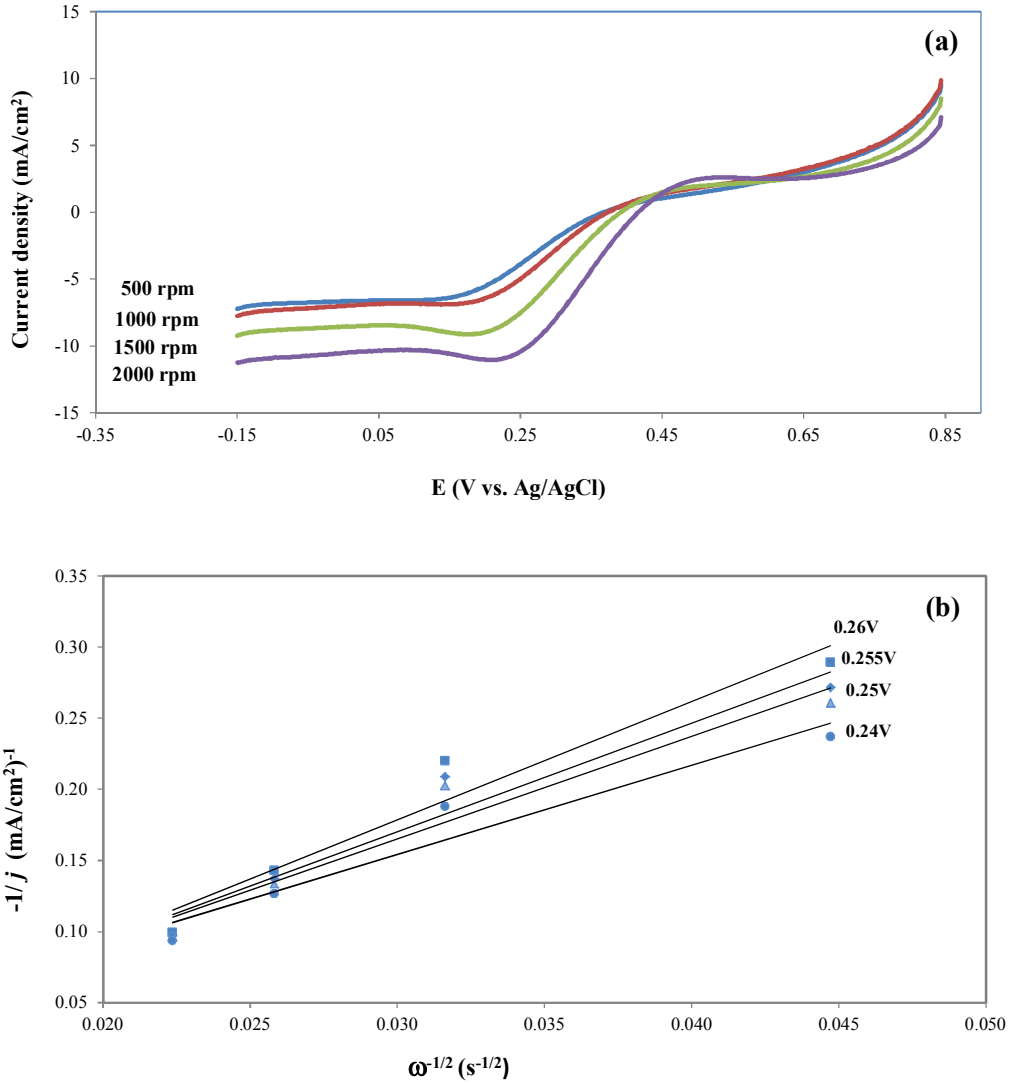

Figure 5.9 The plots for ORR kinetics study of the heat – treated $Ni_{core} - PtRu_{shell}/C$ catalyst (a) the linear sweep voltammograms as a function of rotating rate performed in the continued O_2 bubbling 0.5M H_2SO_4, at a scan rate of 20 mV/s and a scan range (-0.3) – 0.6 V vs. Ag/AgCl. (b) the Levich – Koutecky plot of the selected data in the mixed controlled region.

Table 5.3 The slope ($\frac{1}{B}$) corresponding the Levich – Koutecky plot and the calculated number of electrons transferred in the oxygen reduction reaction for the heat – treated Ni_{core} – $PtRu_{shell}$/C catalyst.

E (V vs. Ag/AgCl)	$\frac{1}{B}$ **(mA/cm^2 s$^{1/2}$)$^{-1}$**	***B* (mA/cm^2 s$^{1/2}$)**	**Number of electrons, *n***
0.260	8.301	0.1205	3.543
0.255	7.622	0.1312	3.859
0.250	7.202	0.1388	4.084
0.245	6.605	0.1514	4.453
		average	3.984

5.3 PEM single cell performance test

The PEM single cell performance test of the heat – treated Ni_{core} – $PtRu_{shell}$/C catalyst as a cathode catalyst was presented in Figure 5.10 (a). The performance test was achieved at 60^{o}C cell temperature with 0.3 mg metal loading/cm^2 for cathode and 0.3 mg Pt loading/cm^2 (commercial Pt/C, Etek) for anode. For a comparison, the performance test of commercial Pt/C (E-tek) with 0.3 mg Pt loading/cm^2 was done as seen in Figure 5.10 (b). Considering the current density per milligram of Pt loading, it could be seen that at 0.6 V of potential, the heat – treated Ni_{core} – $PtRu_{shell}$/C catalyst exhibited a slightly higher current density (229.42 mA/ cm^2· mg Pt) than that of E-tek Pt/C catalyst (209.47 mA/ cm^2· mg Pt) under the same operating condition.

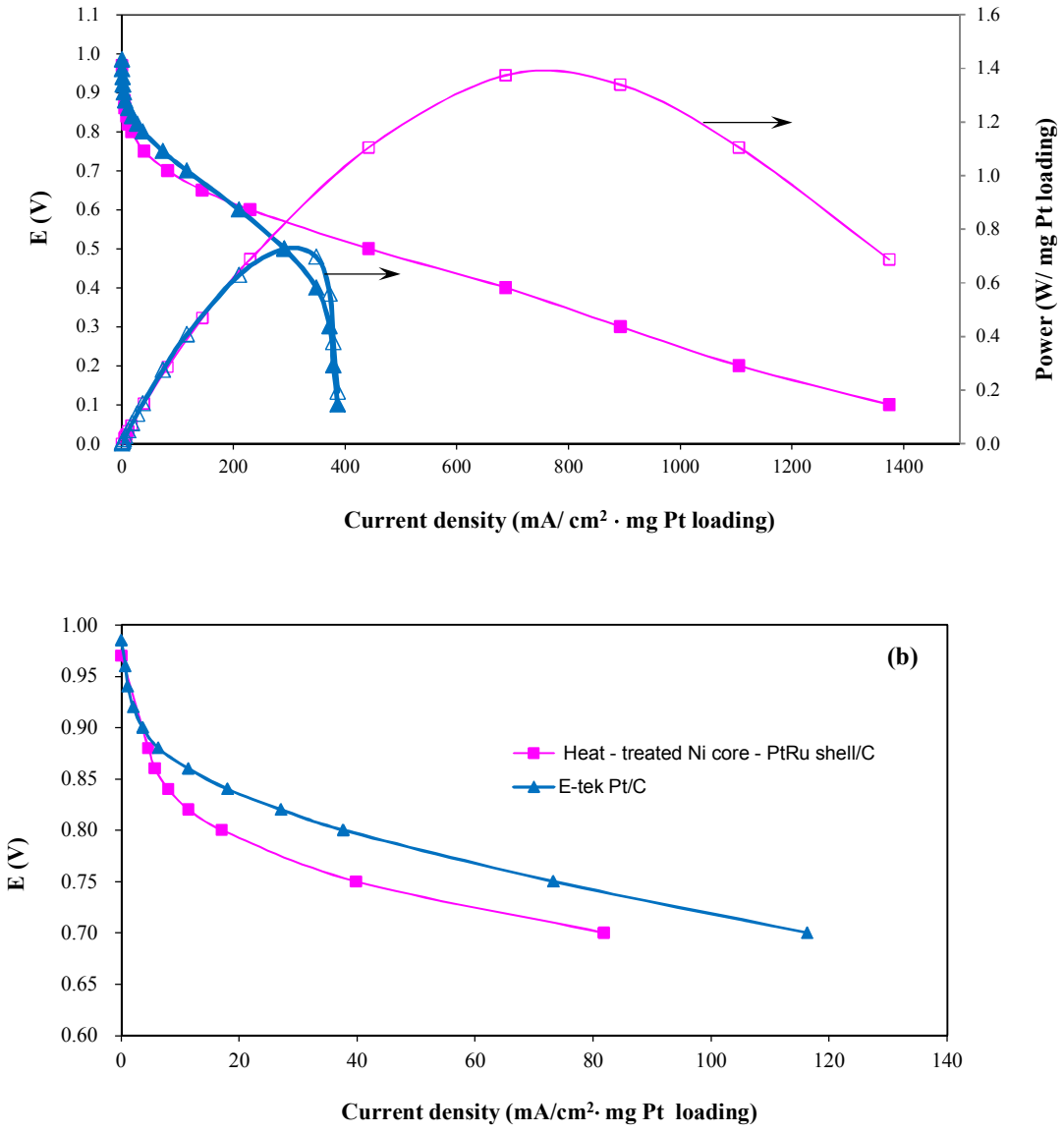

Figure 5.10 (a) PEM single cell performance test of the heat – treated Ni_{core} – $PtRu_{shell}$/C catalyst (■) and E – tek Pt/C (▲) catalyst assayed at 60°C and 1 atm which the filled symbols (■ and ▲) represented the I – V curves and the unfilled symbols (□ and △) represented the I – P curves, respectively and (b) the magnification for the high potential region of the I – V curves.

However, as illustrated in Figure 5.10 (c), for the heat – treated Ni_{core} – $PtRu_{shell}$/C catalyst, the slope of the performance curve at the high potential region slightly decline compared to that of E-tek Pt/C. This declination was majority of the activation loss as a result of the dawdling kinetics of the oxygen reduction reaction [69]. Thus, it could be concluded that the activity in oxygen reduction of the heat – treated Ni_{core} – $PtRu_{shell}$/C catalyst was slightly lower than that of E-tek Pt/C.

5.4 The catalyst durability test

Generally, potential cycling is a technique used for cleaning or activating the surface of electrode. It is found that after potential cycling at high potential region, the Pt dissolution occurs. Moreover, apart from the potential range used, the occurring of this phenomenon also depends on the number of cycles [70-71]. Thus, in this study, the ability of the heat – treated Ni_{core} – $PtRu_{shell}$/C catalyst to endure in the corrosion environment and the change in performance (owing to the loss of EAS) over time was examined by potential cycling. Because of the convenience in using the cyclic voltammogram for evaluating the EAS of the catalyst, the durability study was also performed using the cyclic voltammogram technique with 1,000 cycles of potential cycling. The potential cycling test of E-tek Pt/C catalyst was also investigated for a comparison.

Figure 5.11 represented the cyclic voltammograms as a function of cycle number of (a) E-tek Pt/C and (b) the heat – treated Ni_{core} – $PtRu_{shell}$/C catalyst. The normalized EAS which was corresponding the cyclic voltammogram in Figure 5.11 was determined and presented in Figure 5.12. According to Figure 5.12, for E-tek Pt/C catalyst, it could be seen that the EAS was slightly increased and got the unity at the 100^{th} cycle. For the heat – treated Ni_{core} – $PtRu_{shell}$/C, the similar behavior could be observed but it took more cycle numbers for the EAS to reach the unity (the 200^{th} cycle). This could be due to This could be due to the wetting behavior at the electrode surface and saturation of the Nafion layer that covered the electrocatalyst particle [56].

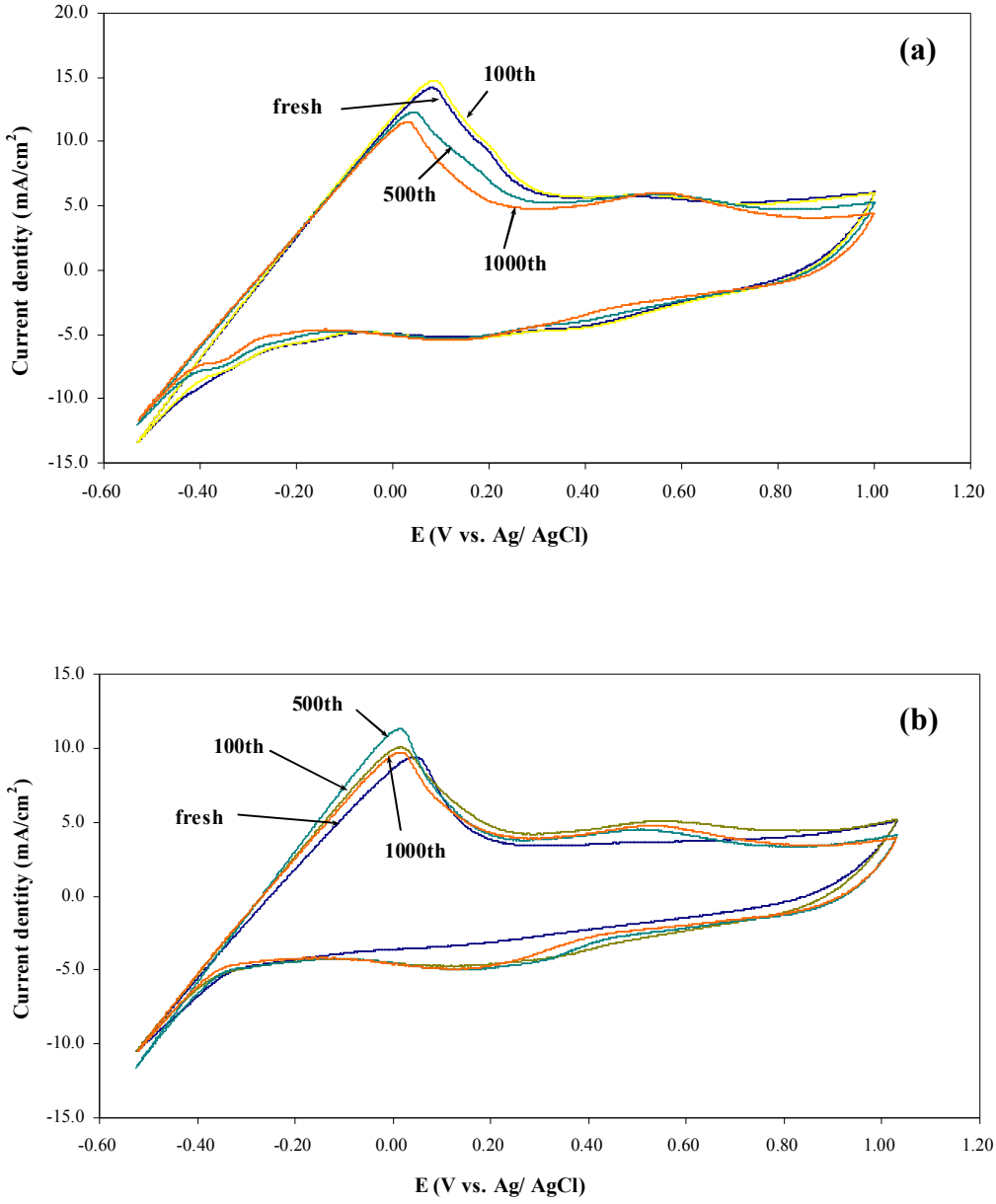

Figure 5.11 The cyclic voltammogram as a function of cycle number of (a) E-tek Pt/C and (b) the heat – treated $Ni_{core} – PtRu_{shell}/C$ assayed in a N_2 saturated 0.5 M H_2SO_4 electrolyte, at a scan rate of 20 mV/s and a scan range of (-0.54) – 1.2 V vs. Ag/AgCl with a constant agitation.

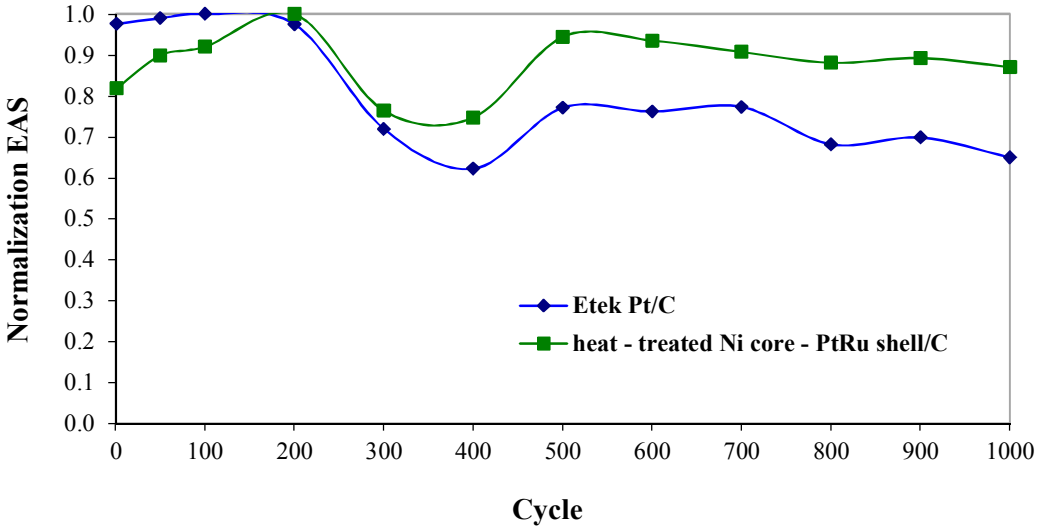

Figure 5.12 The normalized EAS as a function of cycle number of E-Tek Pt/C catalyst and the heat – treated Ni_{core} – $PtRu_{shell}$/C catalyst.

Then, after reaching the unity, both E-tek Pt/C and the heat – treated Ni_{core} – $PtRu_{shell}$/C catalyst exhibited the decreasing of EAS with the increasing of the cycle number. It could be explained by the dependence of potential on the Pt – solubility. When the electrode potential was raised above the particular equilibrium voltage, the dissolution of Pt into the electrolyte occurred. When the electrode potential was decreased below the particular equilibrium voltage, the Pt ion was driven back out of the electrolyte and redeposited on the Pt particle surface. Consequently, the larger catalyst particle was formed and resulted in the decreasing of EAS [70, 72]. However, at 500^{th} cycle, both E-tek Pt/C and the heat – treated Ni_{core} – $PtRu_{shell}$/C catalyst showed a slightly increasing of EAS and then a slightly decreased of EAS was continued until completed 1,000 scanning cycles. The slightly increasing in EAS at 500^{th} cycle might be due to the possibility of the Pt ion that redeposited on the Ni or carbon support surface other than Pt surface and forming a small Pt particle size which provided more EAS to the electrode.

Table 5.4 The comparison of the decreasing in normalized EAS as a function of cycle number between E- tek Pt/C and the heat – treated Ni_{core} – $PtRu_{shell}$/C catalyst.

Cycle number	**% Decrease of normalized EAS at each cycle (relative to Normalized EAS of 1)**	
	Commercial Pt/C (E-tek)	**Heat – treated Ni_{core} – $PtRu_{shell}$/C**
1	-	-
50	-	-
100	Normalized EAS of 1	-
200	2.49	Normalized EAS of 1
300	28.08	23.62
400	37.79	25.29
500	22.88	5.56
600	23.81	6.49
700	22.70	9.28
800	31.83	11.92
900	30.15	10.75
1000	35.05	13.00

The results presented in Table 5.4 revealed that after complete 1000 cycles of potential cycling, the heat – treated Ni_{core} – $PtRu_{shell}$/C showed more durable with a 13% decrease in the normalized EAS than the E-tek Pt/C with 35.05% decrease in the normalized EAS.

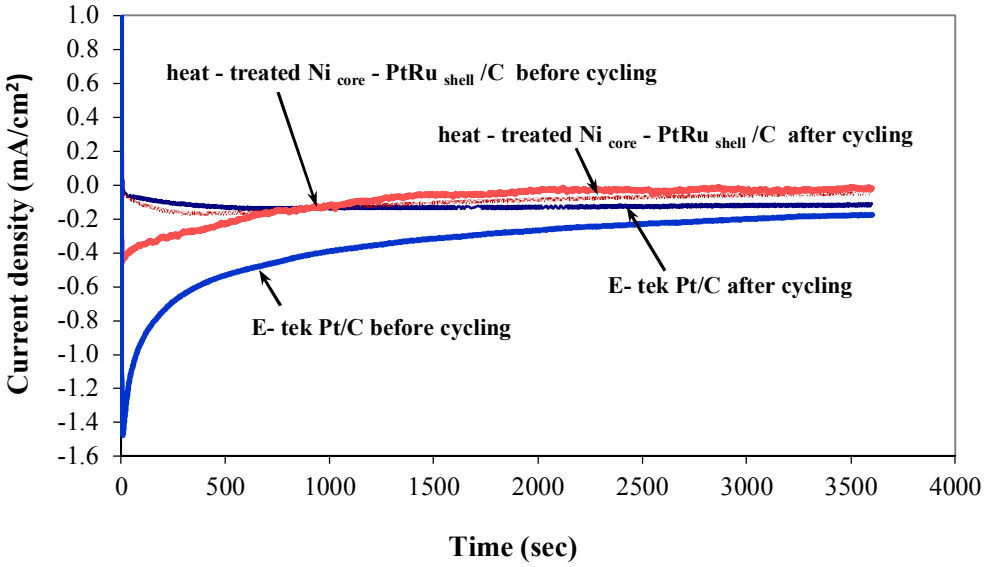

Figure 5.13 Chronoamperometric curves before and after potential cycling of the heat – treated Ni_{core} – $PtRu_{shell}$/C and E-tek Pt/C catalyst in O_2 saturated 0.5 M H_2SO_4 electrolyte, at a scan rate of 20 mV/s and 0.603 V vs. Ag/AgCl.

The chronoamperometry measurement of the heat – treated Ni_{core} – $PtRu_{shell}$/C and E-tek Pt/C catalyst before and after performing potential cycling were investigated. As seen in Figure 5.13, before potential cycling tested, the E- tek Pt/C showed the steady – state cathodic current density of 0.176 mA/cm^2, while the heat – treated Ni_{core} – $PtRu_{shell}$/C expressed the steady – state anodic current density of 0.022 mA/cm^2. This anodic current density at the observed potential (0.603 V vs. Ag/AgCl) might appear corresponding to the oxidation at Ni core nanoparticle surface which partially expose to the electrolyte. This result was conformed to the cyclic voltammogram of heat – treated Ni/C nanoparticle in Figure 5.7 that could observe the oxidation peak at the same potential (0.603 V vs. Ag/AgCl).

After completing the potential cycling tested in the acidic environment, both the heat – treated Ni_{core} – $PtRu_{shell}$/C and E-tek Pt/C could perform the oxygen reduction reaction. The steady – state cathodic current density of E- tek Pt/C catalyst was decreased to 0.119 mA/cm^2 (32.39% decrease) from the initial value. Moreover, the heat – treated Ni_{core} – $PtRu_{shell}$/C expressed the cathodic current density (0.054 mA/cm^2) after the potential cycling. However, the observed steady – state cathodic current density of the E-tek Pt/C catalyst expressed the higher value than that of the heat – treated Ni_{core} – $PtRu_{shell}$/C catalyst. This result was consistent with the performance curve illustrated in Figure 5.10 (c) that E-tek Pt/C provided the higher catalyst activity than the heat – treated Ni_{core} – $PtRu_{shell}$/C catalyst.

CHAPTER VI

CONCLUSIONS AND RECOMMENDATIONS

6.1 Conclusions

The major conclusions of this study can be summarized in the following list and further particularized below.

- In the $Ni_{core} - Pt_{shell}/C$ catalyst synthesis, the catalyst preparation method has an effect on the physical and electrochemical properties of the obtained catalyst.

The conventional method and the modified polyol method are selected for a comparison. The modified polyol method show the lower ability in Pt reduction compare to the conventional method. Besides, the conventional method yields the smaller particle size of the $Ni_{core} - Pt_{shell}/C$ catalyst and gives the higher EAS due to the lower reduction temperature. However, the modified polyol method catalyst shows more stability during the cyclic voltammetry analysis. The evaluated ORR activity from linear sweep voltammetry analysis reveals a slightly difference of the limiting current density from both preparation methods. The slightly positive shift of the onset potential of the conventional method catalyst indicates that more favorable for oxygen reduction than the modified polyol method catalyst

- The type of stabilizer using for the core metal synthesis also affects the physical and electrochemical properties of the synthetic $Ni_{core} - Pt_{shell}/C$ catalyst

The comparison between oleic acid and PVP (mw.10,000) stabilizer is examined with the modified polyol method synthesis. PVP stabilizer provides the higher amount of Ni content in the composition of synthetic catalyst than that using oleic acid stabilizer. The obtained $Ni_{core} - Pt_{shell}/C$ catalyst exhibits the smaller particle size and higher EAS with more stability during the cyclic voltammetry analysis. In the study of ORR activity by linear sweep voltammetry analysis, PVP and oleic acid

expresses the similar limiting current density. However, the oleic acid stabilizer provides a catalyst with more favorable for oxygen reduction reaction than PVP stabilizer since the slightly positive shift of the onset potential is observed in the linear sweep voltammogram of oleic acid stabilizer catalyst.

- The investigation of the parameters relating the modified polyol synthesis of $Ni_{core} - PtRu_{shell}/C$ catalyst by FCC – 2^4 experimental design indicates that the atomic ratio of platinum to ruthenium, the mole ratio of Ni precursor to the PVP stabilizer, the reduction temperature for the PtRu alloy shell formation step and the interaction between the mole ratio of Ni precursor to the PVP stabilizer and the mole ratio of Ni precursor to the PVP stabilizer affect the EAS of the synthetic catalyst.

- The heat treatment of Ni core particle before adding PtRu alloy shell layer can improve the surface of the Ni core nanoparticles.

The XRD pattern of heat treatment Ni core nanoparticle exhibits the Ni characteristic peak comparing to the non – heat treatment Ni nanoparticle. However, Ni nanoparticle shows the increasing in the particle size after heat treatment.

- The reducing agent for the formation of shell layer also affects the formation of shell layer over the core particle.

The modified polyol process with high reduction temperature results in the high reduction rate of shell metal nanoparticle. Then, a number of shell metal nanoparticles being rapidly generated seem to deposit on each other or on the carbon support rather than the core metal nanoparticle.

- The PtRu alloy shell layer for the heat treatment Ni_{core} – $PtRu_{shell}$/C catalyst can be prepared by controlling the PtRu reduction rate through the slowly raising the $NaBH_4$ concentration in the reaction solution.

With this preparation method, the atomic ratio of Pt to Ru of the heat treatment Ni_{core} – $PtRu_{shell}$/C catalyst is similar to the preset condition. The PEM single cell performance test of the heat treatment Ni_{core} – $PtRu_{shell}$/C as the cathode catalyst shows the similar current density per milligram of Pt loading at 0.6 V potential comparing to the commercial Pt/C (E-tek). Moreover, the potential cycling test of the heat treatment Ni_{core} – $PtRu_{shell}$/C showed more durable in the acidic environment than the commercial Pt/C. However, the catalyst activity of the heat treatment Ni_{core} – $PtRu_{shell}$/C is still lower than that of the commercial Pt/C which also confirmed by the chronoamperometry technique.

6.2 Recommendations

In the study of preparation of the carbon supported Ni_{core} – Pt $alloy_{shell}$ catalyst, some points have arisen from this investigation and are interesting for the further study as following:

1. The other type of polymer stabilizer for the metal core nanoparticle.

The different stabilizer and also the different stabilizer concentration provide the different morphology and the particle size of the obtained nanoparticle [63]. Also, in the case of incomplete removal of polymer stabilizer from the surface of core particle, the remaining of the selected stabilizer should promote the desired reaction on the metal nanoparticle surface or should support the electron transfer. The interesting stabilizer for the future study might be the conductive polymer stabilizer.

2. The methodology to remove the remaining stabilizer on the metal nanoparticle surface.

The remaining stabilizer appears as the blockage between the surface of core and shell metal nanoparticle Thus, before applying shell metal layer, the remaining stabilizer should be completely removed. In the future study, the removal methodology should be applied without the alteration of the morphology and core particle size. In case of using heat – treatment method, the interesting parameters for investigation are the heat treatment temperature, time of treatment and the heating rate for increasing the temperature. The microwave – assisted methodology is also interesting for the further study.

3. The reducing agent for shell layer

Since the kinetics of shell metal reduction affects the morphology of the core – shell structure catalyst, the appropriate reducing agent should be selected for the particular shell metal type. The further study should be investigated the effect of the strength of the reducing agent for shell metal on the properties of the obtained core – shell structure catalyst.

REFERENCES

[1]. Larminie, J. and Dicks, A. Fuel Cell System Explained. 2nd edition, John Wiley & Sons Ltd., 2003.

[2]. Wu, J., et al. A review of PEM fuel cell durability: Degradation mechanisms and mitigation strategies. Journal of Power Sources 184 (2008): 104–119.

[3]. Wang, G., Wu, H., Wexler, D., Liu, H. and Savadogo, O. Ni@Pt core – shell nanoparticles with enhanced catalytic activity for oxygen reduction reaction, Journal of Alloys and Compounds 503 (2010): L1 – L4.

[4]. Spiegel, C. Designing and building fuel cells. 1st edition, The McGraw – Hill companies, 2007.

[5]. Li, X. Principles of fuel cells. Taylor & Francis group, 2005.

[6]. Scientific computing world, Fuel for thought on cars of the future [online]. Available from: http://www.scientificcomputing.com/images/scwjanfeb03 fuelcell1.jpg [2010, December 24]

[7]. Fuel cell: Proton Exchange Membrane Fuel Cells (PEMFC) [online], Available from: http://www.e-sources.com/fuelcell-PEMFC.htm [2012, August 6]

[8]. Zhang, J. PEM fuel cell electrocatalysts and catalyst layers: Fundamentals and applications. Springer, 2008.

[9]. Thanasilp, S. and Hunsom, M. Effect of MEA fabrication techniques on the cell performance of Pt–Pd/C electrocatalyst for oxygen reduction in PEM fuel cell. Fuel 89, (2010): 3847–3852.

[10]. Towne, S., Viswanathan, V., Holbery, J. and Rieke, P. Fabrication of polymer electrolyte membrane fuel cell MEAs utilizing inkjet print technology. Journal of Power Sources 171 (2007): 575–584.

[11]. Neyerlin, K.C., Srivastava, R., Yu, C. and Strasser, P. Electrochemical activity and stability of dealloyed Pt–Cu and Pt–Cu–Co electrocatalysts for the oxygen reduction reaction (ORR). Journal of Power Sources 186 (2009): 261–267.

[12]. Ohashi, M., et al. Electrochemical and structural characterization of carbon-supported Pt–Pd bimetallic electrocatalysts prepared by electroless deposition. Electrochimica Acta 55 (2010): 7376–7384.

[13]. Yu, P., Pemberton, M. and Plasse, P. PtCo/C cathode catalyst for improved durability in PEMFCs. Journal of Power Sources 144 (2005): 11–20.

[14]. Camara, G.A., Giz, M.J., Paganin, V.A. and Ticianelli, E.A. Correlation of electrochemical and physical properties of PtRu alloy electrocatalysts for PEM fuel cells. Journal of Electroanalytical Chemistry 537 (2002): 21 – 29.

[15]. Liu, Y., Shindo, D. and Sellmyer, D.J. Handbook of Advanced Magnetic Materials Volume 3: Fabrication and Processing. Springer, 2006.

[16]. Liu, H. and Zhang, J. Electrocatalysis of Direct Methanol Fuel Cells: From Fundamental to Applications. Wiley – VCH, 2009.

[17]. Bai, L. et al. Shape – controlled synthesis of Ni particles via polyol reduction. Journal of Crystal Growth 311(2009): 2474 – 2479.

[18]. Couto, G. G., et al. Nickel nanoparticles obtained by a modified polyol process: Synthesis, characterization, and magnetic properties. Journal of Colloid and Interface Science 311 (2007): 461–468.

[19]. Qi, J., Jiang, L., Jing, M., Tang, Q. and Sun, G. Preparation of Pt/C via a polyol process – Investigation on carbon support adding sequence. International Journal of Hydrogen Energy 36 (2011): 10490 – 10501.

[20]. Park, B. K., et al. Synthesis and size control of monodisperse copper nanoparticles by polyol method. Journal of Colloid and Interface Science 311 (2007): 417–424.

[21]. Zhang, X., et al. Modifying effects of polyethylene glycols and sodium dodecyl sulfate on synthesis of Ni nanocrystals in 1,2 –propanediol. Applied Surface Science. 252 (2006): 8067 – 8072.

[22]. An, B. H., et al. CoPt nanoparticles by a modified polyol process. Colloids and Surfaces A: Physicochem. Eng. Aspects 313–314 (2008): 250–253.

[23]. Ai, F., Yao, A., Huang, W., Wang, D. and Zhang, X. Synthesis of PVP – protected NiPd nanoalloys by modified polyol process and their magnetic properties. Physica E 42 (2010): 1281–1286.

[24]. Lee, K. S., et al. Modified polyol synthesis of PtRu/C for high metal loading and effect of post-treatment. Journal of Power Sources 195 (2010): 1031–1037.

[25]. Kumar, C. Mixed Metal Nanomaterials. Wiley – VCH, 2009.

[26]. Zeng, J., Yang, J., Lee, J.Y., and Zhou, W. Preparation of carbon – supported core – shell Au – Pt nanoparticles for methanol oxidation reaction: the promotional effect of the Au core. Journal of Physical Chemitry B 110 (2006): 24606 – 24611.

[27]. Zhao, H., Li, L., Yang, J. and Zhang, Y. Co@ Pt – Ru core – shell nanoparticles supported on multiwalled carbon nanotube for methanol oxidation. Electrochemistry Communication 10 (2008): 1527 – 1529.

[28]. Kristian, N., and Wang, X., Pt_{shell} – Au_{core} /C electrocatalyst with a controlled shell thickness and improved Pt utilization for fuel cell reaction. Electrochemistry Communication 10 (2008): 12 – 15.

[29]. Wei, Z.D., et al. Electrochemically synthesized Cu/Pt core – shell catalysts on porous carbon electrode for polymer electrolyte membrane fuel cells. Journal of Power Sources 180 (2008): 84 – 91.

[30]. Lee, M.H. and Do, J.S. Kinetics of oxygen reduction reaction on $Co_{rich\ core}$ – $Pt_{rich\ shell}$ /C electrocatalysts. Journal of Power Sources 188 (2009): 353 – 358.

[31]. Wu, Y.N., Liao, S.J., Liang, Z.X., Yang, L.J. and Wang, R.F. High – performance core – shell PdPt@Pt/C catalysts via decorating PdPt alloy cores with Pt. Journal of Power Sources 194 (2009): 805 – 810.

[32]. Ma, Y., et al. High active PtAu/C catalyst with core – shell structure for oxygen reduction reaction. Catalysis Communications 11 (2010): 434 – 437.

[33]. Zhao, Y., Yang, X., Tian, J., Wang, F. and Zhan, L. Methanol electro – oxidation on Ni@Pd core – shell nanoparticles supported on multi – walled carbon nanotubes in alkaline media. International Journal of Hydrogen Energy 35 (2010): 3249 – 3257.

[34]. Mench, M. M., Kumbur, E. C. and Veziroglu, T. N. Polymer electrolyte fuel cell degradation . Elsevier, 2012.

[35]. Ornelas, R., Stassi, A., Modica, E., Arico A. S. and Antonucci, V. Accelerated degradation tests for Pt/C catalysts in sulfuric acid. ECS Transactions 3 (2006): 633-641.

[36]. Bi, W. and Fuller, T. F. Temperature Effects on PEM Fuel Cells Pt/C Catalyst Degradation. Journal of Electrochemical Society 155 (2008): B215-B221.

[37]. Inaba, M., et al. Effect of Core Size on Activity and Durability of Pt Core-Shell Catalysts for PEFCs. ECS Transactions 33 (2010): 231-238.

[38]. Chen, S., et al. Nanostructured polyaniline-decorated Pt/C@PANI core-shell catalyst with enhanced durability and activity. Journal of the American Chemical Society 134 (2012): 13252−13255.

[39]. Huang, S. Y., Ganesan, P. and Popov, B. N. Electrocatalytic activity and stability of titania-supported platinum – palladium electrocatalysts for polymer electrolyte membrane fuel cell. ACS Catalysis 2 (2012): 825−831.

[40]. Chen, Y., et al. Enhanced stability of Pt electrocatalysts by nitrogen doping in CNTs for PEM fuel cells. Electrochemistry Communications 11 (2009): 2071–2076.

[41]. Sugawara, Y., Yadav, A. P., Nishikata, A. and Tsuru, T. Dissolution and surface area loss of platinum nanoparticles under potential cycling. Journal of Electroanalytical Chemistry 662 (2011): 379–383.

[42]. Zignani, S. C., Antolini E., and Gonzalez, E. R. Stability of Pt–Ni/C (1:1) and Pt/C electrocatalysts as cathode materials for polymer electrolyte fuel cells: Effect of ageing tests. Journal of Power Sources 191 (2009): 344–350.

[43]. Z. M. Zhou, et al. Durability study of Pt–Pd/C as PEMFC cathode catalyst. Internataional Journal of Hydrogen Enerygy 35 (2010): 1719 – 1726.

[44]. Wu, H., et al. $Pt_{1-x}Co_x$ nanoparticles as cathode catalyst for proton exchange membrane fuel cells with enhanced catalytic activity. Materials Chemistry and Physics 124 (2010): 841–844.

[45]. Chen, Y., Yang, F., Dai, Y., Wang, W. and Chen, S. Ni@Pt Core-Shell Nanoparticles: Synthesis, Structural and Electrochemical Properties. J. Phys. Chem. C 112 (2008): 1645-1649.

[46]. Long, N.V., Ohtaki, M., Nogami, M., and Hien, T. D. Effects of heat treatment and poly (vinylpyrrolidone) (PVP) polymer on electrocatalytic activity of polyhedral Pt nanoparticles towards their methanol oxidation. Colloid Polym Sci 289 (2011): 1373 – 1386.

[47]. Kanchanarachata, N. Preparation of carbon – supported platinum/ ruthenium catalysts by electroless deposition for PEM fuel cell. Master thesis, Department of Chemical Technology, Faculty of Science, Chulalongkorn University, 2011.

[48]. PEM single cell fuel cell [online]. Available from: http://www.directindustry.com/prod/ eletrochem/pem-single-cell-fuel-cells-22780-686259.html [2013, January 25].

[49]. Sanguanrak, P. Design of proton exchange membrane fuel cell test station. Master thesis, Department of Chemical Technology, Faculty of Science, Chulalongkorn University, 2002.

[50] Bing, Y., Liu, H., Zhang, L., Ghosh, D. and Zhang, J. Nanostructured Pt-alloy electrocatalysts for PEM fuel cell oxygen reduction reaction. Chemical Society Reviews 39 (2010): 2184–2202.

[51]. Zheng, N., Fan, J. and Stucky, G. D. One – step one – phase synthesis of monodisperse noble – metallic nanoparticles and their colloidal crystals. Journal of the American Chemical Society 128 (2006): 6550 – 6551.

[52]. Antolini, E., Salgado, J. R.C., Silva, R. M. D. and Gonzalez, E.R. Preparation of carbon supported binary Pt–M alloy catalysts (M = first row transition metals) by low/medium temperature methods. Materials Chemistry and Physics 101(2007): 395–403.

[53]. Liu H. and Manthiram A. Controlled synthesis and characterization of carbon-supported Pd_4Co nanoalloy electrocatalysts for oxygen reduction reaction in fuel cells. Energy & Environmental Science 2(2009): 124-132.

[54]. Wu, H., Wexler, D. and Wang, G. Pt_xNi alloy nanoparticles as cathode catalyst for PEM fuel cells with enhanced catalytic activity. Journal of Alloys and Compounds 488 (2009): 195–198.

[55]. Esparbé, I., et al. Structure and electrocatalytic performance of carbon-supported platinum nanoparticles. Journal of Power Sources 190 (2009): 201–209.

[56]. Colon-Mercado, H. R., Hansung, K. and Popov, B. N. Durability study of Pt_3Ni_1 catalysts as cathode in PEM fuel cells. Electrochemistry Communications 6 (2004): 795 – 799.

[57]. Takasu, Y. Yoshinaga, N. and Sugimoto, W. Oxygen reduction behavior of RuO2/Ti, IrO2/Ti and IrM (M: Ru, Mo, W, V) Ox/Ti binary oxide electrodes in a sulfuric acid solution. Electrochemistry Communications 10 (2008): 668–672.

[58]. Liang, C., et al. Nanostructured WC_x/CNTs as highly efficient support of electrocatalysts with low Pt loading for oxygen reduction reaction. Energy Environ. Sci 3 (2010): 1121–1127.

[59]. Cao, G. Nanostructures & Nanomaterials: Synthesis, Properties & Applications. London, Imperial College Press, 2004.

[60]. Haque, K. M. A., Hussain, M. S., Alam, S.S. and IsIam, S. M. S. Synthesis of nano-nickel by a wet chemical reduction method in the presence of surfactant (SDS) and a polymer (PVP). African Journal of Pure and Applied Chemistry 4(5) (2010): 58-63.

[61]. Henglein, A. Colloidal silver nanoparticles: photochemical preparation and Interaction with O2, CCl4, and some metal Ions. Chemistry of Materials 10 (1998): 444 - 50.

[62]. Travitsky, N., et al. Pt-, PtNi- and PtCo-supported catalysts for oxygen reduction in PEM fuel cells. Journal of Power Sources 161 (2006): 782 - 9.

[63]. Montgomery, D. C. Design and analysis of experiments. 5th edition, John wiley & sons, Inc., 2001.

[64]. Wang, H., Yuan, X. Z. and Li, H. PEM fuel cell diagnostic tools. CRC press, 2012.

[65]. Wang, H., Kou, X., Zhang, L. and Li, J. Size – controlled synthesis, microstructure and magnetic properties of Ni nanoparticles. Materials Research Bulletin 43 (2008): 3529 – 3536.

[66]. Gan, L., Du, H., Li, B. and Kang, F. Influence of reaction temperature on the particle – composition distributions and activities of polyol – synthesized Pt –Ru/C catalysts for methanol oxidation. Journal of power sources 191 (2009): 233 – 239.

[67]. Toshima, N., Ito, R., Matsushita, T. and Shiraishi, Y. Trimetallic nanoparticles having a Au-core structure. Catalysis Today 122 (2007): 239–244.

[68]. Wang, Z. B., Yin, G. P. and Shi, P. F. The influence of acidic and alkaline precursors on Pt Ru/C catalyst performance for a direct methanol fuel cell. Journal of Power Sources 163 (2007): 688–694.

[69]. Wu, J., et al. Diagnostic tools in PEM fuel cell research: Part I Electrochemical techniques. International journal of hydrogen energy 33(2008): 1735 – 1746.

[70]. Yasuda, K., Taniguchi, A., Akita, T., Ioroi, T. and Siroma, Z. Platinum dissolution and deposition in the polymer electrolyte membrane of a PEM fuel cell as studied by potential cycling. Physical Chemistry Chemical Physics 8 (2006): 746–752.

[71]. Zhang, S., et al. A review of accelerated stress tests of MEA durability in PEM fuel cells. International journal of hydrogen energy 34 (2009): 388 – 404.

[72]. Schmittinger, W. and Vahidi, A. A review of the main parameters influencing long-term performance and durability of PEM fuel cells. Journal of Power Sources 180 (2008):1–14

APPENDICES

Appendix A
The calculation from the XRD analysis

A.1 The calculation of the average particle size from XRD diffraction peak

From Scherer's equation

$$d = \frac{0.9\lambda}{\beta \cos\theta} \qquad \text{(A1)}$$

Where d = the average particle size (nm)

λ = the wavelength of X- ray (0.15406 nm)

β = the width of the peak at half height (radians)
(also called, full width at half maximum, FWHM)

θ = the angle of the peak

The example of average particle size calculation

Data: $Ni_{core} - Pt_{shell}/C$ particle, selected diffraction peak at $2\theta = 44.1^{o}$

then $\theta = 22.05^{o}$ (0.385 radian) and FWHM at selected $2\theta = 2.104^{o}$ (0.0376 radian)

Substitution in the equation A1 (Scherer's equation) then,

$$d = \frac{0.9\ (0.15406)}{(0.0376)\cos(0.385)}$$

$$= 4.072 \text{ nm.}$$

A.2 The calculation of lattice parameter

From Bragg's law

$$\lambda = 2d_{h,k,l} \cdot \sin\theta_{h,k,l} \qquad \text{(A2)}$$

Where λ = the wavelength of X- ray (0.15406 nm)

d = the interplanar spacing (nm)

θ = the incident angle (radian)

After knowing the crystal system of the particle, the interplanar spacing (*d*) can be calculated from Bragg's law following the equation A1. From the relation of the interplanar spacing (*d*), Miller indices (*h, k, l*) and the lattice parameter (*a*) as summarized in Table A-1 below, the calculation of lattice parameter (*a*) can be achieved.

Table A-1 The relation of interplanar spacing (*d*), lattice parameter (*a*) and the Miller indices of some crystal systems [59].

Crystal system	**The interplanar spacing (*d*) , lattice parameter (*a*) , Miller indices (*h*, *k*, *l*)**
Cubic	$\frac{1}{d^2} = \frac{h^2 + k^2 + l^2}{a^2}$
Tetragonal	$\frac{1}{d^2} = \frac{h^2 + k^2}{a^2} + \frac{l^2}{c^2}$
Orthorhombic	$\frac{1}{d^2} = \frac{h^2}{a^2} + \frac{k^2}{b^2} + \frac{l^2}{c^2}$

The example of lattice parameter calculation

Data: $Ni_{core} - Pt_{shell}/C$ particle, cubic with diffraction peaks 44.60^o [111], 51.28^o [200] and 76.24^o [220]

Choosing only one set of data, such as $2\theta = 76.24^o$ then $\theta = 38.12^o$ (0.666 radian)
And the Miller indices (h, k, l) = [220]

Substitution in the equation A2 (Bragg's law) then,

$$0.15406 = 2\, d_{h,k,l} \sin(0.666)$$

$$d_{h,k,l} = 0.1247 \text{ nm.}$$

From the relation of cubic crystal system in Table A-1

$$\frac{1}{d^2} = \frac{h^2 + k^2 + l^2}{a^2}$$

Then, substitute all parameters,

$$\frac{1}{(0.1247)^2} = \frac{2^2 + 2^2 + 0^2}{a^2}$$

The lattice parameter, $a = 0.3528$ nm.

Appendix B

The determination of electrochemical active surface area (EAS) from cyclic voltammetric (CV) analysis

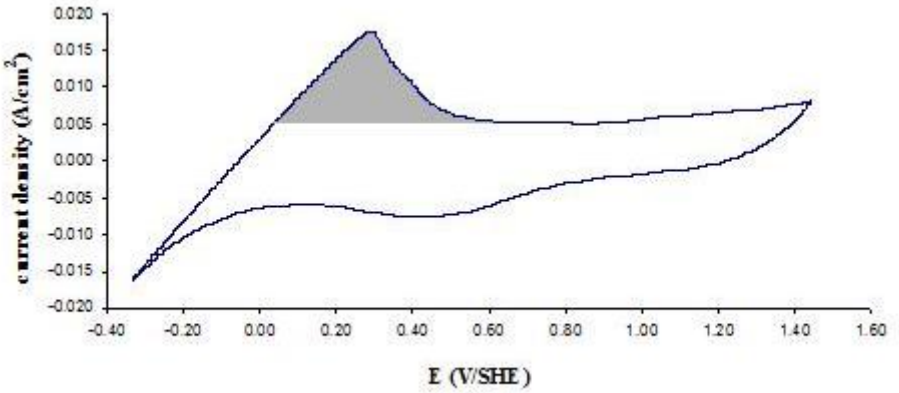

Figure B-1 Illustrate of typical cyclic voltammogram of Pt/C in the N_2 saturated 0.5 M H_2SO_4. The shaded area represents the hydrogen desorption region.

The electrochemical active surface area can be calculated from the equation B1 as shown below [70]

$$EAS(cm^2 Pt / gPt) = \frac{\text{charge}\ (\mu C / cm^2)}{210\ \ (\mu C / cm^2\ \text{Pt}) \times \text{catalyst loading}\ (\text{g Pt} / cm^2)} \qquad \text{(B1)}$$

Where EAS = Electrochemical active surface area (cm^2 Pt/ g Pt).

Charge = The charge needed to remove the monolayer of adsorbed hydrogen on the electrode which obtained from the integration of the area under the hydrogen desorption region of the CV curve ($\mu C/cm^2$).

210 ($\mu C/cm^2$ Pt) = The charge required to remove the monolayer of adsorbed hydrogen on the smooth Pt surface.

Catalyst loading = The total amount of Pt loading in the catalyst layer. (g Pt /cm^2).

The example of EAS calculation

Data:

- $Ni_{core} – PtRu_{shell}/C$ 0.3 mg metal loading/cm^2 (3×10^{-5} g metal loading/cm^2) (58.7wt% Pt in the total active metal).
- Charge obtained from the integration of the area under hydrogen desorption region (by GPEs program) 0.129 coulomb.
- Electrode area for CV measurement 0.786 cm^2.

From data, charge required for this synthetic catalyst = $\frac{0.129\times 10^6}{0.786}$

$= 1.641\times 10^5 \mu C/cm^2$

Substitute all data into equation B1, then

$$EAS = \frac{1.641\times 10^5\ \mu C/cm^2}{210\ \ (\mu C/cm^2\ \text{Pt})\times 3\times 10^{-5}\ (\text{g metal}/cm^2)}$$

$= 2{,}605{,}387.205\ cm^2$ Pt/g active metal

$= 260.54\ m^2$ Pt/ g active metal

However, in this case, the Pt content in the catalyst layer = 58.7 wt%

Thus, the actual EAS for this synthetic catalyst = 260.54 × 0.587

$= 152.94\ m^2$Pt / g Pt

VITA

Miss Saowaluck Bhlapibul was born on December 4, 1981 in Bangkok Thailand. She received her B.Sc. degree in chemical engineering and M.Sc. degree in Chemical Technology from Chulalongkorn University. Saowaluck joined the department of chemical technology, Chulalongkorn University as a Ph.D. student in 2008. She has received the strategic scholarships fellowships frontier research networks from the Higher Education Commission Thailand for her Ph.D. study. Saowaluck also served as a teaching assistant for undergraduate courses “Materials and Energy Balances” and “Physico-Chemical Measurements”. During the last year of Ph.D. student, she spent almost 3 months (August – October 2012) doing research at the department of chemical and biomolecular engineering, faculty of engineer, Yonsei University, Seoul, The Republic of Korea under the supervision of Prof. Yong Gun-Shul. Her paper entitled “The effect of the stabilizer on the properties of a synthetic $Ni_{core} – Pt_{shell}$ catalyst for PEM fuel cells” has been accepted for publication in “The Renewable Energy”. She also presented her work at 1 conference in Singapore and 1 conference in Thailand.